Incorporation and Preservation of Molybdenum and Uranium Isotope Variations in Modern Marine Sediments

by

Stephen J. Romaniello

A Dissertation Presented in Partial Fulfillment
of the Requirements for the Degree
Doctor of Philosophy

Approved July 2012 by the
Graduate Supervisory Committee:

Ariel Anbar, Chair
Hilairy Hartnett
Achim Herrmann
Everett Shock
Meenakshi Wadhwa

ARIZONA STATE UNIVERSITY

August 2012

ABSTRACT

Molybdenum and uranium isotope variations are potentially powerful tools for reconstructing the paleoredox history of seawater. Reliable application and interpretation of these proxies requires not only detailed knowledge about the fractionation factors that control the distribution of molybdenum and uranium isotopes in the marine system, but also a thorough understanding of the diagenetic processes that may affect molybdenum and uranium isotopes entering the rock record.

Using samples from the Black Sea water column, the first water column profile of $^{238}U/^{235}U$ variations from a modern euxinic basin has been measured. This profile allows the direct determination of the $^{238}U/^{235}U$ fractionation factor in a euxinic marine setting. More importantly however, these data demonstrate the extent of Rayleigh fractionation of U isotopes that can occur in euxinic restricted basins. Because of this effect, the offset of $^{238}U/^{235}U$ between global average seawater and coeval black shales deposited in restricted basins is expected to depend on the degree of local uranium drawdown from the water column, potentially complicating the interpretation $^{238}U/^{235}U$ paleorecords.

As an alternative to the black shales typically used for paleoredox reconstructions, molybdenum and uranium isotope variations in bulk carbonate sediments from the Bahamas are examined. The focus of this work was to determine what processes, if any, fractionate molybdenum and uranium isotopes during incorporation into bulk carbonate sediments and their subsequent diagenesis. The results demonstrate that authigenic accumulation of molybdenum

and uranium from anoxic and sulfidic pore waters is a dominant process controlling the concentration and isotopic composition of these sediments during early diagenesis. Examination of ODP drill core samples from the Bahamas reveals similar behavior for sediments during the first ~780ka of burial, but provides important examples where isolated cores and samples occasionally demonstrate additional fractionation, the cause of which remains poorly understood.

ACKNOWLEDGMENTS

Without the support of many, many people, this dissertation would not have been possible, and for that I am deeply indebted. First, I thank my advisory committee and especially Ariel Anbar and Achim Herrmann, who guided, supported, and funded all aspects of my work. I have little doubt that I was, at times, a very challenging student. This dissertation is a testament not only to the strength of my committee's academic support, but also their patience and understanding.

Many other people played a critical role in my professional education at ASU. In particular, I especially thank Gwyneth Gordon, Natalya Zolotova, and Stan Klonowski for the countless hours of analytical training and support they provided. I also thank Brian Kendall and Laura Wasylenki who served as important mentors during my graduate career. Additionally, I thank all of my friends and labmates at ASU who were a constant source of inspiration and companionship both inside the lab and out.

Outside ASU, I thank Albert Colman for collecting the Black Sea samples used in this dissertation while I was still in high school and Pamela Reid for developing and maintaining the Darby Island Research Station, our home base in the Bahamas.

Finally, I thank my wife, Helen Evans, for her love, support, understanding, and companionship throughout my entire graduate career, which has spanned nearly all of nine years of our relationship.

TABLE OF CONTENTS

Page

CHAPTER Page

CHAPTER Page

CHAPTER Page

LIST OF TABLES

LIST OF FIGURES

Figure Page

Chapter 1

INTRODUCTION TO MOLYBDENUM AND URANIUM MARINE ISOTOPE GEOCHEMISTRY

1.1 Non-traditional Stable Isotopes as Redox Proxies

As early as 2001, it was recognized that non-traditional stable isotopes of redox-sensitive metals could be powerful recorders of variations in the redox chemistry of seawater over Earth's history (~35% of total sinks, Barling et al., 2001). Here and throughout this dissertation, the term "redox variation," is used in the colloquial sense common to oceanography to describe the relative abundance of dissolved O_2 and H_2S in seawater and pore waters, but does not necessarily imply a well-defined equilibrium thermodynamic redox potential that can be difficult to determine in low-temperature, environmental systems which may be far from equilibrium.

The solubility of oxyanion forming metals, such as Mo, Re, and U, in seawater is a strong function of the seawater redox state. These metals are soluble and relatively unreactive in seawater containing free dissolved O_2. In contrast, in seawater that is anoxic or contains sulfide as a product of sulfate reduction, these metals become much less soluble either through their chemical or biological reduction as in the case of Re and U, or through the formation of precipitates or particle-reactive species that promote their scavenging from seawater as occurs with Mo (Colodner et al., 1995; Erickson and Helz, 2000; Helz et al., 1996; Morford and Emerson, 1999).

Non-traditional isotope paleoredox proxies work by exploiting isotopic fractionation between various oxidized and reducing sinks for these metals (Anbar, 2004). Given a weathering-derived source of metal to seawater with a restricted isotopic range, the isotopic composition of the metal in seawater will be primarily a function of the relative magnitude of various oxidized and reduced sinks and their fractionation during removal from seawater (Arnold et al., 2004). In the simplest case, given a known isotopic composition of seawater (δ_{sw}), the weathering source (δ_{source}), and the isotopic fractionations associated with a single oxidized and reduced sink (Δ_{ox} and Δ_{sink}, respectively), the relative magnitude of the reduced sink (f_{red}) can be calculated directly:

$$f_{red} = \frac{\delta_{source} - (\delta_{sw} + \Delta_{ox})}{(\Delta_{red} - \Delta_{ox})} \qquad \text{Eq. 1.1}$$

The major potential advantage of this isotopic mass balance approach over more traditional sediment facies analysis and geochemical speciation approaches is that, when the seawater residence time of the metal species greatly exceeds typical ocean mixing time scales (~1500 years), f_{red} reflects the global contribution of reduced sinks (Anbar, 2004). In theory, this allows global marine redox conditions to be estimated from a single core. This is especially useful for understanding redox variations during the Archean and Proterozoic when only sparse geological records remain, and for which it can be especially difficult to precisely correlate cores from geographically distant locations.

Despite this potential, substantial barriers remain to the wide spread and persuasive application of non-traditional stable isotopes as paleoredox proxies.

These problems generally fall into three categories. The first category includes uncertainties in the model parameters invoked in Eq 1.1. Application of Eq. 1.1 requires accurate and precise knowledge of the model parameters, including isotopic composition of the weathering source, which might conceivably vary with time, and the values of the fractionation factors for various sinks. In general, measuring the appropriate fractionation factors for various sinks has proven relatively straightforward. However, significant uncertainty remains regarding the average isotopic compositions of the modern weathering flux for all of these proxies, and the potential for their variation through time remains essentially unexplored.

The second major limitation to the application of non-traditional stable isotope paleoredox proxies is the identification of a reliable means of reconstructing the metal isotopic composition of seawater from the metal isotope variations recorded in the rock record. To date, almost all of these proxies have been reconstructed from variations in black shales. The major advantage of shale over other facies is that shale is relatively impermeable, limiting the potential for post-depositional alteration by fluid migration. However, black shales are not ubiquitous in the geologic record and so our conception of ocean redox evolution may be biased by the conditions of restricted marginal basins where such shales are often deposited. In a search for more widely distributed and representative facies, several different groups have begun exploring trace metal isotope variations in other facies, such as carbonates and banded iron formations

(Brennecka et al., 2011a; Frei et al., 2009; Voegelin et al., 2010; Voegelin et al., 2009).

The third and perhaps most fundamental limitation facing non-traditional stable isotope paleoredox proxies is that the global marine budgets of all these metals includes more than two quantitatively important sinks. The presence of multiple sinks makes the solution to Eq 1.1 non-unique and requires that additional constraints be defined, either from combination of multiple isotope systems or by imposing relationships between the magnitude of various sinks. Most researchers in the field now recognize at least three quantitatively important sinks for redox-sensitive oxyanion-forming metals: oxic sinks dominated by adsorption and coprecipitation of metals to Fe and Mn-oxides, anoxic/suboxic sinks dominated by the reduction of metals in the water column or pore waters, and euxinic sinks where the chemistry is governed by high concentrations of sulfide in the water column (e.g., Barnes and Cochran, 1990; Dunk et al., 2002; McManus et al., 2006; Miller et al., 2011; Montoya-Pino et al., 2010; Scott et al., 2008; Weyer et al., 2008). Ultimately, even this classification scheme may prove to be too simple, as sediments tend to grade between these classifications and the scheme ignores other potential sinks such as carbonates, cherts, and hydrothermal deposits. A more detailed discussion of the magnitude and isotopic composition of Mo and U sources sinks is given in Sections 1.2 and 1.3.

The underlying theme of this dissertation is an attempt to address some of these limitations, thereby enabling more reliable paleoredox reconstructions. Two major focuses are the development U isotopes as a paleoredox proxy and the

reconstruction of Mo and U isotope records from carbonates. Development of multiple paleoredox proxies will allow intercomparison of results and increase the reliability of reconstructions, much in the same way that multiple radiogenic isotope systems are combined to validate radiometric ages. Moreover, if Mo and U isotope records can be simultaneously extracted from the same samples, a new generation of multiple isotope proxies may help resolve ambiguities inherent in systems with three or more sinks.

1.2 Isotope Geochemistry and Marine Budget of Molybdenum

Mo has seven stables isotopes with abundances ranging from 9-24%. This large number of isotopes combined with a relatively flat isotope distribution makes the mass spectrometry of Mo analytically attractive and was one of the original drivers for studying Mo isotope geochemistry instead of other redox sensitive metals (Anbar, 2004). Mo has three common environmental redox states (+IV, +V, +VI), although little is known about stable isotope fractionation involving the +IV and +V redox states.

Recent studies of Mo isotope fractionation typically express variations as $\delta^{98/95}$Mo [$=1000\times(^{98}Mo/^{95}Mo_{smpl}/^{98}Mo/^{95}Mo_{std}-1)$] although older literature also expressed variations as $\delta^{97/95}$Mo. In the absence of an agreed upon international isotopic standard, isotopic compositions are generally referenced to intercalibrated in-house ICP standards (e.g., “RochMo2”, Johnson Matthey Specpur, Lot #802309E) and sometimes referenced against open ocean seawater as a common external standard, which has a $\delta^{98/95}$Mo value of 2.3±0.1‰ on the

RochMo scale (Arnold et al., 2004; Barling et al., 2001; Neubert et al., 2008; Siebert et al., 2003). The observed natural range of Mo isotope variations, expressed as $\delta^{98/95}$Mo, is approximately -0.7 to +2.3‰ (Barling and Anbar, 2004; Barling et al., 2001; Kendall et al., 2009; Kendall et al., 2011; Siebert et al., 2003). The processes responsible for the fractionation of Mo isotopes in marine environment are described in the following sections.

1.2.2 Mo Sources

The two main sources of Mo to the ocean are rivers (~90%, 1.9×10^8 mol yr^{-1}) and low-temperature hydrothermal inputs (~10%, 2.2×10^7 mol yr^{-1}) (Morford and Emerson, 1999; Wheat et al., 2002). The magnitude of the ground water Mo fluxes is not well known, but estimates of direct submarine groundwater discharge range from 6-10% of riverine runoff (Garrels and Mackenzie, 1971; Zektser and Dzhamalov, 1981) and groundwater Mo concentrations are typically ~1ppb , so it is likely that groundwater Mo discharge is in the range of 2-4 $\times 10^7$ mol yr^{-1} (Ayotte et al., 2011; Garrels and Mackenzie, 1971; Zektser and Dzhamalov, 1981). In a survey accounting for 22% of global riverine discharge, Archer and Vance (2008) found an average $\delta^{98/95}$Mo of 0.7‰, a value substantially heavier than the average $\delta^{98/95}$Mo of continental rocks (0.09±0.24 ‰), including granites, basalts and clastic sediments (Barling et al., 2001; Siebert et al., 2003). The reason for this discrepancy remains unresolved, but on-going research is addressing the role of incongruent weathering of Mo, preferential retention of isotopically light Mo during weathering, preferential

scavenging of isotopically light Mo into the bed load of rivers, or the weathering of isotopically heavy marine sediments (Archer and Vance, 2008; Neubert et al., 2011; Pearce et al., 2010; Voegelin et al., 2012).

To date, there have been only two isotopic studies of Mo in fluids from hydrothermal systems. McManus et al. (2002) measured the Mo isotopic composition of hydrothermal ridge-flank, low-temperature hydrothermal system (Baby Bare basaltic outcrop, Juan de Fuca Ridge) and reported a dilution-corrected Mo concentration of 297 nmol kg^{-1} (2.8 × that of seawater) and a $\delta^{98/95}$Mo of 0.8‰. Pearce et al. (2010) reported a single measurement from an Icelandic hot spring (Deildartunguhver hydrothermal spring) that also had an elevated Mo concentration of 211 nM and a $\delta^{98/95}$Mo of -3.44‰, by far one of the lightest $\delta^{98/95}$Mo values reported to date. More measurements are needed before conclusions can be drawn about the average $\delta^{98/95}$Mo of hydrothermally-derived Mo, but the overall impact of this uncertainty on the isotopic Mo budget is damped by the relatively small size of the hydrothermal source. A similar argument can be made for groundwater Mo inputs, for which there are no published isotopic data.

Together, riverine and hydrothermal Mo sources account for ~2.1×10^{8} mol yr^{-1} with an isotopic composition between -0.3 and +0.7‰. Given an oceanic Mo inventory of ~1.4×10^{14} moles, the residence time of Mo in the modern ocean is calculated to be ~650 ky.

1.2.3 Mo Sinks

Broadly speaking, most researchers recognize three marine Mo sinks: oxic sinks, suboxic/anoxic sinks, and euxinic sinks. Oxic sinks describe sediments where ferromanganese oxides persist for at least several centimeters below the sediment-water interface. Mo is absorbed onto the surface ferromanganese sediments, accounting for a burial flux 0.7×10^8 mol Mo yr^{-1} (~35% of total sinks, Kendall et al., 2009; Scott et al., 2008). Both direct measurements and extensive laboratory experiments have demonstrated the Mo absorbed to Mn- and Fe-oxides is isotopically light, confirming that this sink has a $\delta^{98/95}$Mo of -0.7‰ (Barling and Anbar, 2004; Brucker et al., 2009; Goldberg et al., 2009; Goldberg et al., 2012; Siebert et al., 2003; Wasylenki et al., 2008; Wasylenki et al., 2011).

Euxinic sinks describes settings with sufficient sulfide (H_2S) in the water column to convert soluble, relatively unreactive molybdate (MoO_4^{2-}) to tetrathiomolybdate (MoS_4^{2-}) which is strongly particle-reactive and readily removed from the water column (Erickson and Helz, 2000; Helz et al., 1996). This process results in rapid, almost quantitative removal of Mo from sulfidic water columns, but occurs only in small regions of the modern ocean such as the Black Sea, some fjords, and submarine brine pools. As a result, loss of Mo to euxinic sinks accounts for only 0.1×10^8 mol Mo yr^{-1} (~5% of global marine Mo sinks, Kendall et al., 2009; Scott et al., 2008). Because this reaction is quantitative in the presence of sufficient sulfide, the isotopic composition of Mo removed in euxinic sinks matches that of seawater Mo with $\delta^{98/95}$Mo = 2.3‰ (Arnold et al., 2004; Neubert et al., 2008).

Suboxic/anoxic Mo sinks include the entire range of marine sediments between oxic and euxinic sinks. Although this sink was not originally recognized in early Mo isotope mass balance models (Arnold et al., 2004), it is now thought to be the largest Mo sink in the modern ocean, accounting for 1.2×10^8 mol Mo yr^{-1}, (~60% of global marine sinks, Kendall et al., 2009; McManus et al., 2006; Scott et al., 2008). Because this sink spans a continuum of settings that transition from nearly oxic to nearly euxinic, $\delta^{98/95}$Mo also varies, ranging from -0.5 to 1.8‰, and is correlated with bottom water redox conditions (Brucker et al., 2009; Poulson et al., 2006; Siebert et al., 2006). Within this range however, anoxic sites such as those found on the Pacific margins of Mexico and Peru, are uniquely large sinks with a consistent and well-characterized $\delta^{98/95}$Mo value of 1.6‰ (Brucker et al., 2009).

High-temperature hydrothermal systems represent a fourth possible sink for Mo, but a recent study has suggested that this sink is very small at present, 2.6×10^6 mol Mo yr^{-1} (0.4% of total sinks, Miller et al., 2011). The isotopic composition of this sink is not known, but is unlikely to play a significant role in the marine Mo isotope budget unless it is highly fractionated.

1.3 Isotope Geochemistry and Marine Budget of Uranium

Uranium (U) has two naturally-occuring primordial isotopes, ^{235}U ($\tau_{1/2} \approx$ 703 Ma) and ^{238}U ($\tau_{1/2} \approx 4.5$ Ga). In addition, the α-decay of ^{238}U indirectly produces a third short-lived U nuclide ^{234}U ($\tau_{1/2} \approx 245{,}000$ a). Both ^{235}U and ^{238}U have long, non-overlapping decay chains that have been used extensively for

radiometric dating applications since the 1950's (Edwards et al., 2003b; Henderson and Anderson, 2003). In addition to its well-known use in geochronology, U has two common environmental redox states (IV, VI) that make it useful as a tracer of redox geochemistry. In circum-neutral to slightly basic natural settings, U undergoes reduction from U(VI) to U(IV) at about the same redox potential as Fe(III)/Fe(II), although the kinetics of this reduction can be significantly inhibited by the formation of uranyl carbonates (e.g., UO_2CO_3) and ternary Ca-U-CO_3 complexes (Anderson et al., 1989a; Hua et al., 2006; Stewart et al., 2007). In the laboratory, U(V) is also a well-known oxidation state of U, but U(V) rapidly disproportionates into U(VI) and U(IV). Recent studies have shown that microbial reduction of U(VI) takes place via an obligatory U(V) step, suggesting that U(V) is likely an important but understudied environmental intermediate (Renshaw et al., 2005).

Two different isotope ratios of U are discussed in this dissertation, $^{234}U/^{238}U$ and $^{238}U/^{235}U$. Unlike Mo, where all of the isotopes display similar mass-dependent behavior, these two U isotope systems behave in fundamentally different ways and so it essential to distinguish between these two systems.

^{234}U is a decay product of ^{238}U and also undergoes further α-decay to ^{230}Th. In a closed system, the isotopic abundance of ^{234}U will evolve until the decay activity ratio of ($^{234}U/\ ^{238}U$) = 1, which is also defined as $\delta^{234/238}U = 0‰$. Measurements of ^{230}Th, ^{234}U, and ^{238}U began in earnest in the late 1950's and early 1960's for the purpose of dating marine carbonates (Edwards et al., 2003b). Initially, it was assumed that ^{234}U should be in secular equilibrium with ^{238}U, but

it was soon realized that rivers could be enriched in ^{234}U by several hundred permil, and that the $\delta^{234/238}U$ of seawater was enriched by ~146‰ (Ku, 1965; Thurber, 1962). The reason for this excess is the increased mobility of ^{234}U relative to other U isotopes, caused by the recoil of daughter nucleus during the α-decay of ^{238}U. The ejection of an α-particle from the ^{238}U nucleus not only results in the translocation of the resulting ^{234}Th atom by ~550 angstroms in the opposite direction, possibly ejecting the daughter from the host mineral grain, but also damages the mineral crystal lattice resulting in preferential leaching of ^{234}U further down the decay chain (Kigoshi, 1971). The resulting $^{234}U/^{238}U$ disequilibrium is very useful for dating materials and determining the origin of U in modern marine sediments but is not preserved in samples older than ~2 My.

The uranium isotope system that is the primary focus of this thesis is $^{238}U/^{235}U$. Until recently, it was widely believed the modern ratio of $^{238}U/^{235}U$ was constant in all solar system materials at a value of 137.88. Although the absolute ratio of $^{238}U/^{235}U$ has changed through time due to the differential decay of the two isotopes, this effect is eliminated when expressed as $\delta^{238/235}U$ because the ^{238}U and ^{235}U in the sample and standard decay at the same rate. The first reliable reports of terrestrial variation in natural $\delta^{238/235}U$ were published by Stirling et al. (2007) and Weyer et al. (2008), following an earlier report by Rademacher et al. (2006) of $\delta^{238/235}U$ fractionation in ^{235}U-enriched U during the biotic reduction of U(VI) to U(IV). The entire range of measured $\delta^{238/235}U$ variations in terrestrial materials spans ~1.6‰ from -0.9‰ to +0.5‰ with an internationally available standard reference material, SRM950a, serving as the standard reference material

(seawater has a value of -0.41‰ on this scale). The primary driver of these variations appears to be redox chemistry, with U(IV) enriched in ^{238}U by 0.4-0.8‰, but a smaller -0.2‰ fractionation has also been demonstrated for absorption of U onto birnessite (Bopp et al., 2009; Bopp et al., 2010; Brennecka et al., 2010a; Brennecka et al., 2011b; Weyer et al., 2008). Although the $^{238}U/^{235}U$ system is relatively new, the following sections summarize what is known about the magnitude and $^{238}U/^{235}U$ of U sources and sinks to the global ocean.

1.3.2 U Sources

Like Mo, the main source of U to the oceans is rivers that ultimately derive their U from the weathering of crustal and sedimentary rocks. The estimated global riverine U flux is 42×10^6 mol yr^{-1}, with an additional 9×10^6 mol yr^{-1} from ground water discharge, and 2×10^6 mol yr^{-1} from dust (Dunk et al., 2002). The average U concentration of seawater is 13.9 nM, giving an oceanic inventory of 19×10^{12} mol and a residence time of ~350 ky (Chen et al., 1986; Ku et al., 1977). The $\delta^{238/235}U$ of the riverine U flux is thought to be similar to crustal rocks (-0.2 to -0.4‰) and was confirmed by direct measurements of riverine $\delta^{238/235}U$ between -0.17 and -0.38‰ (Noordmann et al., 2009; Weyer et al., 2008). The $\delta^{238/235}U$ of average ground water discharge is not currently known and is difficult to constrain based on theoretical considerations alone. The $\delta^{238/235}U$ of dust is likely to be similar to that of average crustal rocks.

1.3.3 U Sinks

By combining recent reviews of the marine U budget with available published surveys of $\delta^{238/235}U$ in various materials, one can identify four major isotopically-distinct U sinks: euxinic sediments, suboxic/anoxic sediments, oxic sediments, and hydrothermal settings (Dunk et al., 2002; Stirling et al., 2007; Weyer et al., 2008). The reduction of soluble U(VI) to insoluble U(IV) is a major process responsible for U removal from seawater, and imparts a large isotopic fractionation (Barnes and Cochran, 1990; Bopp et al., 2009; Brennecka et al., 2010a; Klinkhammer and Palmer, 1991; Weyer et al., 2008). Euxinic sediments, defined by the presence of free sulfide in the overlying water column, account for the removal of 2.1×10^6 mol U yr^{-1}, with the largest portion of this occurring in the Black Sea (Dunk et al., 2002). The $\delta^{238/235}U$ of sediments in the Black Sea range from 0‰ to +0.4‰, implying that euxinic sinks are 0.4 to 0.8‰ heavier than seawater (Weyer et al., 2008).

Suboxic/anoxic sediments are the largest oceanic U sink and can be further subdivided into several subcategories (Barnes and Cochran, 1990; Dunk et al., 2002). Anoxic sediments, such as those found off the Peru Margin, account for 4.3×10^6 mol U yr^{-1} (Dunk et al., 2002). Uranium accumulation rates in oxygen-depleted sediments of the continental shelf and slope are an order of magnitude slower than in anoxic settings on an areal basis, but they cover a much larger area of the seafloor, and thus account for 13×10^6 mol U yr^{-1} (Dunk et al., 2002). Weyer et al. (2008) measured sediments from the Peru margin and found $\delta^{238/235}U$ values slightly heavier than seawater (-0.37 to -0.16‰). Although U

captured in these settings is likely to be U(IV), similar to euxinic settings, the overall apparent magnitude of fractionation appears to be smaller (0.1 – 0.2‰). The reason for this is not yet known, but may involve diffusion-limitation as the window of U-reduction moves deeper into the sediment, or a role for isotopically-light uranium delivered to sediments via absorption to Fe- and Mn-oxides. Dunk et al. (2002) identified mangroves, salt marshes, and estuaries as a separate sink accounting for 11×10^6 mol U yr^{-1}. No measurements of $\delta^{238/235}U$ exist for these settings yet, but as they are likely similar to other reducing suboxic/anoxic sediments; these coastal sinks are included with other anoxic/suboxic sinks in this discussion. Finally, Weyer et al. (2008) and Dunk (2002) both identified carbonates as a separate U sink. However, results in Chapter 3 and 4 suggest that U in bulk carbonate sediments behaves similarly to U in suboxic settings, undergoing reductive authigenic accumulation from reduced pore water with an isotopic offset of ~0.2‰. Because of this, the U burial flux in carbonates is included with other suboxic settings here, accounting for an additional 13×10^6 mol U yr^{-1}. This gives a total suboxic/anoxic/carbonate sink of 41×10^6 mol U yr^{-1}.

The third major U sink is via absorption to Fe -and Mn-oxides. It is estimated that the size of the modern oxic sink is small, at 1.4×10^6 mol U yr^{-1} similar to dust fluxes and modern euxinic sinks (Dunk et al., 2002). Laboratory experiments and analysis of environmental samples both imply that U absorbed to birnessite is depleted in $\delta^{238/235}U$ by 0.2‰ (Brennecka et al., 2011b; Stirling et al., 2007; Weyer et al., 2008). Measurements of samples from banded iron formations

suggest a wider range of variation for Fe-oxides, with measured $\delta^{238/235}U$ values between -0.29 and -0.88‰. It is not clear whether these reflect variable isotopic fractionation, variation in seawater $\delta^{238/235}U$ through time, or some other environmental process (Weyer et al., 2008).

The fourth major U sink is hydrothermal circulation through the seafloor. The estimated size of this sink is 5.7×10^{6} mol U yr^{-1} (Dunk et al., 2002). Because U appears to be removed quantitatively from hydrothermal fluids, it is likely that this process is quantitative, producing no isotope fractionation (Wheat et al., 2002).

Several additional sinks for U exist that are either small at present or for which insufficient data are available to assess. The two most important of these are likely to be siliceous sediments and phosphorites. Dunk (2002) estimated the modern U sink via precipitation of biogenic silica to be 0.6×10^{6} mol U yr^{-1}. U concentrations in phosphorites can be extremely high (70-150 ppm) but relatively low phosphorite accumulation rates (3 mmol P cm^{-2} kyr^{-1}) and their rare occurrence in the modern ocean (<0.1% of the seafloor) limit the maximum size of this sink to 1×10^{6} mol U yr^{-1} (Filippelli, 2002; Veeh et al., 1974). Although these sinks are small at present, large chert and phosphorite deposits exist in the geologic record, suggesting these might have been more important sinks at times in the past. No published measurements of $\delta^{238/235}U$ exist for cherts or phosphorites, so it is difficult to assess the potential significance of these sinks on the marine U isotope budget.

Chapter 2

FRACTIONATION OF $^{238}U/^{235}U$ IN THE WATER COLUMN OF THE BLACK SEA

2.1 Introduction

Recent analytical and conceptual advances have suggested the use of $^{238}U/^{235}U$ uranium (U) isotope fractionation as a marine paleoredox proxy (Bopp et al., 2010; Brennecka et al., 2010a; Stirling et al., 2007; Weyer et al., 2008). This suggestion is based on the observation of significant fractionation of $\delta^{238/235}U$ in marine sediments deposited under oxidizing versus reducing conditions (Bopp et al., 2010; Brennecka et al., 2010a; Weyer et al., 2008). These ideas have already been applied to interpret the $\delta^{238/235}U$ record of oceanic anoxia during OAE2 and the end-Permian extinction (Brennecka et al., 2011a; Montoya-Pino et al., 2010). In this study, we present a $\delta^{238/235}U$ profile from the water column of a modern sulfidic basin. We use these results to calculate an updated isotopic fractionation factor for U removal to sediments under euxinic conditions and demonstrate the importance of Rayleigh fractionation during partial U removal from the water column of restricted marine basins.

The marine geochemistry of U is sensitive to the redox state of seawater. Under oxic conditions, U is present in the oxidized U(VI) state that forms soluble $Ca\text{-}UO_2\text{-}CO_3$ complexes (Dong and Brooks, 2006). Due to the stability and solubility of these complexes, U in the modern ocean has a residence time of 3.2–5.6×10^5 years (Dunk et al., 2002). In its oxidized state, U is primarily removed from seawater via incorporation into carbonates. This process is slow however,

accounting for only 28% of U removal despite widespread carbonate precipitation in the surface ocean. Under oxygen-depleted conditions, U may be reduced to U(IV) which is poorly soluble and rapidly removed from seawater. Because of this, suboxic and anoxic marine sediments presently account for ~56% of U removal from seawater despite covering only ~6% of the seafloor (Dunk et al., 2002).

The U paleoredox proxy depends on the balance between the removal of isotopically fractionated U into marine sediments underlying reducing bottom waters and the removal of unfractionated or isotopically light U into carbonates and (Fe,Mn)-hydroxides (Brennecka et al., 2008; Montoya-Pino et al., 2010; Weyer et al., 2008). For example, in an oxygen-replete ocean, there would be minimal fractionation during removal, and so the U isotopic composition of seawater would be close to that of average riverine inputs. On the other hand, in an oxygen-depleted ocean, it is expected that the widespread removal of isotopically heavy U would cause the isotopic composition of seawater to become light. This relationship has been quantified and inverted such that, given an estimate of the U isotopic of seawater in the past, one can determine the proportion of reducing and non-reducing sinks (Montoya-Pino et al., 2010):

$$f_{anox} = \frac{\delta^{238/235}U_{inputs} - \delta^{238/235}U_{seawater}}{\Delta^{238/235}U_{reduced}} \qquad \text{Eq. 2.1}$$

where $\delta^{238/235}U_{inputs}$ is the isotopic composition of U inputs to seawater, $\delta^{238/235}U_{seawater}$ is the isotopic composition of U in seawater, $\Delta^{238/235}U_{reduced}$ is the

isotopic fractionation during removal to reducing sinks, and f_{anox} is the fraction of total U burial occurring in reduced sediments.

Several lines of evidence suggest U removed from seawater into reducing marine sediments is isotopically heavy (enriched in ^{238}U). Foremost, measurements of reduced marine sediments indicate values heavier than average seawater (Stirling et al., 2007; Weyer et al., 2008). In addition, low-temperature, redox-dependent U ores are generally heavier than high-temperature and non-redox dependent U ores (Bopp et al., 2009; Brennecka et al., 2010a). Similarly, U-contaminated groundwater becomes isotopically lighter during experimental stimulation of U bioreduction, suggesting the reduced U precipitate is isotopically heavy (Bopp et al., 2010). All these measurements generally agree with first-principle calculations that predict U(IV) in equilibrium with U(VI) should be isotopically heavy (Abe et al., 2008). Curiously however, two independent laboratory investigations of U reduction have failed to confirm to this effect. In abiotic experiments where U(VI) was reduced on the surface of zero-valent iron and zinc powder, no U isotopic fractionation was measured during reduction (Rademacher et al., 2006; Stirling et al., 2007). In microbial reduction experiments, a negative isotopic fractionation was observed, which is opposite the direction observed in natural environments (Rademacher et al., 2006).

These contradictory results motivated this study to confirm and better constrain the isotopic fractionation for U removal into reduced sediments by examining the isotopic composition of U in the water column of the Black Sea. The euxinic water column of the Black Sea provides an ideal laboratory for

studying isotope U fractionation during reductive removal from seawater. The Black Sea water column is stably stratified due to a large inflow of dense, salty Mediterranean water that results in slow overturn of the deep basin waters. Due to high-productivity and limited vertical mixing, the water column is anoxic and sulfidic below a depth of approximately 100 meters (Fig. 2.1a). Under these conditions, U concentrations decrease with depth through the anoxic water column (Fig. 2.1b). Deep Black Sea sediments are enriched in U and are known to be isotopically heavy relative to open ocean seawater (Weyer et al., 2008). If the removal of isotopically-heavy reduced U is indeed occurring in this modern marine setting, we hypothesized that the remaining U in the Black Sea water column should be isotopically light and the concentration and isotopic composition of U in the water column should be strongly correlated.

2.2. Samples and Methods

Black Sea water samples were collected during the 2001 R/V Knorr Black Sea cruise and stored under trace metal clean conditions in our laboratory. 2-4L samples were collected using a standard CTD-Rosette, sampled directly from the Niskin bottle into acid-washed contiainers using a triple bag methodology to prevent atmospheric contamination, and immediately acidified with 10 mL/L of trace metal grade concentrated HCl to pH < 1.

Sample aliqouts containing 250 ng U (75-200 mL) were spiked with a ^{233}U-^{236}U double spike, dried, and treated with concentrated nitric acid and 32% hydrogen peroxide to oxidize potential organic inferences. U was separated from

the sample matrix using Eichrom UTEVA resin, and analyzed via MC-ICP-MS utilizing established methodology (Weyer et al., 2008). U isotope data are reported in standard delta notation relative to the U standard SRM-950a:

$$\delta^{238/235}\mathrm{U} = 1000 \cdot \left(\frac{{}^{238}\mathrm{U}/{}^{235}\mathrm{U}_{\mathrm{sample}}}{{}^{238}\mathrm{U}/{}^{235}\mathrm{U}_{\mathrm{SRM\text{-}950a}}} - 1 \right) \qquad \text{Eq. 2.2}$$

With this method, it is possible to measure $\delta^{238/235}\mathrm{U}$ with a 2σ precision of ±0.07‰ on 100 ng U samples (Brennecka et al., 2010b).

U concentrations in the Black Sea water column (determined by isotope dilution) reflect mixing between seawater and riverine source waters, as well as U drawdown into sediments. In order to facilitate the deconvolution of these processes, we present salinity-normalized U concentrations to account for conservative mixing. Salinity-normalized U is calculated as the ratio of the observed U concentration divided by the conservative U concentration expected by the mixing between seawater and average riverine inputs to the Black Sea (Colodner et al., 1995):

$$\mathrm{U}_{\mathrm{normalized}} = \frac{\mathrm{U}_{\mathrm{observed}}}{\mathrm{U}_{\mathrm{river}} + \frac{\mathrm{S}_{\mathrm{observed}}}{\mathrm{S}_{\mathrm{seawater}}}\left(\mathrm{U}_{\mathrm{seawater}} - \mathrm{U}_{\mathrm{river}}\right)} \qquad \text{Eq. 2.3}$$

where open ocean seawater salinity and U are 36 psu and 14.1 nmol U kg^{-1} respectively, and the average U concentration of rivers flowing into the Black Sea is 4 nmol U kg^{-1} (Colodner et al., 1995; Nikolayev et al., 1977). Observed salinity data were recorded at the time of sample collection (Murray, 2006).

2.3. Results

U concentrations increased from 7.9 to 8.7 nM U between 0-100 meters depth before decreasing monotonically to 5.7 nM U at 2000 m (Fig. 2.1b), in agreement with previous results (Anderson et al., 1989a). These variations are driven by a combination of U removal from the sulfidic water column below 100 m, overlain on a mixing trend between inflowing saline, U-rich Mediterranean seawater and fresh, U-poor water from rivers and precipitation. Normalizing the U concentrations to salinity (Eq. 2.3) removes the mixing trend, and clearly demonstrates a monotonic pattern of increasing removal of U from the water column with depth (Fig. 2.1d). At 2000 m, the maximum U removal is approximately 44%.

Based on previous measurements of isotopically heavy U in deep Black Sea sediments, we expected the U remaining in the water column would be isotopically light. The first measured profile of $\delta^{238/235}U$ in the Black Sea confirms this hypothesis (Fig. 2.1c). Our results show that $\delta^{238/235}U$ decreases monotonically with depth. In the oxic upper 100 m of the water column, where drawdown of U is minimal, $\delta^{238/235}U$ values are similar to those in the open ocean. At 2000 m, where U concentrations are depleted by ~44% relative to conservative mixing, $\delta^{238/235}U$ is 0.28‰ lighter than open ocean seawater. As expected, $\delta^{238/235}U$ in the water column is always lighter than that of the deep Black Sea sediments.

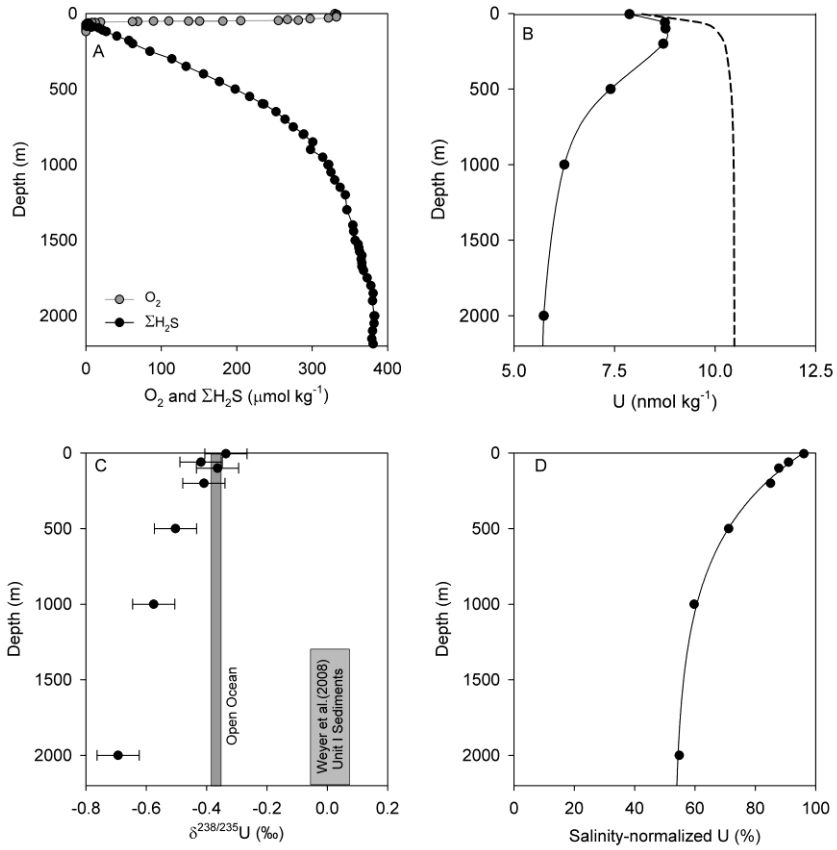

Figure 2.1. Black Sea water column geochemical profiles. (A) Distribution of dissolved O_2 (gray circles) and $\sum H_2S$ (black circles) emphasizing euxinia below ~100 m. (B) Total dissolved U concentration (black circles) compared with the concentration expected based mixing between Mediterranean sea water and average Black Sea river inputs (dashed line). (C) $\delta^{238/235}U$ isotope variation (black circles) compared with average open ocean seawater and surface sediments from the Black Sea abyssal plain (gray bars). (D) Salinity-normalized U concentration; on this scale, a value of 100% implies no U removal from solution.

2.4. Discussion

The strong correlation between $\delta^{238/235}U$ and salinity-normalized U (R^2 = 0.94, $p<0.0005$) clearly demonstrates that isotopically heavy U is being removed from the euxinic water column of the Black Sea, resulting in Rayleigh-type isotope fractionation (Fig. 2.2). Fitting the cross-plot of these variables with a Rayleigh model yields a best-fit apparent fractionation factor of $\alpha = 1.00061 \pm 0.00012$ ($\Delta^{238/235}U = +0.61 \pm 0.12‰$). This value falls within the range of previous published estimates ranging from +0.4 to ~+1‰ (Abe et al., 2008; Bopp et al., 2010; Brennecka et al., 2010a; Weyer et al., 2008).

Even though the data can be fit to a Rayleigh model, the isotopic composition of U in the Black Sea water column is the result of a complex mixing between different source waters and water masses. Such mixing violates the Rayleigh model assumption that fractionation occurs from a well-mixed reactant pool. To verify that the fractionation factor determined above is not biased by these effects, we implemented a simple model of U isotope fractionation in a 1-D reaction-transport model of Black Sea circulation previously calibrated with temperature, salinity, CFC-12, and ^{14}C (Romaniello and Derry, 2010). Briefly, the model assumes that U enters the Black Sea through two sources, the Bosphorus inflow and rivers. The Bosphorus Inflow is specified with [U] = 14.1 nmol kg^{-1}, $\delta^{238/235}U$ = -0.41‰ (Weyer et al., 2008). Rivers are specified with [U] = 4 nmol kg^{-1} and $\delta^{238/235}U$ = -0.18‰ (Nikolayev et al., 1977; Stirling et al., 2007). Further, the model assumes that below 100m, authigenic U accumulates in Black Sea sediments with $\delta^{238/235}U$ enriched by +0.61‰ from the overlying water column at

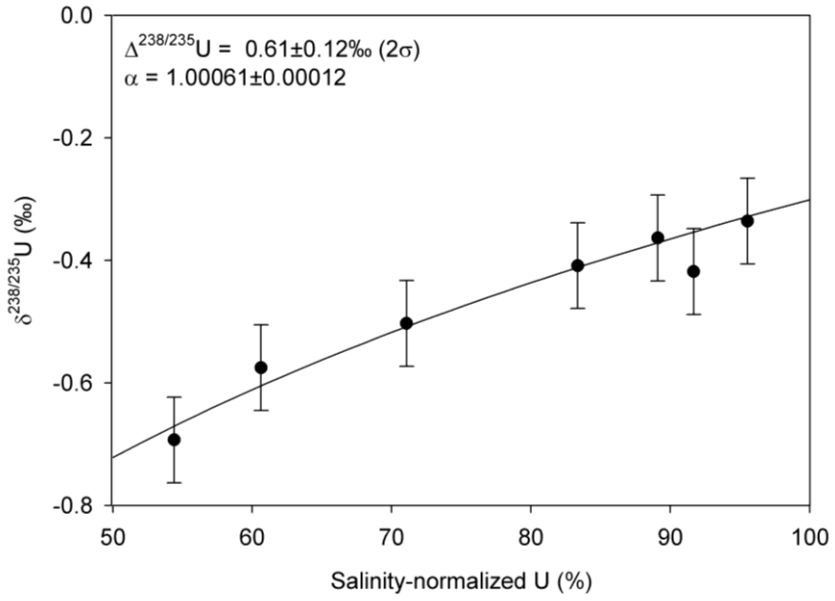

Figure 2.2. Rayleigh isotope fractionation model fit to the observed Black Sea U isotope and salinity-normalized U concentration data.

a rate of 0.42 mg U m^2 yr^{-1} (Barnes and Cochran, 1991; Colodner et al., 1995; Teodoru et al., 2007). The simulated U concentration and $\delta^{238/235}U$ show good agreement with the available data, providing independent confirmation that the fractionation factor determined above is accurate (Fig. 2.3). In the case of the Black Sea, the Rayleigh model probably agrees well with the reaction-transport model because most of the U entering the Black Sea comes from the Mediterranean inflow (i.e., mixing between Mediterranean and riverine U is unimportant) and because the surface outflow of Black Sea water to the Mediterranean has an isotopic composition close to that of open ocean seawater, so this sink does not affect the isotopic balance.

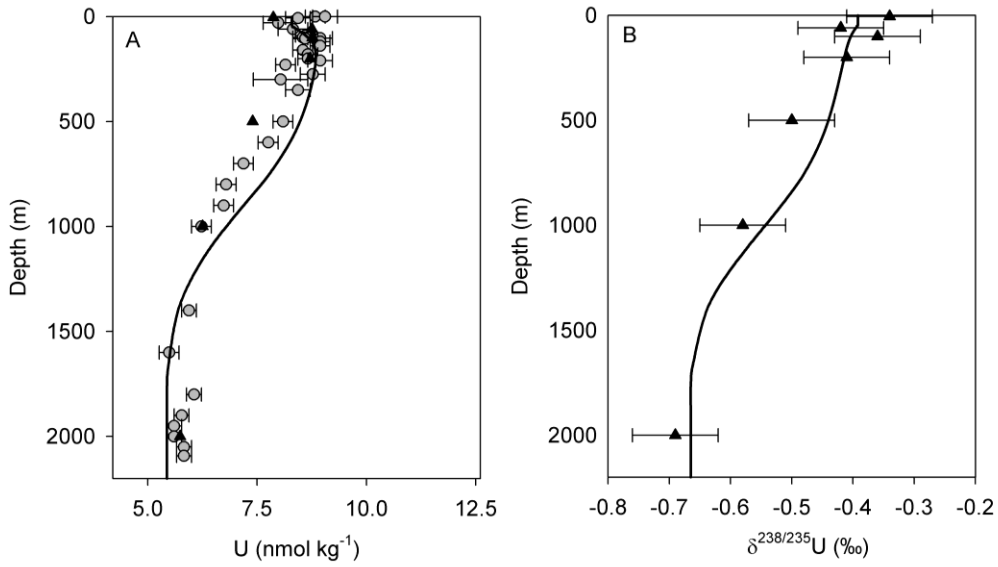

Figure 2.3. Comparison of the Black Sea U reaction-transport results with observations. (A) Simulated concentration profile (solid line) compared to measurements from this study (black diamonds) and from Anderson et al. (1989, gray circles). (B) Simulated water column U isotope profile (solid line) compared data from this study (black diamonds).

Weyer et al. (2008) previously determined a U isotopic fractionation factor of ~+0.4‰ for the Black Sea by comparing the $\delta^{238/235}U$ of modern deep Black Sea sediments with global average seawater. However, as pointed out by Montoya-Pino (2010) and demonstrated in this study, partial drawdown of U in restricted basins suppresses the apparent magnitude of isotopic fractionation between open ocean seawater and the restricted basin sediments.

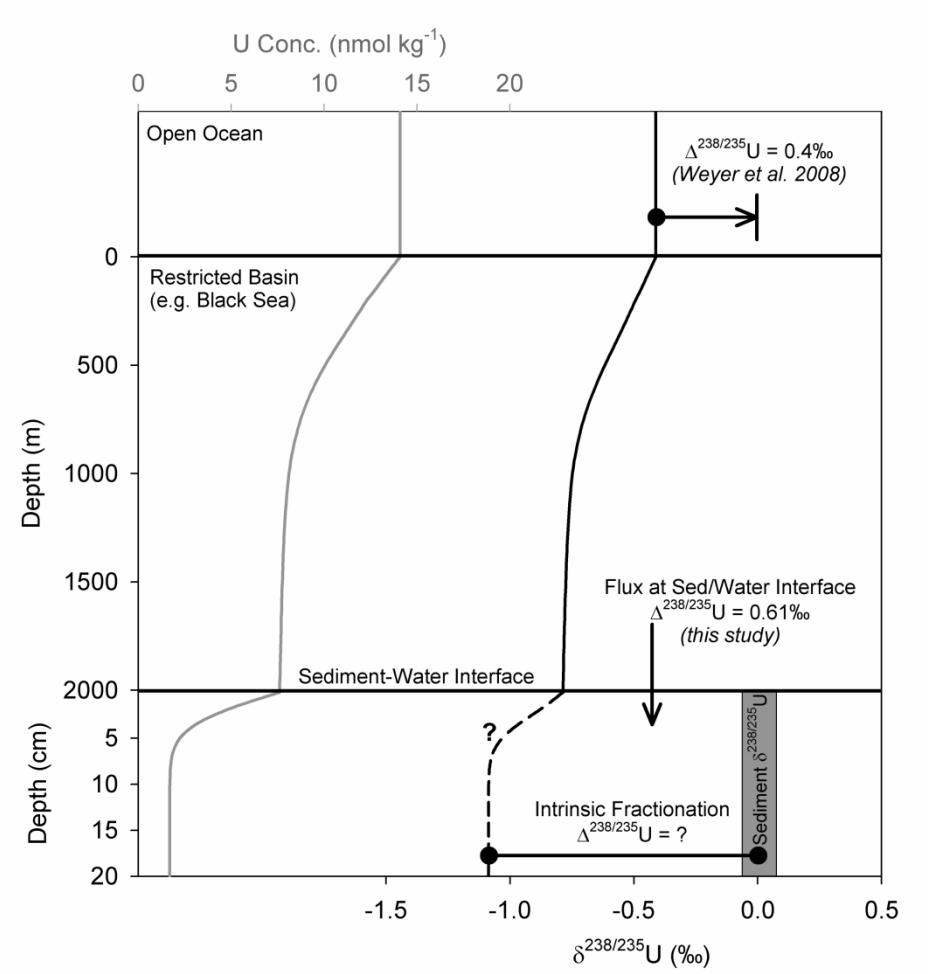

Figure 2.4. Relationship between the intrinsic and apparent isotopic fractionation factors during U deposition in a restricted marine basin, considering basin pore waters (lower panel), basin water column (middle panel) and global average seawater (upper panel). Partial restriction of both the sediment pore waters and basin water column suppress the apparent magnitude of the isotopic fractionation factor compared with intrinsic *in situ* fractionation factor.

This occurs because the preferential removal of ^{238}U into sediments leaves the restricted water column lighter than seawater, and subsequent authigenic U accumulating in sediments records this offset to light values (Fig. 2.4).

It is important to note the U isotopic fractionation factor determined in this study is also an apparent rather than intrinsic value. This is because the removal of U from the dissolved to solid phase in anoxic basins appears to occur only at or below the sediment water interface. Previous work has shown that U is not present as reduced U(IV) in either the Black Sea water column or sediment trap samples, despite the thermodynamic potential for the reduction of U(VI) to U(IV) in the Black Sea water column (Anderson et al., 1989a). The apparent absence of U(VI) reduction in the water column is consistent with laboratory studies that demonstrate that the reduction of U(VI) to U(IV) by sulfide is strongly inhibited by the formation of $UO_2(CO_3)_x$ species (Hua et al., 2006). Pore water profiles from the Black Sea indicate that U concentrations drop rapidly in the uppermost 1-5 cm of sediment, and this drop is accompanied by an accumulation of U in solid phase (Barnes and Cochran, 1991). Under these conditions, we expect that diffusion limitation will result in pore waters that are isotopically light compared to bottom water due to the removal of isotopically heavy U(IV) from the pore water – a situation analogous the discussion of the Black Sea water column above. Because of this, the apparent fractionation factor determined in this study is likely smaller than the intrinsic fractionation factor (Clark and Johnson, 2008).

Variations in the apparent magnitude of U isotope fractionation during U reduction have important implications for interpreting records of $\delta^{238/235}U$ as a

paleoredox proxy. Theoretical predictions of the isotopic fractionation of $\delta^{238/235}U$ during reduction of U(VI) to U(IV) are close to +1‰ (Abe et al., 2008). In the Black Sea, U drawdown in sediment pore water suppresses this intrinsic fractionation factor to an apparent fractionation factor of +0.62‰ across the sediment water interface. Furthermore, the removal of isotopically heavy U depletes the isotopic composition of dissolved U and results in a net difference of only +0.4‰ between modern Black Sea sediments and global average seawater. Variations in pore water U reduction rates and the degree of restriction of local ocean basins will be reflected in the apparent offset between global seawater and local sediments. Unless corrected for these effects, the $\delta^{238/235}U$ paleoredox proxy will tend to underestimate the importance of restricted basin and overestimate the extent of global anoxic events. For example, Montoya-Pino et al. (2010) estimate that 40±20% of the global U flux was removed to anoxic and euxinic sinks during OAE2 assuming a fractionation factor +0.5‰ derived in part from the difference between restricted Black Sea sediments and global average seawater. However, because anoxic conditions during OAE2 were not restricted, the value of 0.62‰ determined in this study should better represent deposition conditions during the anoxic event. In this case, only ~20% of the global U flux must be removed into anoxic sediments, toward the lower end of estimates made by Montoya-Pino et al. (2010).

2.5 Conclusions

Compared with the better established molybdenum (Mo) isotope paleoredox proxy, the U paleoredox proxy offers a number of advantages and disadvantages. One of the main disadvantages is that U is not quantitatively removed to sediments under reducing conditions. Whereas Mo concentrations are depleted to ~2% of seawater in the deep Black Sea, U concentrations are drawn down by only 44% relative to the concentration expected by conservative mixing. As a result, the Mo isotope composition of deep Black Sea sediments matches that global average seawater, whereas the U isotope composition of Black Sea sediments is significantly heavier than that of global average seawater. It seems unlikely that this offset is a simple constant factor as proposed by Weyer et al. (2008). Instead, as discussed by Montoya-Pino et al. (2010) and demonstrated in this study, the U isotopic offset between global average seawater and reduced sediments in restricted basins is likely to be a function of the degree of U drawdown from the water column.

Because of this effect, attempts to use $\delta^{238/235}U$ records from black shales deposited in restricted or partially restricted basins to infer global marine paleoredox conditions may be be hampered by the need to constrain the degree of local U drawdown from the water column. When the degree of U drawdown is slight, the offset between global seawater and the reduced sediments will be fully expressed (0.62‰). On the other hand, when the degree of U drawdown is significant, the fractionation will be suppressed (~0.4‰ in the modern Black Sea

for example). In the end-member case of nearly complete U drawdown, no fractionation will expressed similar to the situation for Mo isotopes.

Reconstructing marine paleoredox conditions from $\delta^{238/235}U$ recorded in black shales deposited in unrestricted marine basins should be free of these complications. In these settings, the fractionation factor determined in this study, 0.62‰, provides the best current estimate of the offset between seawater and co-deposited black shales. Further development in this area would benefit from studies that address the intrinsic magnitude and mechanism of U isotope fractionation in marine pore waters under anoxic and euxinic conditions, as well as the controls on the extent of apparent fractionation at the sediment-water interface.

Chapter 3

FRACTIONATION OF $^{238}U/^{235}U$ IN MODERN PRIMARY CARBONATES AND SHALLOW SEDIMENTS FROM THE EXUMA ISLANDS, BAHAMAS

3.1 Introduction

Recent analytical advances have made it possible to resolve small variations in the $^{238}U/^{235}U$ isotopic ratio of uranium (U), spanning a range of ~1.3‰ ($\delta^{238/235}U$, defined below) for a variety of crustal and marine samples (Stirling et al., 2007; Weyer et al., 2008). While non-redox processes such as U(VI) absorption to birnessite have been shown to cause U isotope fractionation (Brennecka et al., 2011b), the largest observed natural $^{238}U/^{235}U$ fractionation occurs during the reduction of U(VI) to U(IV) (Bopp et al., 2009; Bopp et al., 2010; Brennecka et al., 2010a; Stirling et al., 2007; Weyer et al., 2008). Because the marine geochemistry of U is highly redox sensitive and because these redox variations produce relatively large isotopic shifts, a number of recent authors have suggested that $\delta^{238/235}U$ variations in ancient marine sediments could record temporal variations in ocean redox conditions (Brennecka et al., 2011a; Montoya-Pino et al., 2010; Weyer et al., 2008).

In theory, a U isotope paleoredox proxy should have a number of advantages over better established complementary techniques, such as molybdenum (Mo) isotope variations and iron (Fe) speciation (Anbar, 2004; Poulton et al., 2004; Raiswell and Canfield, 1998). Like Mo, U has a long marine residence time (~350ka, Dunk et al., 2002). Because of this, the U isotope composition of open ocean seawater should be uniform and provide a globally

integrated record of paleoredox conditions. In sediments, U reduction occurs under anoxic, Fe-reducing conditions (Barnes and Cochran, 1990; Klinkhammer and Palmer, 1991; Morford et al., 2009), and thus should be a more sensitive proxy for mildly-reducing anoxic conditions than Mo, which is widely regarded to require sulfidic conditions for removal from marine waters (Arnold et al., 2004; Erickson and Helz, 2000; Neubert et al., 2008). Most importantly, while Mo and Fe paleoredox proxies have been developed primarily for use in black shales, U is also incorporated into marine carbonate minerals and carbonate sediments. Although black shales offer low permeability and excellent preservation potential for geochemical records, they occur only sporadically in the geological record and often form in partially restricted marine basins, which may introduce a bias into the paleoredox record. The development of a paleoredox proxy for use in carbonates would not only provide independent confirmation of shale-based proxies, but also allow more complete coverage of the geological record, since carbonate sediments are common on ocean-facing marine margins. Better still, initial measurements of $\delta^{238/235}U$ in modern and fossil corals suggested that carbonate minerals might directly record the isotopic composition of seawater (Stirling et al., 2007; Weyer et al., 2008). This idea was invoked by Brennecka et al. (2011a), who measured $\delta^{238/235}U$ variations in a carbonate section spanning the end-Permian mass extinction, and interpreted the resulting variations as directly reflecting seawater variations.

Carbonate-hosted proxy records also face a number of well-known potential problems. While it is sometimes assumed that elemental and isotopic

profiles in carbonate sediments reflect the direct coprecipitation of elements along with the primary carbonate precipitate, this assumption is often unjustified (Derry, 2010; Knauth and Kennedy, 2009). For example, oceanographers have long known that diagenetic alteration is a major concern even for relatively young and extremely well-preserved foraminifera, even when hand-picked from sediments, meticulously cleaned, and individually screened for alteration (e.g., Henderson and Onions, 1995; Kontakiotis et al., 2011; Regenberg et al., 2007; Sexton and Wilson, 2009). Moreover, because precise measurement of $\delta^{238/235}U$ requires ~75 ng U using the current technology, performing large numbers of measurements on hand-picked separates would be very labor intensive, and it is essentially impossible in lithified sediments. As a result, bulk carbonate sediments, which may have experienced significant diagenetic alternation during sedimentation and subsequent lithification, will likely be used for U isotope-based paleoredox studies in the near future. During burial, these bulk sediments integrate the composition of the primary precipitate and any included organic or siliciclastic detritus, as well as geochemical alternation during shallow burial including the influence of local pore water chemistry and the precipitation of secondary mineral phases. Because carbonates can be highly porous and permeable, further alteration during longer term burial is also common, particularly when fluids migrate through carbonate rocks at elevated water/rock ratios (Banner and Hanson, 1990; Derry, 2010; Jacobsen and Kaufman, 1999). Nevertheless, by carefully studying the processes by which elements become incorporated into carbonate sediments and understanding the diagenetic processes

by which their distributions are altered, it has been possible to carefully select well-preserved samples and develop reliable long term isotopic records from marine carbonates in some cases.

The goals of this study were to determine (1) whether or not all primary carbonate precipitates directly record the $\delta^{238/235}U$ isotopic composition of seawater, regardless of initial mineralogy or biotic/abiotic origin, and (2) whether or not the isotopic composition of shallow bulk carbonate sediments directly reflects the isotopic composition of local primary precipitates. A more complete understanding of uranium isotope fractionation during incorporation into bulk carbonate sediments will improve estimates of seawater $\delta^{238/235}U$ values reconstructed from $\delta^{238/235}U$ measurements of marine carbonate rocks.

3.2 Materials and Methods

3.2.1 Sampling Sites

The study region consisted of a 2 km × 12 km area in the southern Exuma Islands, Bahamas, extending northwest from Lee Stocking Island to Little Darby Island (Fig. 3.1, Table 3.1). As one of the largest and best studied Holocene carbonate platforms, the Bahamas are an outstanding region for the study of carbonate sediment deposition and diagenesis. Their location far from continental land masses produces sediments that contain very little siliciclastic detritus, and thus simplifies the process of separating primary and authigenic inputs from detrital siliciclastic inputs. Samples were collected during January and July of 2011. Collection of primary carbonate precipitates was conducted throughout our

study region, but focused most heavily in the north end of the channel between Darby and Little Darby Islands. Cores 1 and 2 were collected in this same area, with two additional cores collected west of Lee Stocking Island and in Norman's Pond (Fig. 3.1). Core 1 was collected in a small lagoon open to the ocean, that was dominated by dense turtle grass (*Thalassia testudium*) and green calcareous algae (*Halimeda incrassata*). The sediment was stabilized by *Thalassia* rhizomes and consisted of abundant *Halimeda* fragments and fine-grained carbonate sand. Large (30 cm) mounds and burrows produced by shimp (*Callianassa sp.*) were abundant at this site, but the location of the core was chosen to avoid these mounds. Core 2 was collected approximately 100 m southeast of Core 1 on a shallow tidal flat just below the low tide line. The surface at the Core 2 was unvegetated, and the sediment was composed of fine carbonate sand containing a mixture of pellets, ooids, and small fragments of coarser materials that appeared homogenous in composition throughout the core. Core 3 was collected west of Lee Stocking Island in a large, dense *T. testudium* flat approximately 4 m deep. The sediments were similar to those in Core 1, but they were finer and lacked abundant *Halimeda* fragments. Core 4 was collected in a large tidal pond on Norman's Pond Cay. The ~80 acre pond was used as a salt production facility

Table 3.1. Coordinates of coring locations.

Core	Latitude (°N)	Longitude (°W)	Water Depth (m)	Site Description
Core 1	23.85812	76.22627	1.5	*T. testudium* flat
Core 2	23.85713	76.22552	0.5	tidal flat
Core 3	23.76851	76.11293	4	*T. testudium* flat
Core 4	23.76898	76.12950	0.5	tidal pond

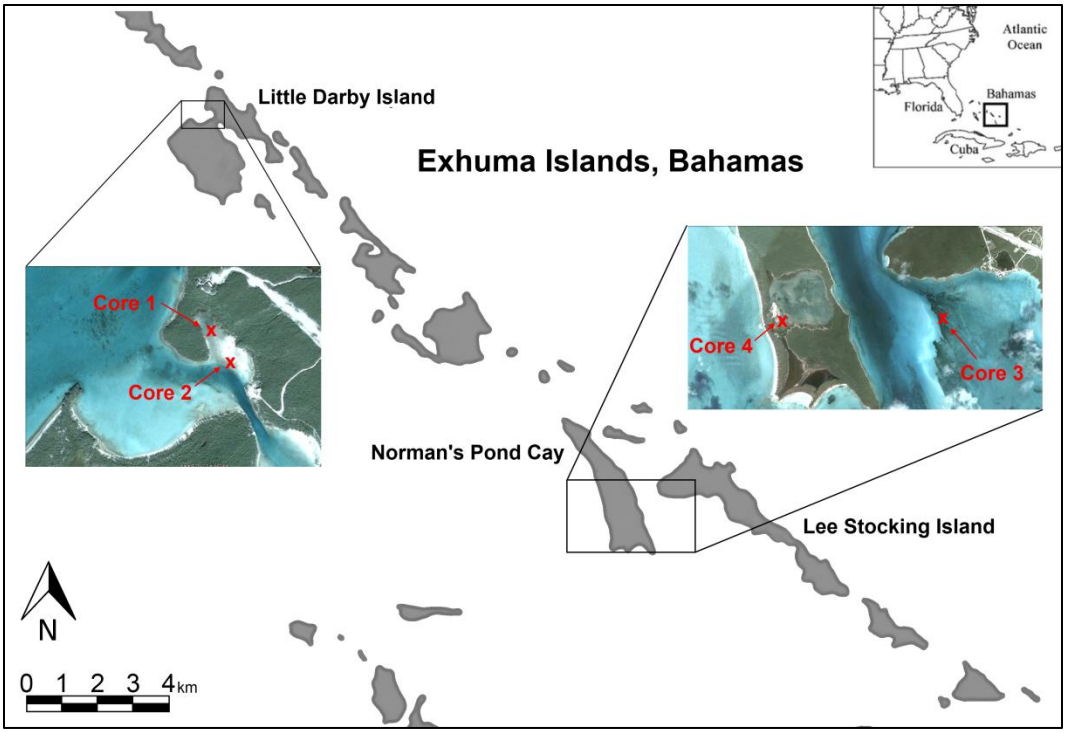

Figure 3.1. Map of the study region, located in the southern Exuma Islands, Bahamas. Insets show a broader regional map and aerial photographs marked with the location of each core.

from the 17th to 19th centuries (Feldmann and McKenzie, 1998; Hein and Winsborough, 2001). A manmade channel connects the pond to the ocean, but a partial dike maintains the pond level 60 cm above low tide, while allowing seawater to enter the pond at high tide (Wicklund et al., 1991). The pond sediment is a dark black, carbonate mud that contains intervals rich in marine gastropod shells and buried layers of laminated microbial mats.

3.2.2 Samples

In order to determine whether or not primary carbonate precipitates directly record the $\delta^{238/235}U$ of seawater, a wide variety of common biological and abiological precipitates, representing aragonitic and high-magnesium calcite mineralogies were collected and analyzed. Samples included corals, calcifying green and red algae, mollusks, and ooids. Primary carbonate precipitates were collected in the field and air-dried prior to transport to the laboratory. Push cores were collected by manually inserting 7.5 cm diameter core liners into the sediment. During extraction from the sediment and transport back to the field laboratory (< 1 hr), the cores were sealed and kept vertical. This method resulted in minimal core compression (<2 cm) with clear overlying waters and a well-defined sediment interface. When sampling laminated salt pond sediments, little or no disturbance of the laminations was observed near the core walls, suggesting vertical smearing of the solid sediment was negligible. An additional core was taken at each site for porosity measurements. Pore water samples were collected using acid-washed, trace-metal-clean Rhizon pore water samplers (Rhizosphere Research Products P/N 19.21.22F) connected to acid-washed 10 mL polypropylene syringes via a 3-way polycarbonate stopcock. The syringes were held in custom-made polycarbonate frames that allowed the syringe plungers to be gently drawn back using a rubber band during sampling. Once flow was established, any headspace bubbles were ejected via the 3-way stopcock, and sampling was continued for ~20 minutes using the rubber band to extract 6-10 mL of pore water. *In situ* pore water samples were collected by inserting the Rhizon

pore water samplers directly into the sediment a known depth normal to the sediment surface. *Ex situ* pore water samples were collected from cores immediately upon return to the field laboratory by drilling small holes in the core liner and inserting the Rhizon pore water samplers parallel to the sediment surface. Following pore water sampling, cores were drained and either extruded and sectioned in the field or packed whole for shipment back to W. M. Keck Foundation Stable Isotope Laboratory for Environmental Biogeochemistry ("Keck Lab") at Arizona State University. Wet, intact porosity cores were extruded into pre-weighed plastic bags at the field laboratory, sealed, and shipped back to the laboratory for wet/dry weight determination.

3.2.3 Analytical Methods

Following sampling, pore water samples were sealed without a headspace inside 10 mL syringes using a 3-way stockcock until all pore water samples could be processed (<4 hours). All samples were processed with identical controls containing DI water and IAPSO standard seawater. Dissolved oxygen and suflide measurements were initiated immediately following collection. Sulfide was determined using the traditional Cline assay measuring the absorption in a 1 cm cell at 670 nm (Cline, 1969). Sulfide samples were diluted 1:50 using deionized water immediately prior to measurement. Dissolved oxygen was determined by placing 0.5 mL of pore water onto the sensor of an inverted galvanic oxygen electrode (IQ Scientific), calibrated using fully-oxygenated IAPSO seawater and Oakton Zero-Oxygen calibration solution (P/N 00653-00), which contains sodium

sulfite to scavenge O_2 from the test solution. Laboratory tests using He-degassed water demonstated that even freshly prepared O_2-free solutions read artificially high when calibrated when the sensor was calibrated using the Zero-Oxygen solution. In order to correct for this effect, a manual calibration curve was used to correct measured % O_2 saturation values to actual values (Fig. 3.2).

Sample pH and total alkalinity (ALK_{tot}) measurements were completed within 3 hours of sample collection using micro-titration of precisely-weighed 1 mL aliquots of pore water. Initial sample pH was measured using an ISFET pH electrode (IQ Scientific), calibrated using NBS buffers. The samples were titrated with 0.0100 N HCl (Ricca P/N 3590) dispensed from a ditigal tritator (Hach P/N 1690001). Total alkalinity was determined using the fast titration method (Almgren et al., 1983):

$$\mathrm{ALK_{tot}\,(mol/L)} = \left[10^{-\mathrm{pH_{initial}}}\,\mathrm{v_0}\,f_{H^+}^{-1} + \mathrm{v_{HCl}c_{HCl}} - 10^{-\mathrm{pH_{final}}}\left(\mathrm{v_0} + \mathrm{v_{HCl}}\right)f_{H^+}^{-1}\right] \Big/ \mathrm{v_0} \qquad \text{Eq. 3.1}$$

Total alkalinity was calculated as the average of 3 serial titrations to pH end points of ~3.5, 3.4, and 3.3, assuming a H^+ activity of f_{H^+} = 0.729 (Perez and Fraga, 1987). Measurement precision using this method averaged 5.5% for repeat analysis of IAPSO seawater.

Dissolved inorganic carbon (DIC) samples (~1 mL) were stored in preweighed, evacuated, 13 mL screw top exetainers that were pre-loaded with 0.1 mg of $HgCl_2$ to inhibit microbial activity. Samples were analyzed using a Thermo Scientific GasBench II connected to a Finnigan MAT 253 mass spectrometer following standard methods. DIC measurements were corrected for the presence of a field blank amounting to 9.3 ± 0.7% of the IAPSO standard based on the

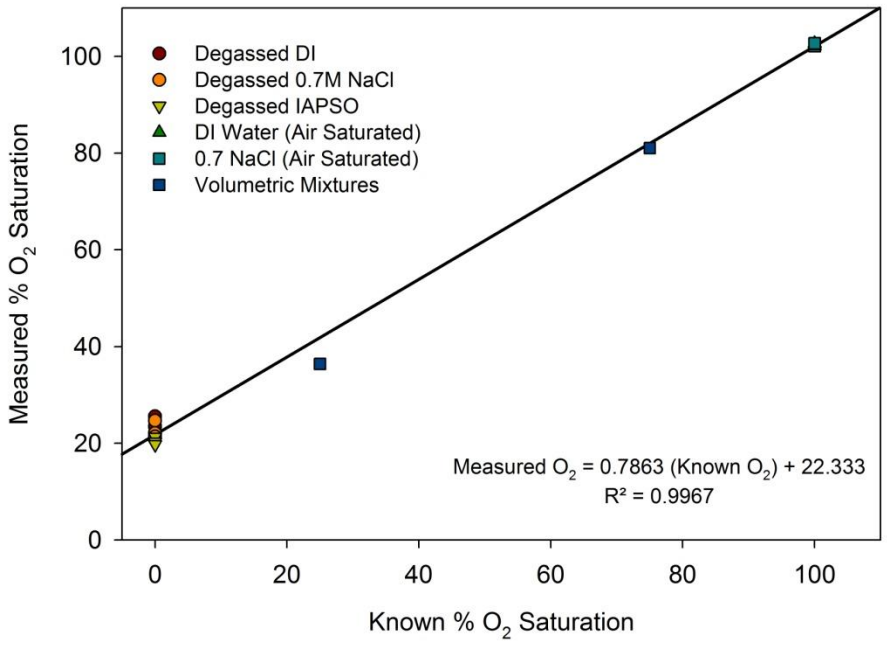

Figure 3.2. Calibration curve used to correct measured pore water O_2 to actual concentrations. The galvanic sensor was initially calibrated using air-saturated DI water and an Oakton Zero-Oxygen solution to create a two-point calibration. However, thoroughly degassed water standard cluster around 20-25% saturation with this method, necessitating a secondary correction.

analysis of replicate field blanks from multiple days. The overall precision of DIC concentrations obtained using this method was estimated at 2.5% based on replicate analysis of IAPSO seawater treated identically to samples.

Carbonate equilibrium calculations were performed using measured DIC and ALK_{tot} data and the CO2SYS program available from the Carbon Dioxide Information Analysis Center at Oak Ridge National Laboratory (van Heuven et al., 2011). Prior to entering data into the software, the contribution of HS^- was

subtracted from total alkalinity following Millero (1995). Measured salinity values were used for each sample (obtained using a salinity refractometer), while average July water and laboratory temperatures were estimated at 30°C. Calculated sample pH generally agreed with measured values to within 0.5 pH units. Calculated carbonate ion concentrations were used along with measurements of Ca concentrations (discussed below) to calculate the calcite and aragonite saturation factors in pore waters following Millero (1995).

Pore water trace metal samples (~1 mL) were acidfied with 65 μL of 5 M trace metal grade nitric acid and stored in acid-washed 4 mL HDPE bottles. Major and trace elements were analyzed in triplicate at a 1:3 dilution using a Thermo Scientific X-series 2 quadrapole ICP-MS located in the Keck Lab. NASS-5 was spiked with an additional multielement mixture to form a concentration calibration series. CASS-5 was used to verify measurement accuracy. The precision of replicate measurements varied from 2%-20% depending on the concentration, isotopic abundance, sensitivity and interference spectra for each element.

Solid phase major and trace element concentrations and U isotopes were also determined in the Keck Lab. Primary precipitate samples were cleaned with DI water and dried for >24 hours in a 105°C oven. Larger samples were crushed using a trace-metal-clean silicon carbide mortar and a ceramic pestle. Core samples were dried for >24 hours and powdered in a ball mill equipped with trace-metal-clean silicon carbide mortars (SPEX). Aliquots of primary precipitate and powder sediment samples containing approximately 250-1000 ng U (0.5-10 g

of sample) were weighed into acid-washed ceramic crucibles, covered, and ashed for 24 hours at 750°C. This temperature is sufficient to calcinate the calcium carbonate matrix, allowing complete oxidation of organic matter intimately associated with the carbonate matrix and eliminating the tendency for violent CO_2 release during sample dissolution. After cooling, samples were quantitatively transferred to 50 mL centrifuge tubes and dissolved overnight in 10-50 mL of 3 M nitric acid, leaving little or no visible residue. Following dissolution, major and trace element concentrations were determined on sample aliquots at 1:2000 dilution using a Thermo X-series 2 quadrapole ICP-MS.

Preliminary U concentrations were used to prepare a portion of the sample containing 250-1000 ng U spiked with ^{233}U-^{236}U doublespike (IRMM3636, Verbruggen et al., 2008) at a 0.0363 spike:sample molar ratio. Spiked samples were purified and preconcentrated using the UTEVA resin protocol described by Weyer et al. (2008). Following column chemistry, samples were evaporated in a mixture of concentrated nitric acid and 32% hydrogen peroxide repeatedly (3X) to oxidize any organic materials leached from the UTEVA resin. U isotopes ($^{238}U/^{235}U$ and $^{234}U/^{238}U$) and final U concentrations (via isotope dilution) were determined on a Thermo Neptune MC-ICP-MS equipped with an ESI Apex desolvating nebulizer. The analytical and double spike method of Weyer et al. (2008) was modified to measure ^{234}U on the axial secondary electron multiplier. This allows precise $^{234}U/^{238}U$ ratios to be collected simultaneously with $^{238}U/^{235}U$ ratios. The accuracy of the resulting ^{234}U data depend critically on the correction for the residual ^{234}U in the IRMM3636 spike and peak tailing effects from ^{233}U

and ^{235}U on ^{234}U. These corrections were made using the certified isotopic composition of the IRMM3636 spike (Verbruggen et al., 2008) and by estimating the peak tailing effects from a series of standard analyses spiked at different spike-sample ratios. Isotope data are reported as:

$$\delta^{238/235}U\ (‰) = 1000 \times [(^{238}U/^{235}U_{sample}) / (^{238}U/^{235}U_{standard}) - 1] \quad \text{Eq. 3.2}$$

and

$$\delta^{234/238}U\ (‰) = 1000 \times [(^{234}U/^{238}U_{sample}) / (^{234}U/^{238}U_{standard}) - 1]. \quad \text{Eq. 3.3}$$

Although Weyer et al. (2008) reported their $\delta^{238/235}U$ results against the SRM950a standard, this standard is no longer available. Instead, CRM145 was used as the isotopic standard. Intercalibration of SRM950a and CRM145 has shown no $\delta^{238/235}U$ offset between these reference materials (Condon et al., 2010). In addition, the $\delta^{234/238}U$ of CRM145 has been measured by a large number of groups and found to be depleted by -36 to -37‰ relative to secular equilibrium (summarized in Andersen et al., 2004). To correct for small amounts of instrument drift, every two samples in a measurement session were bracketed by an identically double-spiked aliquot of CRM145 and the samples were reported relative to the average of the bracketing CRM145 standards assuming $\delta^{238/235}U$ and $\delta^{234/238}U$ of the standard to be 0.00‰ and -36.7‰, respectively. All samples were analyzed at least three times and the precision reported as two standard deviations. Average measurement precision was 0.12‰ for $\delta^{238/235}U$ and 1.1‰ for $\delta^{234/238}U$.

3.3 Results

3.3.1 Primary Precipitates

Uranium concentrations in these samples ranged from 0.017 to 3.47 ppm, reflecting a variation in mineralogy and the mechanisms of carbonate precipitation (Fig. 3.3, Table 3.2). The $\delta^{238/235}U$ results demonstrate that regardless of primary mineralogy or biologic origin, the $\delta^{238/235}U$ of primary carbonate minerals in the Bahamas are indistinguishable from that of seawater U, which has a $\delta^{238/235}U$ of -0.41‰ (Weyer et al., 2008). As expected, the $\delta^{234/238}U$ data demonstrate that that these primary precipitates are also very close to the established $\delta^{234/238}U$ composition of seawater (146.8 ± 0.1‰, Andersen et al., 2010). The one exception to this is the much lighter $\delta^{234/238}U$ for sample 6, a tiger lucine shell (*Codakia orbicularis*), collected from the Norman's Pond outflow channel.

3.3.2 Sediment Cores

Shallow sediment cores were collected from 4 locations in the study region to determine whether or not the $\delta^{238/235}U$ of sediments was similar to that observed in primary precipitates. Analysis of the solid bulk carbonate sediment revealed that U concentrations increased downcore. This increase was most prominent in Cores 1 and 4, while Cores 2 and 3 displayed a smaller degree of enrichment. The highest U concentrations observed for primary precipitates were 2.7-3.0 ppm for corals and 3.5 ppm for ooids. In contrast, core samples averaged

Table 3.2. Summary of U isotope data from primary precipitates.

Sample #	Sample Description	Primary Mineral	Mg/Ca (mol:mol)	U Conc. (ppm)	$\delta^{238/235}$ U (‰)	2σ err	$\delta^{234/238}$U (‰)	2σ err
Corals								
1	*Diploria strigosa*	Arag.	0.005	2.74	-0.34	0.08	150.1	3.5
2	*Siderastrea radians*	Arag.	0.007	2.79	-0.33	0.12	145.4	2.3
3	*Porites divaricata*	Arag.	0.006	2.55	-0.32	0.09	148.2	2.2
4	*Porites asteroids*	Arag.	0.006	2.97	-0.35	0.18	148.5	3.8
Mollusks								
5	*Tellina listeri*	Arag.	0.002	0.031	-0.4	0.19	144.0	3.6
6	*Codakia orbicularis*	Arag.	0.001	0.014	-0.36	0.05	129.7	3.5
7	*Cittarium pica*	Arag.	0.001	0.059	-0.46	0.03	148.2	2.9
Green Algae								
8	*Acetabularia crenulata* (whole)	Arag.	0.035	0.84	-0.35	0.07	147.0	3.5
9	*Acetabularia crenulata* (stalk)	Arag.	0.022	1.26	-0.33	0.21	147.6	2.9
10	*Acetabularia sp.* (head)	Arag.	0.046	0.581	-0.35	0.13	146.4	3
12	*Rhipocephalus phoenix* (stalk)	Arag.	0.027	1.61	-0.44	0.23	147.8	1.5
13	*Rhipocephalus phoenix* (leaves)	Arag.	0.024	2.40	-0.4	0.05	147.9	3.4
15	*Penicillus capitatus* (stalk, collected dead)	Arag.	0.039	1.87	-0.47	0.19	147.7	2.8
17	*Penicillus capitatus* (stalk, collected live)	Arag.	0.030	1.94	-0.29	0.09	147.2	1.6
18	*Penicillus capitatus* (head, collected live)	Arag.	0.024	2.01	-0.45	0.10	146.4	2.4
Red Algae								
19	*Neogoniolithon strictum* (Collected Dead)	HMC	0.240	0.535	-0.39	0.37	144.5	1.3
20	*Neogoniolithon strictum* (Collected Live)	HMC	0.371	0.246	-0.48	0.09	148.5	2.6
Ooids								
11	Ooids (Lee Stocking Island)	Arag.	0.005	3.47	-0.28	0.12	143.4	2.3
	Average				**-0.38**	**0.13**	**146.0**	**8.9**

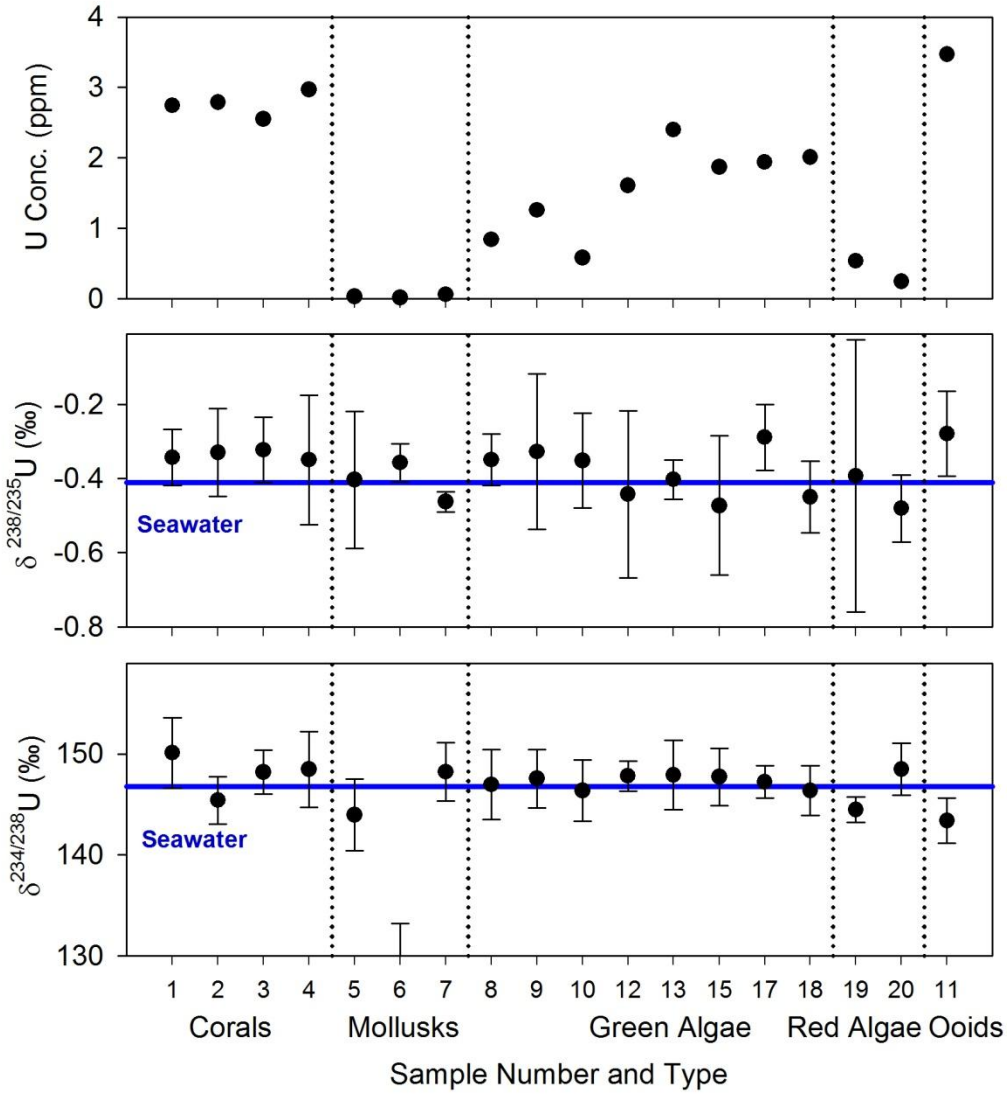

Figure 3.3. U concentrations, $\delta^{238/235}U$, and $\delta^{234/238}U$ variations in primary carbonate precipitates. Error bars represent the 2σ precision of replicate analyses of the same solutions. Estimated U concencentration errors are smaller than the symbol size. Horizontal solid lines indicate the composition of average seawater. Vertical dotted lines separate different sample types.

4.2, 3.9, 3.5, and 4.7 ppm U for Cores 1-4 respectively; concentrations equal to, or exceeding, the highest concentrations observed in primary precipitates.

Isotopic analysis of $\delta^{238/235}U$ in bulk core sediments further reveals a significant isotopic shift from values observed in primary precipitates. While primary precipitates shared a similar $\delta^{238/235}U$ with average seawater (-0.41‰), core samples were generally heavier, averaging -0.06, -0.16, -0.20, and -0.30‰ for Cores 1-4 respectively. For Cores 1 and 4, $\delta^{238/235}U$ values also generally correlated with downcore variations in U concentrations, becoming isotopically heavier as U concentrations increased. Even Cores 2 and 3, which have the lowest levels of U enrichment and no significant downcore trends in U concentrations, demonstrate significantly heavier $\delta^{238/235}U$ values beginning within 3-4 cm of the core top (the shallowest resolution afforded by our sampling).

In contrast to $\delta^{238/235}U$, $\delta^{234/238}U$ in Cores 1-3 generally shows good agreement with primary precipitates. For these cores (which are all below the low tide line), $\delta^{234/238}U$ is indistinguishable from that of the primary precipitates at the level of the measurement precision ($2\sigma = \sim 1‰$).

Compared to Core 1-3, Core 4, which was collected in a tidal pond, is exceptional in two ways. First, the $\delta^{234/238}U$ values are persistently light. Even at the top of the core, $\delta^{234/238}U$ values are 10‰ lighter than those of seawater U. Second, both $\delta^{234/238}U$ and $\delta^{238/235}U$ display a pronounced shift toward lower values in the lower portion of this core that is strongly correlated with a shift toward elevated Mg/Ca values.The significance of this observation is discussed further in Section 3.3.4.

Table 3.3. Summary of U isotope data from shallow sediment cores.

	Depth (cm)	Mg/Ca (mol:mol)	U Conc. (ppm)	$\delta^{238/235}$U (‰)	2σ err	$\delta^{234/238}$U (‰)	2σ err
Core 1							
	0-3	0.041	2.99	-0.19	0.14	149.8	2.2
	4-6	0.043	3.35	-0.12	0.29	149.2	1.6
	8-11	0.043	3.61	-0.15	0.09	148.8	1.5
	12-14	0.042	4.15	-0.13	0.04	148.5	0.9
	16-18	0.041	4.69	-0.16	0.05	148.5	1.5
	24-26	0.038	5.01	0.03	0.17	149.0	1.5
	32-34	0.041	4.73	0.07	0.19	150.8	1.8
	40-42	0.043	5.44	0.14	0.25	148.7	0.2
Core 2							
	0-3	0.018	3.78	-0.16	0.04	147.7	1.3
	6-9	0.018	3.91	-0.13	0.03	148.1	1.0
	12-15	0.020	3.98	-0.21	0.11	147.5	0.5
	18-21	0.020	3.97	-0.19	0.05	148.4	1.0
	21-24	0.020	3.96	-0.12	0.16	147.3	0.6
Core 3							
	1-4	0.057	3.13	-0.23	0.15	148.7	0.3
	6-9	0.052	3.44	-0.24	0.14	148.2	1.5
	10-14	0.055	3.43	-0.16	0.17	148.6	1.4
	17-21	0.056	3.52	-0.18	0.09	147.8	1.4
	19-22	0.053	3.92	-0.18	0.15	148.3	1.4
Core 4							
	0-4	0.132	3.93	-0.22	0.10	136.9	0.6
	4-8	0.141	4.42	-0.17	0.04	137.0	0.9
	8-12	0.105	5.29	-0.03	0.13	141.4	1.1
	12-16	0.138	5.42	-0.06	0.11	139.0	0.8
	16-20	0.199	5.44	-0.27	0.08	133.8	0.4
	24-28	0.459	3.86	-0.71	0.18	102.5	1.0
	28-30	0.452	4.53	-0.65	0.18	112.1	1.6

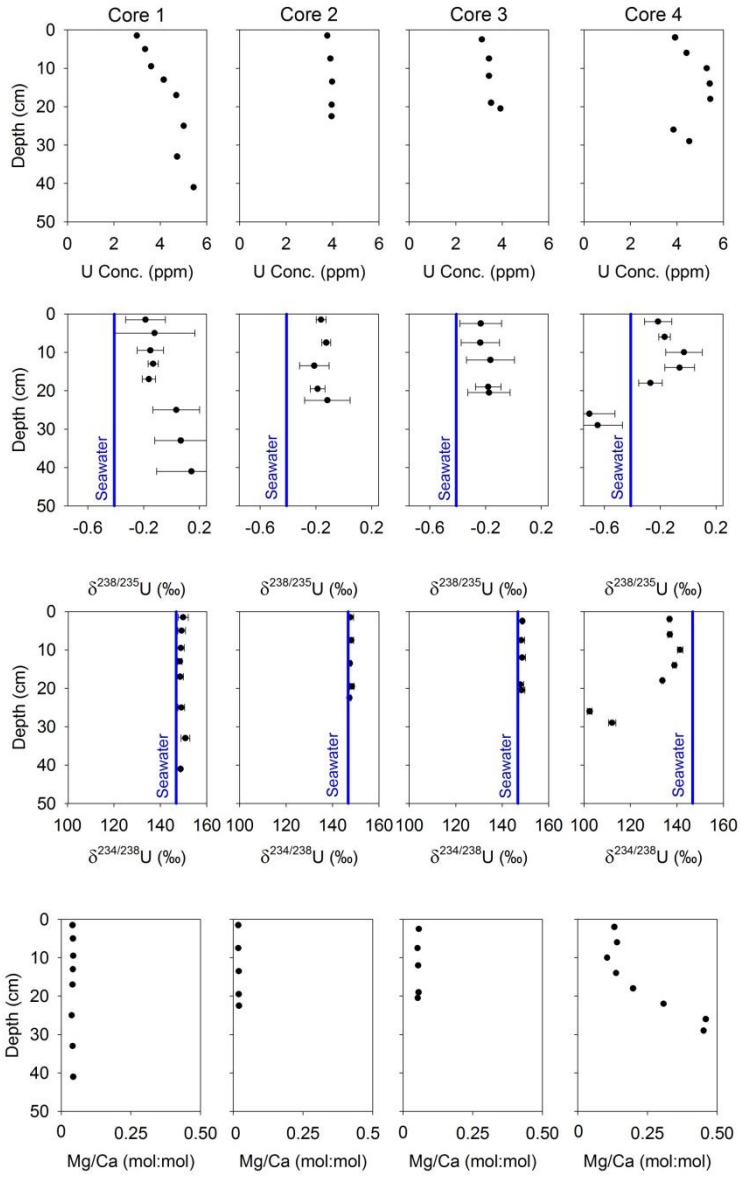

Figure 3.4. Solid-phase U concentrations, $\delta^{238/235}U$, $\delta^{234/238}U$, and Mg/Ca variations in shallow sediment cores. Error bars represent 2σ errors. Uncertainity in the U concentrations and Mg:Ca ratios are smaller than the symbol size. Vertical lines represent the average U isotope composition of open ocean seawater.

3.3.3 Pore waters

The shallow sediments sampled in Cores 1-4 consist primarily of highly permeable 0.5-1 mm carbonate sand. The high permeability of these sediments makes precise pore water sampling extremely difficult. *In situ* sampling has been preferred by recent authors in order to limit disturbance of the pore water profile (Burdige et al., 2010; Burdige and Zimmerman, 2002; Burdige et al., 2008). However, we found that this method of sampling can sometimes result bottom water intrusion along the axis of the sampling probe. On the other hand, the alternative of *ex situ* sampling via small holes drilled perperdicularly through liner of an extracted core is also problematic because bottom water trapped at either end of the core can easily flow through the core and atmospheric O_2 is easily entrained at the sampling site (an anaerobic sampling chamber was unavailable at the time of sampling). For comparison, we present data collected using both sampling techniques.

Figure 3.5 and Table 3.4 present porewate O_2, H_2S, and U concentrations for each core. Elevated downcore O_2 concentrations are most likely due to contamination during sampling. Given the high concentrations of H_2S in these cores and the short half life of H_2S in the presence of O_2, oxygen would not be expected to persist past the first 1-2 cm of depth, except where burrows or seagrass rhizomes provide a local oxygen source. Because of this, the O_2 in the deeper portion of each core should be mainly regarded as in indication of bottom water or atmospheric contamination, and the measured H_2S profiles as minimum estimates due to the potential for partial oxidation of sulfide. Despite the potential

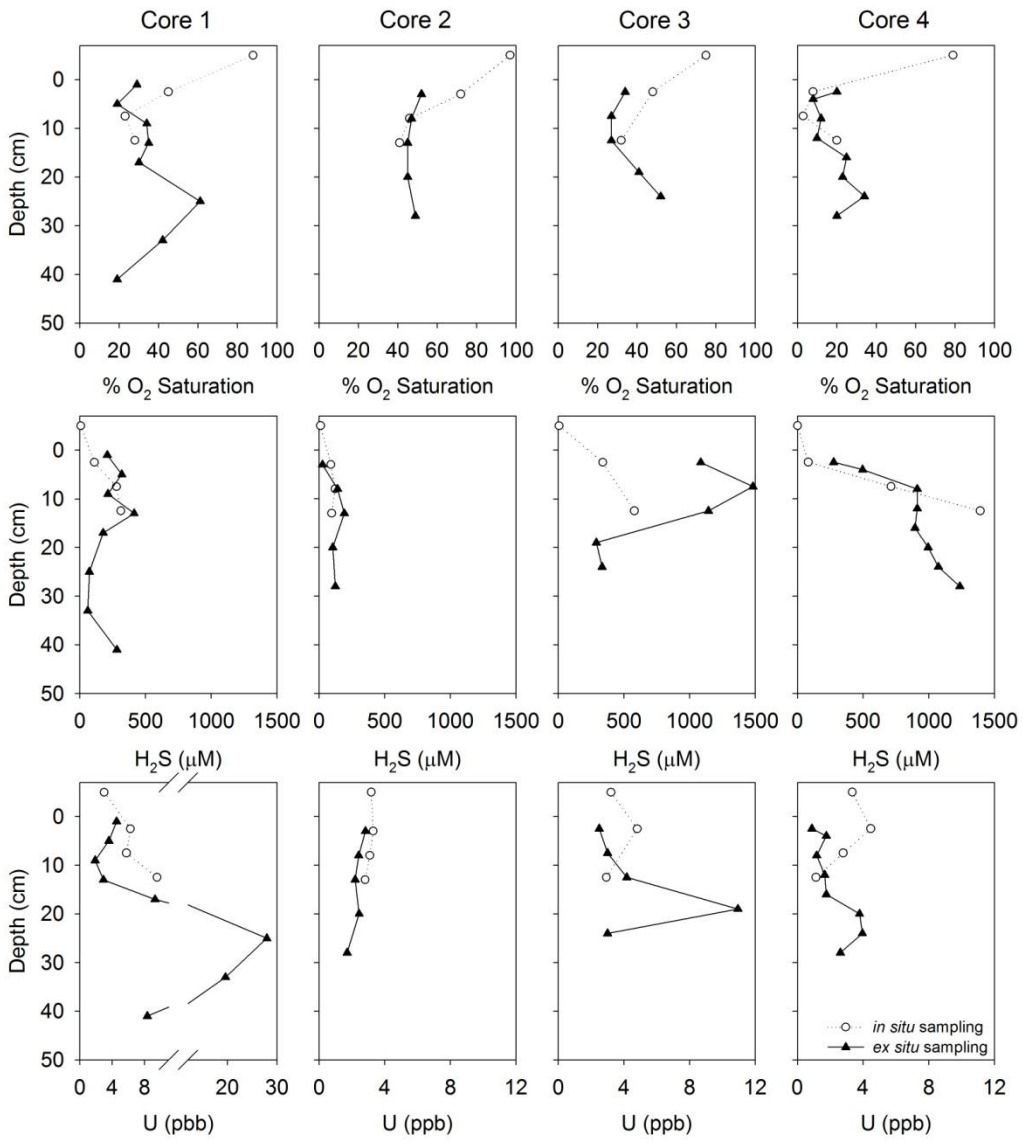

Figure 3.5. Dissolved O_2, H_2S and U concentrations in pore water samples. Dissolved O_2 primarily reflects contamination of samples with bottom water and atmospheric O_2, and should not be interpreted as the *in situ* concentration. See Section 3.3.3 for details.

for reoxidation, measured H_2S concentrations were generally high, ranging from ~100 μM in Core 2 to >1200 μM in Cores 3 and 4. This is consistent with visibly abundant macroscopic organic matter in each core and the potential for high rates of respiration and sulfate reduction.

Dissolved U profiles behaved somewhat erratically with concentrations both above and below that of the overlying bottomwater (3.2 ppb). These variations vastly exceeded the analytical error of replicate analysis of each sample (3%) and cannot be explained by sampling blanks, which were negligible. Instead, it is likely that elevated U concentrations are caused by rapid oxidation of U(IV) phases in the solid sediment, especially for those samples in which U concentrations greatly exceed seawater. This is a well-known sampling artifact that often occurs during sampling of marine pore waters, even when extreme caution is taken to prevent oxidation (Anderson et al., 1989b; Cochran et al., 1986; Henderson et al., 1999; Toole et al., 1984).

Figure 3.6 presents the data on the state of the carbonate system in the pore waters of all 4 cores. Low pH and high DIC concentrations are indicative of high respiration rates and consistent with the observed presence of significant amounts of organic matter and high concentrations of H_2S. Undersaturation of calcite and aragonite along with high alkalinities provide evidence of significant carbonate dissolution in response to respiration. These data are consistent with previously published Bahamas pore water profiles collected in the same region (Burdige et al., 2010; Burdige and Zimmerman, 2002; Burdige et al., 2008). Pore water data are tabulated in Table 3.4.

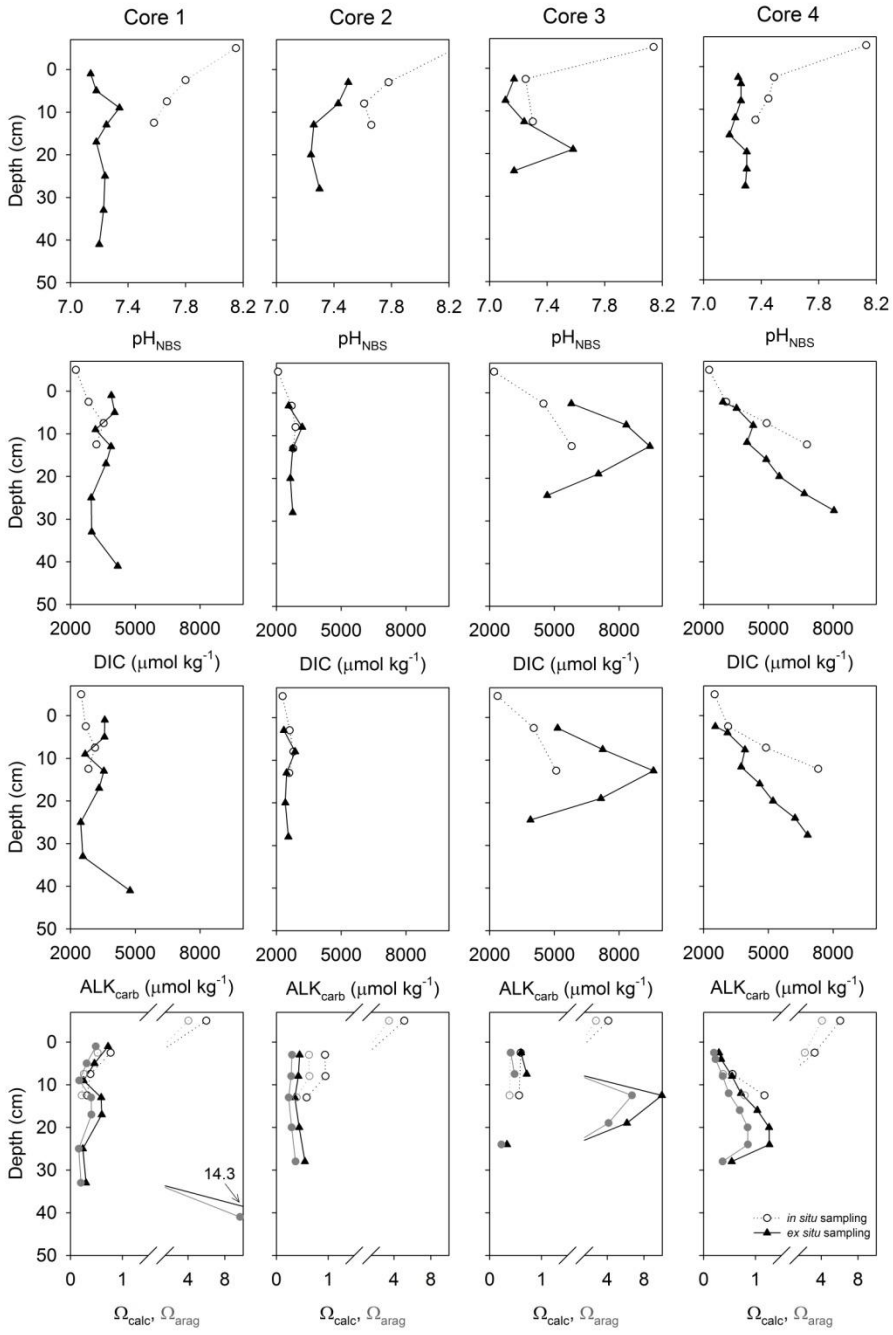

Figure 3.6. Porewater profiles of pH, DIC, ALK, and calcite and aragonite saturation state.

Table 3.4. Summary of pore water data

Sample	Depth (cm)	Sal. (ppt)	O_2 (% Sat.)	$\sum H_2S$ (μM)	pH_{NBS}	DIC (uM)	ALK_{tot} (uM)	ALK_{carb} (uM)	pH_{NBS} (Calc)	ΔpH_{NBS}	Ω_{calc}	Ω_{arag}	Mg (ppm)	Ca (ppm)	Sr (ppb)	U (ppb)
Estimated Err. (1σ)	2	0.5	5	10	0.05	3%	5%	5%					6%	6%	3%	3%
Core 1 IAPSO		35.0			7.95	2166	2381	2310	7.81	0.1	3.89	2.61	1235	392	7998	3.1
Core 2 IAPSO		35.0	88	8	8.02	2117	2304	2234	7.74	0.3	3.31	2.22	1194	379	7972	3.0
Core 3 IAPSO		35.0			7.97	2226	2165	2150	7.09	0.9	0.80	0.54	1222	391	8441	3.3
Core 4 IAPSO		35.0	88	13	8.03	2113	2468	2350	8.01	0.0	5.86	3.94	1214	388	8264	3.1
Core 1 Bottom Water	-5	37.0	88	8	8.15	2250	2610	2498	8.01	0.1	5.99	4.03	1194	379	8036	3.0
Core 1 *in situ* 1	2.5	37.5	45	111	7.80	2840	2808	2708	7.01	0.8	0.77	0.52	1371	435	9311	6.3
Core 1 *in situ* 2	7.5	38.0	23	280	7.67	3536	3323	3140	6.68	1.0	0.38	0.26	1315	433	9071	5.8
Core 1 *in situ* 3	12.5	38.0	28	313	7.58	3209	3036	2835	6.66	0.9	0.32	0.22	1238	403	8617	9.6
Core 1 *ex situ* 1	**1**	38.0	29	209	7.14	3895	3747	3590	6.83	0.3	0.72	0.49	1335	440	9558	4.6
Core 1 *ex situ* 2	**5**	38.0	19	320	7.18	4045	3785	3578	6.67	0.5	0.46	0.31	1262	426	9317	3.6
Core 1 *ex situ* 3	**9**	37.5	34	213	7.34	3159	2804	2681	6.54	0.8	0.25	0.17	1261	408	9122	1.9
Core 1 *ex situ* 4	**13**	37.0	35	413	7.25	3877	3839	3546	6.79	0.5	0.59	0.40	1297	434	9328	2.9
Core 1 *ex situ* 5	**17**	37.5	30	178	7.18	3647	3460	3330	6.79	0.4	0.60	0.41	1320	439	9637	9.3
Core 1 *ex situ* 6	**25**	38.0	61	73	7.24	2962	2519	2476	6.50	0.7	0.24	0.16	1367	436	9813	28.0
Core 1 *ex situ* 7	**33**	37.5	42	61	7.23	2985	2611	2571	6.58	0.7	0.30	0.20	1262	414	9045	19.6
Core 1 *ex situ* 8	**41**	38.0	19	282	7.20	4190	5160	4761	8.10	-0.9	14.4	9.66	1331	442	10060	8.4
Core 2 Bottom Water	-5	37.5	97	12	8.25	2076	2398	2289	7.98	0.3	5.12	3.45	1257	404	9019	3.2
Core 2 *in situ* 1	3	37.5	72	92	7.78	2705	2708	2617	7.10	0.7	0.94	0.63	1270	406	8578	3.3
Core 2 *in situ* 2	8	37.0	46	123	7.61	2892	2903	2788	7.08	0.5	0.95	0.64	1335	432	9406	3.1
Core 2 *in situ* 3	13	37.0	41	98	7.66	2779	2679	2597	6.89	0.8	0.58	0.39	1343	432	9156	2.8
Core 2 *ex situ* 1	**3**	37.0	52	27	7.50	2566	2373	2347	6.79	0.7	0.45	0.30	1295	412	9274	2.8
Core 2 *ex situ* 2	**8**	37.5	47	142	7.43	3197	2965	2866	6.71	0.7	0.42	0.28	1270	410	9249	2.4
Core 2 *ex situ* 3	**13**	37.5	45	192	7.26	2757	2600	2469	6.71	0.6	0.35	0.24	1285	409	9164	2.2
Core 2 *ex situ* 4	**20**	37.5	45	104	7.24	2645	2495	2416	6.79	0.5	0.44	0.30	1248	399	8964	2.4
Core 2 *ex situ* 5	**28**	37.5	49	125	7.30	2753	2657	2557	6.87	0.4	0.55	0.37	1247	396	8535	1.7

Table 3.4 (cont.). Summary of pore water data

Sample	Depth (cm)	Sal. (ppt)	O_2 (% Sat.)	$\sum H_2S$ (μM)	pH_{NBS}	DIC (uM)	ALK_{tot} (uM)	ALK_{carb} (uM)	pH_{NBS} (Calc)	ΔpH_{NBS}	Ω_{calc}	Ω_{arag}	Mg (ppm)	Ca (ppm)	Sr (ppb)	U (ppb)
Estimated Err. (1σ)	2	0.5	5	10	0.05	3%	5%	5%					6%	6%	3%	3%
Core 3 Bottom Water	-5	37.5	75	8	8.14	2210	2455	2372	7.84	0.3	4.12	2.77	1307	417	8423	3.2
Core 3 *in situ* 1	2.5	38.0	48	340	7.25	4498	4277	4047	6.73	0.5	0.60	0.40	1338	458	9771	4.8
Core 3 *in situ* 3	12.5	38.0	32	580	7.30	5806	5448	5089	6.64	0.7	0.57	0.38	1356	469	9559	2.9
Core 3 *ex situ* 1	**2.5**	38.0	34	1084	7.17	5784	5849	5150	6.69	0.5	0.61	0.41	1363	464	10463	2.5
Core 3 *ex situ* 2	**7.5**	37.5	27	1483	7.11	8332	8131	7242	6.61	0.5	0.71	0.48	1266	455	10171	3.0
Core 3 *ex situ* 3	**12.5**	37.5	27	1144	7.24	9424	10677	9591	7.49	-0.3	9.96	6.70	1278	482	10815	4.2
Core 3 *ex situ* 4	**19**	37.5	41	290	7.58	7041	7461	7159	7.48	0.1	6.15	4.14	1309	485	10719	10.9
Core 3 *ex situ* 5	**24**	37.5	52	334	7.17	4670	4075	3894	6.5	0.7	0.34	0.23	1270	432	9546	3.0
Core 4 Bottom Water	-5	39.0	79	2	8.13	2254	2624	2514	8.03	0.1	6.07	4.09	1332	432	9183	3.4
Core 4 *in situ* 1	2.5	39.0	8	83	7.49	3044	3260	3138	7.58	-0.1	3.29	2.21	1332	430	9463	4.5
Core 4 *in situ* 2	7.5	39.0	3	714	7.45	4922	4914	4889	7.29	0.2	0.56	0.37	1364	455	9987	2.8
Core 4 *in situ* 3	12.5	39.0	20	1393	7.36	6791	7391	7311	7.86	-0.5	1.17	0.79	1328	470	10689	1.1
Core 4 *ex situ* 1	**2.5**	38.0	20	276	7.24	2890	2714	2539	6.64	0.6	0.30	0.20	1358	441	9576	0.9
Core 4 *ex situ* 2	**4**	38.5	8	497	7.26	3529	3419	3106	6.65	0.6	0.34	0.23	1323	439	9547	1.8
Core 4 *ex situ* 3	**8**	38.0	12	913	7.26	4298	4554	3919	6.78	0.5	0.55	0.37	1318	444	9797	1.2
Core 4 *ex situ* 4	**12**	38.0	10	913	7.22	4012	4422	3741	6.88	0.3	0.72	0.48	1300	437	10031	1.7
Core 4 *ex situ* 5	**16**	38.0	25	896	7.18	4904	5278	4598	6.91	0.3	1.04	0.70	1190	409	9765	1.8
Core 4 *ex situ* 6	**20**	39.0	23	996	7.30	5509	5995	5217	6.97	0.3	1.26	0.85	1356	469	10551	3.8
Core 4 *ex situ* 7	**24**	40.0	34	1073	7.30	6668	7039	6235	6.9	0.4	1.27	0.85	1405	488	11066	4.0
Core 4 *ex situ* 8	**28**	40.5	20	1238	7.29	8039	7512	6819	6.54	0.8	0.54	0.36	1344	474	10928	2.6

3.4 DISCUSSION

3.4.1 Primary Precipitates

The results demonstate that a wide variety of primary carbonate precipitates have $\delta^{238/235}U$ values that are very to close to that of seawater (-0.41‰). Our sample set includes abiotic precipitates (e.g., ooids) and biotic precipitates representing both aragonitic and high-magnesium calcite mineralogies (Table 3.2). The wide variability of U concentrations incorporated in these materials (0.014-3.471 ppm) reflects significant differences in the precipitation mechanism (Chung and Swart, 1990). The finding that $\delta^{238/235}U$ is nearly uniform across all these materials supports the assertion that the origin of primary carbonate precipitates will not have a significant direct effect on the $\delta^{238/235}U$ of marine carbonate rocks.

As has long been established, the $\delta^{234/238}U$ of the primary carbonate precipitates are also indistiguishable from seawater (+146.8‰, Robinson et al., 2004), with only one exception discussed below. The processes responsible for generating the large observed isotopic fractionations of $\delta^{234/238}U$ in nature (which can exceed 100‰) are qualitatively different from those responsible for $\delta^{238/235}U$ fractionation. ^{234}U is a decay product of ^{238}U (via ^{234}Th and ^{234m}Pa). Radioactive decay of ^{238}U to ^{234}U in a mineral results in damage to the local crystal lattice which can result in preferential leaching of ^{234}U from a sample, a process known as the alpha recoil effect (Kigoshi, 1971). One sample in this study, a slightly weathered tiger lucine shell (*C. orbicularis*) may show evidence for this type of selective ^{234}U leaching. However, the fresh appearance of this shell suggests that

it may not be old enough to have undergone significant ^{234}U decay required for preferential leaching. Alternatively, this shell may have incorporated uranium with light $\delta^{234/238}U$ during formation from sediments in Norman's Pond outflow channel where it was collected. As discussed below, sediments at this site display light $\delta^{234/238}U$ (<110‰) providing a potential source material for the isotopically light shell composition.

3.4.2 Sedimentary Diagenetic Environment

Before discussing possible alteration of U isotope signals during diagensis, it is useful to discuss the downcore diagentic processes suggested by the pore water and solid phase data.

This study focused on shallow water (< 5 m) sites that represent the proximal end-member of the shore-shelf-slope profile present in the Bahamas and often recorded in geological sequences. These sites often host highly productive biotic communities, such as sea grass flats, which provide the source of abundant macroscopic organic detritus observed in shallow sediment cores. Pore water measurements reveal relatively low pH, high pCO_2, and significant H_2S concentrations consistent with high rates of respiration and sulfate reduction (Fig. 3.5, Fig. 3.6, Table 3.4). High rates of respiration drive significant carbonate dissolution, as indicated by the low carbonate and aragonite saturation states and high alkalinity of the pore waters. These results are consistent with previously published results for shallow Bahamanian sediments that estimate areally-

averaged dissolution rates equivalent to 0.3-0.5 cm sediment/yr (Burdige et al., 2010; Burdige and Zimmerman, 2002; Burdige et al., 2008).

Subtidal Cores 1-3 have solid phase Mg:Ca ratios in the range of 0.02-0.05 mol:mol, similar to the range typical for primary aragonite precipitates (0.001-0.05). In contrast, Core 4 (Norman's Pond) has significantly higher Mg:Ca ratios ranging from 0.11-0.56 mol:mol, with the lowest ratios near the sediment surface and a sharp increase between 16-30 cm depth. The highest values occur between 24-30 centimeters and are strongly correlated with a sharp shift toward low $\delta^{238/235}U$ and $\delta^{234/238}U$ values (discussed below). The high Mg/Ca ratio provides evidence for a high-Mg phase, likely high-magnesium calcite (HMC) or dolomite. The replacement or cementation of aragonite with dolomite is well known process occuring in Bahamian salt ponds (Dix, 2001; Furman et al., 1993; Miller, 1961) and supratidal settings (Lasemi et al., 1989; Shinn et al., 1965). While many of these settings are thought to involve evaporative brines, there is evidence that dolotimization can also occur at normal seawater salinities (Teal et al., 2000; Whitaker et al., 2009). Given Norman's Pond's complicated land use history as a salt production facility (Feldmann and McKenzie, 1998; Hein and Winsborough, 2001), including the construction of a manmade channel to the ocean (Wicklund et al., 1991), it is difficult to determine whether or not dolotimization is ongoing at present or occurred under past conditions that may have differed significantly from present conditions. Through detailed sediment dating and mineralogical work, future studies should be able to identify and quanitify the Mg-rich phase(s) and better constrain the timing and conditions of deposition.

3.4.3 Evidence for the Authigenic Accumulation of Isotopically Heavy U(IV)

Authigenic accumulation of U into reducing sediments is a well-known process that has been described in a variety of marine settings with bottom water redox conditions ranging from fully oxic to sulfide-rich (Barnes and Cochran, 1991; McManus et al., 2006; Morford et al., 2005; Morford et al., 2009). Soluble U(VI) is readily converted to nearly insoluble U(IV) at a redox potential similar to that required for the reduction of Fe(III) to Fe(II) (Morford et al., 2009). This reaction can occur abiotically, with sulfide as the reductant for example, or can be directly biologically-mediated (Hua et al., 2006; Lovley et al., 1993). Under oxic bottom water conditions, reductive authigenic accumulation into bulk sediment occurs as U diffuses or is otherwise mixed into anoxic or sulfidic pore waters and is reduced. It is often assumed that the U(IV) forms a dispersed U(IV) precipitate (such as uraninite) in sediments, but U(IV) may also be associated with organic phases or substitute for Ca in calcite (Barnes and Cochran, 1991; Sturchio et al., 1998).

Several lines of evidence point to the authigenic accumulation of U in cores collected in this study. First, sulfide concentrations in the pore water of all cores were elevated even at the shallowest sampling depth (1-3 cm depth). Sulfide concentrations at the shallowest depths measured in each core ranged from 27-1084 μM. As discusssed in Section 3.3.3, the co-occuring O_2 measured in pore water samples is almost certainly an artifact of sampling, but implies that *in situ* sulfide concentrations may be, if anything, higher than the measured concentrations due to partial redoxiation of H_2S during sampling.

Concommitent with the observation of pore water sulfide, the average solid phase U concentrations for each core (4.23, 3.92, 3.48, and 4.70 ppm for Cores 1-4 respectively) were equal to, or exceeded, the highest concentration in primary precipites measured (ooids, 3.47 ppm), and downcore U concentrations increased by 5-82% relative to the most surficial sample. Pore water profiles of dissolved U show a mix of concentrations both above and below average seawater and measured bottom water concentrations. Despite the sometimes elevated concentrations, many of the samples contain U concentrations below that of seawater suggesting that U is being removed from the pore water, likely via the formation of reduced U(IV) phases. These phases could then be oxidized when inadvertantly exposed to O_2 sampling, giving rise to the higher U concentrations observed in sporatic samples. Given the highest observed pore water U concentration, 28 ppb, the sediment porosity at this site, 68%, and the sediment U concentration, 3.1 ppm, and a typical density for seawater and $CaCO_3$ of 1.023 g cm^{-3} and 2.7 g cm^{-3}, it is possible to calculate that a maximum of 0.7% of the solid phase U could have been oxidized during sampling:

$$\frac{\mu g \text{ dissolved U } cm^{-3}}{\mu g \text{ solid phase U } cm^{-3}} = \frac{28\ ng/g \times 10^{-3}\ \mu g/ng \times 68\% \times 1.023\ g/cm^3}{3.1\ \mu g/ng \times 32\% \times 2.7\ g/cm^3} = 0.7\% \quad \text{Eq. 3.2}$$

Because the porportion of oxidized U is small, the solid phase U concentration and isotopes could not have been significantly affected by reoxidation during sampling, but the impact on porewater U concentrations is very significant. Given this, it is difficult to precisely estimate what fraction of the observed pore water U concentrations was actually present *in situ*, but the pore water profile for Core 2

shows a smooth, consistent downcore decrease in U which might be interpreted as an approximation of the true profile. While partial dissolution of carbonate sediments and reprecipitation of secondary carbonate phases with higher U/Ca ratios could possibly explain down core increase in solid phase U concentrations, low pore water U concentrations are incompatible with this suggestion. Higher U/Ca ratios in the secondary precipitate would require elevated U/Ca ratios in pore water fluids, unless the partition coefficient was significantly higher for the incorporation of U in the the secondary precipitate. This is unlikely because secondary precipitates are expected to be calcite, which has a much lower U/Ca partition coefficient (Reeder et al., 2000; Reeder et al., 2001)

Finally and mostly importantly for this study, unlike the primary carbonate precipitates, the $\delta^{238/235}U$ of bulk carbonate sediments is significantly heavier than that of average seawater U by 0.2-0.4‰. This result is consistent with the authigenic accumulation of reduced U(IV) that has been shown to be isotopically heavy in a wide variety of reducing environmental samples including modern marine sediments, black shales, uranium ores, and groundwater (Bopp et al., 2009; Bopp et al., 2010; Brennecka et al., 2010a; Stirling et al., 2007; Weyer et al., 2008). Taken together with the solid-phase and porewater U concentration data, the most likely explanation for the accumulation of isotopically heavy U in bulk carbonate sediments is that a portion of uranium in the sediment porewater is reduced to U(IV) and incorporated into the sediment either as U(IV) bound in the carbonate lattice or present as dispersed uraninite (Sturchio et al., 1998). This reduced U(IV) carries the heavy isotopic signature. If porewater U reduction was

complete, there would be no isotopic fractionation because of isotope mass balance constraints. However, if the isotopically-light residual U(VI) in the porewater exchages with seawater, then the incorporation of isotopically-heavy U(IV) into sediments can be balanced by an isotopically heavy net flux of U(VI) into sediments, allowing authigenic enrichment to continue.

An alternate possibility for the observed $\delta^{238/235}U$ offset is that different carbonate minerals composing the bulk sediment matrix carry different $\delta^{238/235}U$, and that the partial dissolution of one or more of these phases results in the observed isotopic shift. However, it seems unlikely that partial dissolution and/or reprecipitation of secondary aragonite or high-magnesium carbonate would alter the $\delta^{238/235}U$ of bulk sediment because $\delta^{238/235}U$ does not seem to fractionate upon incorporation into these phases as observed in primary precipitates. Furthermore, secondary calcite phases should contain lower U concentrations due to the lower partition U/Ca partition coefficient for calcite (Reeder et al., 2000; Reeder et al., 2001). This is at odds with elevated solid-phase concentrations observed in the cores samples. As a result, when the heavy $\delta^{238/235}U$ observations are taken together with the above evidence for the reduction of U, reductive authigenic accumulation of U seems to be the simplest explanation for all of the available data.

3.4.4 Evidence for a High-Mg Carbonate Phase with Very Light $\delta^{238/235}U$

During the diagnesis of carbonate rocks, the formation of high-Mg phases, particularly magnesian calcite, calcic dolomite, and dolomite, is a common and

important process. Despite the abundance of dolomite in the geologic record, the formation of dolomite in modern, surficial environments is rare. Nevertheless, Bahamian salt ponds and supratidal environments are well-known for the occurrence of recently deposited dolomite (Dix, 2001; Furman et al., 1993; Lasemi et al., 1989; Miller, 1961; Shinn et al., 1965).

As discussed in Section 3.3.2, Core 4 collected in Norman's Pond is characterized by high solid phase Mg:Ca ratios increasing from 0.1 near the surface of the core to 0.46 at the bottom of the core. These high Mg concentrations (up to 31 mole % Mg) are indicative of the presence of a high-Mg carbonate phase.

The presence of this unidentified phase is strongly correlated with the presence of depleted $\delta^{238/235}U$ and $\delta^{234/238}U$ bulk sediment isotope ratios (Fig. 3.7). Attempts to indentify other environmental parameters that correlate with these sharp U isotope variations were unsuccessful. While the $\delta^{234/238}U$ measurements could be easily explained by an admixture of uranium at secular equilibrium (0‰) for example, the $\delta^{238/235}U$ data in this core are already among the lightest naturally fractionationed compositions ever measured in terrestrial samples. Because of this, it seems difficult to indentify any known material with an even lighter $\delta^{238/235}U$ value to serve as a mixing end-member. Likewise, the strong depletion of $\delta^{234/238}U$ makes it unlikely that this high-Mg phase precipitated directly from seawater with its present isotopic composition, because $\delta^{234/238}U$ is nominally unfractionated during carbonate precipitate and certainly does not undergo 40‰ shifts in any case.

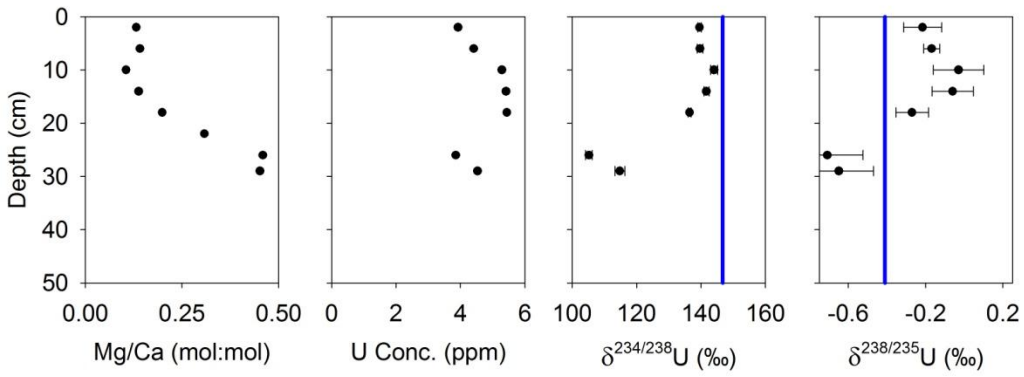

Figure 3.7. Correlation between Mg/Ca ratio of bulk sediment and $\delta^{234/238}U$ and $\delta^{238/235}U$ in Core 4.

Production of the light $\delta^{234/238}U$ via direct diagentic alteration also seems unlikely. Preferential removal of ^{234}U via the alpha recoil and preferential leaching process can only occur once ^{238}U has had time to decay to ^{234}U in a given precipitate. Even if we assume that all of the ^{234}U produced by ^{238}U decay was preferentially leached or overwise scavenged, given the 246 ky half life of ^{234}U, the 40‰ shift in $\delta^{234/238}U$ would be just barely accomodated if the sediments were 14.4 ky old. If this was the case, then the sediments were likely deposited in a freshwater pond, because sea level was well below the present level at that time (Smith et al., 2011).

Here, two additional hypotheses are put forth that do not seem to be excluded by the available data and could be testable in future work. The first hypothesis is that the core samples precipitated from a non-seawater fluid containing U with lower $\delta^{238/235}U$ and $\delta^{234/238}U$ either at the time of primary deposition or during subsequent diagenesis. While the Bahamas groundwaters are typically enriched in $\delta^{234/238}U$ due to alpha recoil effects (Henderson et al., 1999),

it is not impossible that dissolution of the presumably Pleistocene-age carbonate bedrock in this region could produce waters depleted in $\delta^{234/238}U$. Moreover, if this water was anoxic, preferential removal of isotopically heavy $\delta^{238/235}U$ into reduced phases could produce a final derived fluid with lower $\delta^{234/238}U$ and $\delta^{238/235}U$ from which the Core 4 precipitates could be derived.

The second hypothesis is that the high-Mg phase and lower $\delta^{238/235}U$ and $\delta^{234/238}U$ ratios were produced by the direct reworking and/or dolotimization of Pleistocene-age bed rock. This could have occurred via natural processes, or perhaps more likely, as a result of the salt production operations in Norman's Pond occuring over the last 200 years (Feldmann and McKenzie, 1998; Hein and Winsborough, 2001). Bubb and Atwood (1968) described the dolotimization of several inches of Pleistocene carbonate in a region underlying salt production facilities on Great Inagua Island, Bahamas. While the relict brine ponds visible from aerial imagery taken over Norman's pond are located >100 m from our sampling site, we cannot determine whether or not brine pools existed at other locations in the past given the lack of detailed knowledge about the history of land use at this site. This mechanism could explain the lower $\delta^{234/238}U$ signal observed in pond sediments, but would require an additional unidentified mechanism to produce lower $\delta^{238/235}U$. Unfortunately, a sample of the bed rock was not collected from this location.

Future work could perhaps exclude one or both of these hypotheses and/or provide new explanations based on careful dating, sedimentology, and sequential and microscale analysis of Norman's Pond sediments.

3.5 Conclusions

The purpose of this study was to investigate some of the emerging paradigms in the development of $\delta^{238/235}U$ for use as a paleoredox proxy in carbonates (Brennecka et al., 2011a; Weyer et al., 2008).

Our results demonstrate that a broad range of modern biological and abiological primary carbonate precipitates directly record the $\delta^{238/235}U$ of seawater, as has been assumed from the analysis of corals (Stirling et al., 2007; Weyer et al., 2008). The data set in this study includes corals, representatives of the green and red algae, mollusks (gastropods and bivalves), and ooids, and encompases both aragonitic and HMC mineralogies.

However, the most important finding of this study is that although primary carbonate precipitates appear to directly record seawater U isotope compositions, the shallow sediments examined did not directly record sea water. Based on evidence for reducing pore water conditions, authigenic accumulation of U into the bulk sediment, and $\delta^{238/235}U$ ratios generally elevated by 0.2-0.4‰ above seawater, it appears that U undergoes substantial reductive authigenic accumulation into shallow carbonate sediments even under fully oxic bottom water conditions.

Although this study involved only a small number of cores from a single region, our results suggest that $\delta^{238/235}U$ analysis in shallow water carbonates with evidence for sulfidic pore waters might still be a viable route for reconstructing past variations in the $\delta^{238/235}U$ of seawater, if a correction factor of 0.2-0.4‰ is subtracted from the $\delta^{238/235}U$ measured in sediment. For this to be a robust

correction, future work will be required to assess whether or not this offset is representative of carbonates from different regions, to develop a mechanistic explanation for the magnitude of this offset, and to address the cause of the 0.2‰ variation within and between cores.

Another important finding from this study was the unexpected discovery of strongly depleted $\delta^{238/235}U$ and $\delta^{234/238}U$ values in the bulk sediment of a tidal pond core, approaching -0.7‰ and 102‰ respectively. Analysis of a variety of contextual geochemical data reveal a strong correlation only between the high Mg/Ca ratio in the bulk sediment (up to 31% mole percent Mg) and the strongly depleted $\delta^{238/235}U$ and $\delta^{234/238}U$ values. While several potential hypotheses can be ruled out, the presently available data, combined with the uncertain details regarding the construction and use of the tidal pond as a salt production facility, are insufficient to draw specific conclusions about the origin of these sediments. In order to accommodate the lower $\delta^{234/238}U$ values, the two possible hypotheses presented here invoke the formation of a high Mg-phase that is either the host for or contemporaneous with U derived from the Pleistocene-age bed rock. It is proposed that one or more unidentified steps during this process must also drive $\delta^{238/235}U$ toward depleted isotopic compositions. While further work is needed to fully explain the origin of these depleted U isotope ratios, their co-occurrence with a Mg-rich phase suggests the need for caution when interpretting $\delta^{238/235}U$ ratios in carbonates that may have experienced dolomitization at any point during their diagenetic history.

Chapter 4

FRACTIONATION OF $^{238}U/^{235}U$ DURING CARBONATE DIAGENESIS: RESULTS FROM THE ODP LEG 166 BAHAMAS TRANSECT

4.1 Introduction

Recent work has suggested that the $^{238}U/^{235}U$ ratio of seawater is sensitive to oceanic redox conditions (Weyer et al., 2008). Records of these variations preserved in marine shales and limestones potentially provide a powerful way of reconstructing paleoredox changes over Earth's history (Brennecka et al., 2011a; Montoya-Pino et al., 2010). However, before this proxy can be fully exploited, it is essential to understand the processes by which $^{238}U/^{235}U$ is recorded in the rock record and how it might be altered during diagenesis. In Chapter 3, measurements of U concentrations and $^{238}U/^{235}U$ variations in primary carbonate precipitates and shallow (20-40 cm) push cores from the Bahamas demonstrated that authigenic accumulation of reduced U(IV) from sulfidic pore water plays an important role in controlling the U isotope composition of bulk carbonate sediments during early diagenesis. As a result, even though primary carbonate precipitates have $^{238}U/^{235}U$ ratios similar to that of seawater, the shallow bulk carbonate sediments examined were typically enriched in ^{238}U by 0.2-0.4‰.

The primary goal of this study is to build on the results of Chapter 3 by looking at later diagenetic alteration of $^{238}U/^{235}U$ during the first 780 ka of diagenesis in sediments on the western margin of Grand Bahama Bank. Henderson et al. (2002) previously examined these sediments for apparent variations in $\delta^{234/238}U(T)$—the decay-corrected $\delta^{234/238}U$ at the time of sediment

deposition. $\delta^{234/238}U(T)$ values in marine carbonates that deviate from seawater ($\delta^{234/238}U = 146.8‰$) are usually assumed to reflect diagenetic alteration of sediments (Edwards et al., 2003a). Here we seek to test the hypothesis that diagenetic variations $\delta^{234/238}U(T)$ might be correlated with $\delta^{238/235}U$ variations if U mobility was the common driver of diagenetic alteration. Alternatively, it is possible that $\delta^{238/235}U$ will be uncorrelated with variations in $\delta^{234/238}U(T)$. This is possible because the major drivers of $\delta^{238/235}U$ fractionation are redox and absorption chemistry, while $\delta^{234/238}U$ can be independently fractionated through α-recoil effects (Brennecka et al., 2010a; Brennecka et al., 2011b; Henderson et al., 2000; Kigoshi, 1971; Weyer et al., 2008).

In either case, observations of $\delta^{238/235}U$ variations along the Bahamas margin will prove extremely useful for paleooceanographic research. While $\delta^{234/238}U$ variations are erased on a timescale of ~1 My via decay to secular equilibrium, $\delta^{238/235}U$ variations can be preserved for billions of years. The Grand Bahamas Bank provides a modern analog for ancient carbonate platforms in the geologic record. There are many well preserved examples of carbonate platforms in the geologic record where the entire platform margin and slope can be easily identified and traced in a context very similar to the Bahamas margin. Examples include the Archean-age platforms, such as the Campbellrand-Malmani platform, as well as numerous Proterozoic and Phanerozoic examples, such as the Nama Group in Namibia, the Barremian (La Montagnette) carbonate platforms in France, and Guadalupe Mountains in Texas (Grotzinger, 1989; Kendall et al., 2010). These readily identifiable structures provide a unique opportunity to

reconstruct not only temporal records, but also paleo-depth transects in a manner not usually possible with shales. The Bahamas ODP transect provides an ideal analog where one can observe depositional and diagenetic trends along a modern carbonate platform margin.

4.2 Site Description and Samples

The samples used in the study were obtained from the western margin of Grand Bahamas Bank during ODP Leg 166 (Fig. 4.1. Eberli et al., 1997; Swart et al., 1997). During this leg, sediment cores were collected from 5 sites that form a transect extending approximately 25 km offshore from the platform margin between 300-660 m water depth. The deepest of these cores penetrated 1235 meters below seafloor (mbsf) and provided a nearly continuous sediment record from the late Oligocene to present. During Leg 166, two additional sites, 1008 and 1009, were also drilled approximately 100 km south of the Bahamas transect to provide additional examples of slope-toe sediments.

All of the samples obtained for this study were previously discussed in the context of U/Th dating as summarized by Henderson et al. (2002), except that for 7 of the 42 samples, sample material was no longer available, so an adjacent sample was used from 1 cm away. Using independent age constraints from sea-level high stands, biostratigraphic dating, and paleomagnetism, Henderson et al. (2002) provided evidence for diagenetic alteration of the $^{238}U/^{234}U/^{230}Th$ system in many of the samples used in this study. A primary goal of this study is to

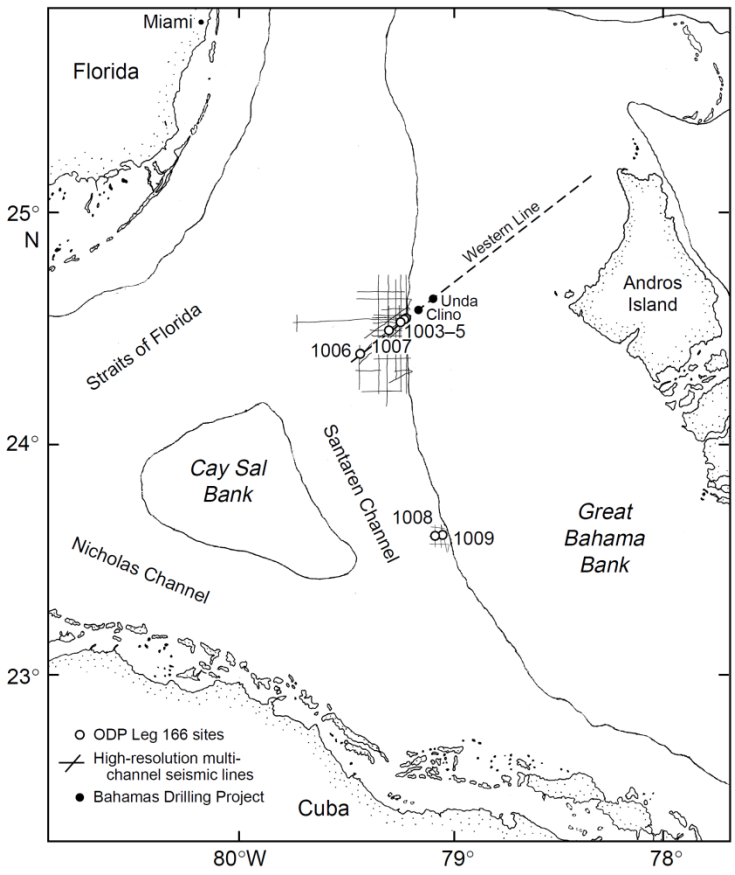

Figure 4.1. ODP Leg 166 site map. From Eberli et al. (1997).

determine whether or not diagenetic alteration of the $^{238}U/^{234}U/^{230}Th$ system also results in $^{238}U/^{235}U$ shifts.

Approximately half of the samples in this study (22 of 42 samples) come from Site 1006. Site 1006 is the deepest site in the Bahamas Transect and is the most distal site from the bank margin (Shipboard Scientific Party, 1997). Cores at this site provide a continuous record of sedimentation from the middle Miocene to present. Samples used in this study come from the upper 27.1 m meters of Unit I and are Holocene to Pleistocene in age. Unit I sediment consists of alternating

intervals of bank-derived, aragonite-rich material that was rapidly deposited during sea level high stands when the bank top was flooded, and intervals of mostly pelagically-derived low-magnesium calcite deposited during sea level low stands (Eberli, 2000; Kroon et al., 2000b; Rendle et al., 2000). This interpretation was confirmed by a strong correlation between sediment aragonite content and variations in oxygen isotopes (Kroon et al., 2000a). All of the Site 1006 samples used here correspond to the last 9 consecutive sea-level high stands (marine isotope stages: 1, 5, 7, 9, 11, 13, 15, 17, and 19), which allow the samples ages to be independently constrained via the known timing of each interglacial. These ages were independently validated by biostratigraphic dating using calcareous nannofossils and planktonic foraminifera and U/Th dating (Henderson, 2002; Henderson et al., 2000; Robinson et al., 2002; Wright and Kroon, 2000). Compared to other sites in the Bahamas Transect, sediments at Site 1006 appear to be less affected by diagenesis, as indicated by excellent preservation of foraminifera and only modest changes in pore water $\delta^{18}O$ that would indicate equilibrium with recrystallizing carbonate minerals (Shipboard Scientific Party, 1997; Swart, 2000). Compared with other sites on Leg 166, Site 1006 is also unique in that while pore water sulfate concentrations continuously decrease to zero in the upper 200 meters, this was the only site where pore water sulfide was not detected (Shipboard Scientific Party, 1997). Based on clear evidence for sulfate reduction and abundant disseminated pyrite throughout the core, it was argued that excess reactive iron scavenges sulfide from the pore water (Shipboard Scientific Party, 1997). This same process also appears to buffer pore

water pH in the range of 7.1-7.3, higher than the values of ~6.5 observed at other sites.

Another third of the samples in this study (15 of 42) come from slope sediments cored at Sites 1003, 1004, and 1005. The sediments at these sites are similar to those of Site 1006, but contain a higher proportion of bank-derived material and are interrupted by hiatuses and erosion features presumably due to down-slope transport of sediment (Henderson et al., 2000). Because the sediments at these sites are non-continuous, they can be difficult to precisely correlate with other Leg 166 cores, where age models strongly depend on continuous records $\delta^{18}O$ and aragonite content. For this reason, most of the samples from these sites where chosen within a meter of the Brunhes/Matayama magnetic reversal indentified at Sites 1003 and 1004. This event has a well-dated age of 780 ka (McNeil and Kislak, 2000).

The remaining samples (5 of 42) were chosen from cores at Sites 1008 and 1009. These sites are located approximately 100 km south of the Bahamas Transect in 437 m and 308 m of water, respectively. Sediments at these sites provide continuous, extremely expanded, Holocene and Pleistocene sediment records (Robinson et al., 2002). Coherency of radiocarbon and U/Th dates at Sites 1008 and 1009 suggest that homogenization or erosion of sediment via slumping and turbidite flows is minor (Robinson et al., 2002; Slowey et al., 2002). Reliable U/Th ages with initial $\delta^{234/238}U$ ratios similar to modern seawater suggest the U isotopes have remained undisturbed for at least the last 230 ky at these sites (Robinson et al., 2002).

4.3. Fluid Flow and Diagenetic Setting

All of the sites cored during Leg 166 show evidence for substantial subsurface fluid flow and down-core diagenetic dissolution and reprecipitation of solid-phase carbonate species. Profiles of subsurface temperature and conservative and non-conservative pore water constituents are uniform to depths of 30-40 m in all cores. These uniform profiles have been interpreted as evidence for extensive pore water flushing of sediments to this depth (Eberli et al., 1997; Henderson et al., 1999; Kramer et al., 2000; Swart, 2000). Below the bottom of this flushed zone, temperature and pore water chloride concentrations increase monotonically, governed by geothermal gradients and diffusional communication with a deeper brine fluid or evaporite deposit (Eberli et al., 1997; Kramer et al., 2000; Swart, 2000). Below the zone of pore water flushing, elevated pore water Sr concentrations and $\delta^{18}O$ provide evidence for ongoing diagenesis with preferential dissolution of aragonite and recrystallization of low-magnesium calcite (Kramer et al., 2000; Malone et al., 2001; Swart, 2000). This is similar to diagenetic patterns observed in earlier cores drilled in the northern Bahamas during ODP Leg 101 (Dix and Mullins, 1988; Droxler et al., 1988; Swart and Guzikowski, 1988). Quantitative analysis of sediment mineralogy confirms the interpretation of pore water analyses, demonstrating conversion of metastable bank-derived aragonite and high-Mg calcite to diagenetic low-Mg calcite and minor dolomite (~1 wt. %) on timescales of ~1 My (Kramer et al., 2000; Malone et al., 2001; Melim et al., 2002). In contrast to the bank top sediments that experience subaerial exposure and meteoritic diagenesis during sea level low stands, all of

the sites in this study have undergone only seafloor and marine burial diagenesis (Melim et al., 2002).

4.4. Methods

All samples were analyzed at the W. M. Keck Foundation Laboratory for Environmental Biogeochemistry at Arizona State University using standard trace-metal-clean techniques, including the use of acid-washed plasticware and trace-metal-grade acids. Prior to analysis, samples were dried and homogenized. Weighed sample aliquots (0.5-1.2g) were ashed at 750°C for 24 hours to oxidize organics and calcinate the carbonate material. Ashed samples were quantitatively transferred to 50 mL polypropylene centrifuge tubes and dissolved overnight in 10 mL of 3M nitric acid. In some samples, a small amount (<2%) of fine suspended matter was allowed to settle, and only the clear supernatant was used for subsequent analyses. Samples aliquots were analyzed for major and trace metal concentrations at 1:2000 dilution using an Thermo X-Series 2 Q-ICP-MS. This data was used to prepare sample aliquots containing 1500 ng U spiked with a ^{233}U-^{236}U double-spike at a 0.0363 spike:sample molar ratio (Verbruggen et al., 2008; Weyer et al., 2008).

Spiked samples were purified and preconcentrated using the Eichrom UTEVA resin protocol described by Weyer et al. (2008), except that column chemistry was performed using a novel automated chromatography system (Elemental Scientific PrepFAST MC). The system uses a computer-controlled

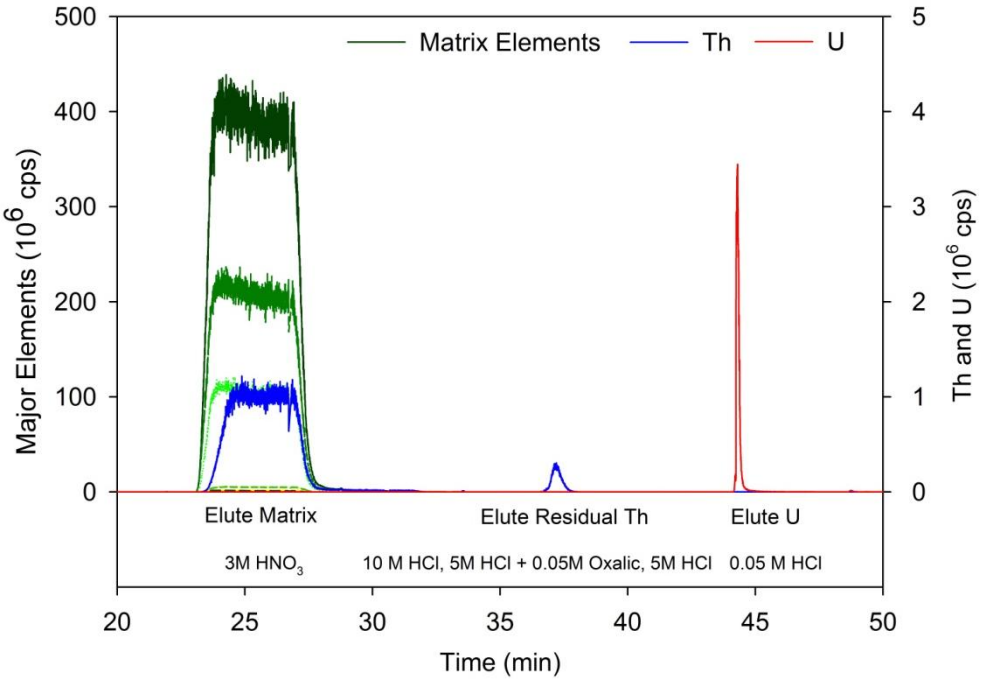

Figure 4.2. Typical U elution profile using the ESI PrepFAST MC. The separation column contained 600 µL of Eichrom UTEVA resin. The elution profile was collected online in real time by directly connecting the PrepFAST MC to a Thermo Element 2 Q-ICP-MS, using an aliquot of BCR-2 basalt standard as the sample. Matrix elements plotted here include Ca, Mg, and Fe, and are typical for all other matrix elements measured. The automated cleaning step (t = 0-20 min) is not plotted, but is indistinguishable from baseline at this scale.

autosampler and a series of valves and syringe pumps, featuring an all Teflon flow path, to completely automate column chromatography. The system includes a fully-automated column cleaning step, allowing a single column containing 600 µL of UTEVA resin to be reused at least 30 times. A typical chromatography

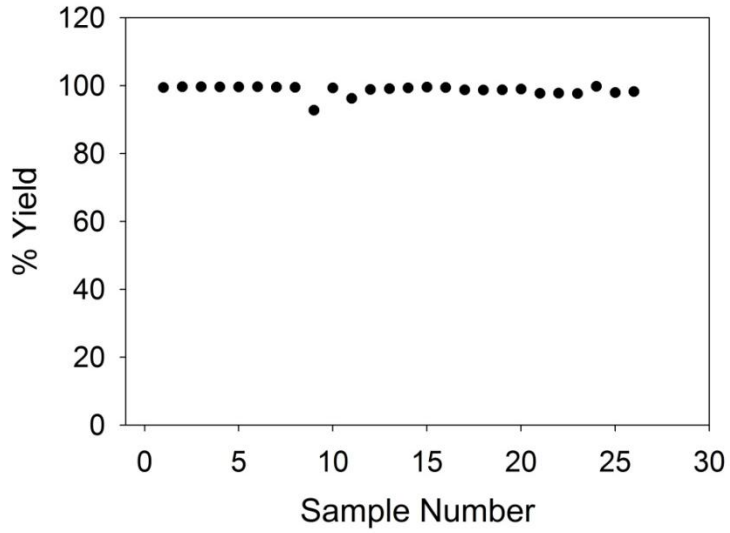

Figure 4.3. Typical uranium column yields for a series of 26 samples prepared with the PrepFAST MC. The average yield was 97.8% and the minimum yield was 92%.

elution profile is shown in Figure 4.2 and typical column yields are shown in Figure 4.3.

Following column chemistry, samples were evaporated in a mixture of concentrated nitric acid and 32% hydrogen peroxide repeatedly (3X) to oxidize any organic materials leached from the UTEVA resin. U isotopes ($^{238}U/^{235}U$) and final U concentrations (via isotope dilution) were determined on a Thermo Neptune MC-ICP-MS equipped with an ESI Apex desolvating nebulizer, following methods described in Chapter 3. Figure 4.4 demonstrates that the external reproducibility for 10 aliquots of CRM145 standard, interspersed with samples and independently processed through chemistry using the PrepFAST MC system, was 0.03‰ (2sd). Internal precision for the replicate measurement of

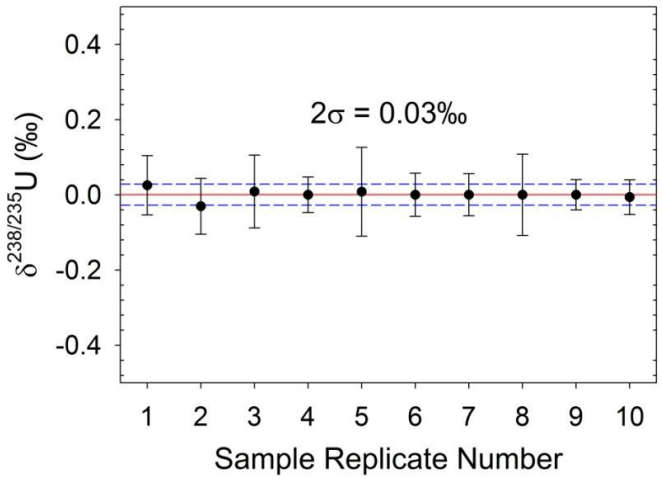

Figure 4.4. External reproducibility of $\delta^{238/235}U$ for 10 aliquots CRM145 independently processed through chemistry over a 1 week period using the ESI PrepFAST MC. Standards were processed interspersed with natural samples (not shown). Errors bars indicate the 2σ precision of replicate measurements on a single sample aliquot (N≥3). The red solid line represents the mean value for all sample aliquots, and the blue dashed lines indicate the 2σ precision for the means of all sample aliquots.

samples was generally larger than this, averaging 0.08‰ (2sd) with a maximum of 0.19‰.

4.5 Results

4.5.1 Variations in $\delta^{238/235}U$

The range of $\delta^{238/235}U$ measured for all samples in this study was -0.31 to 0.16‰. Notably, all of the 42 samples measured had $\delta^{238/235}U$ values significantly heavier than that of modern seawater (-0.41‰, Weyer et al., 2008). The down core profile of $\delta^{238/235}U$ at Sites 1006 is primarily vertical, with an overall average

value of -0.17±0.19‰ (all errors 2sd) (Fig. 4.5a). The variance is dominated by excursions to ~0‰ in three samples. When these points are excluded, the average of the remaining data is -0.20±0.08‰. It is not clear why these three samples sharply diverge from the remaining data set. In 2 of the 3 cases, a nearby sample taken from 10 cm away was determined to have $\delta^{238/235}U$ value similar to the remaining average, with values of -0.20‰ and -0.23‰ respectively. This suggests these anomalous samples likely reflect intermittent periods of high frequency variability or disturbance, perhaps due to the deposition of turbidites or extensive bioturbation. Indeed, similarly high $\delta^{238/235}U$ values were observed in Core 1 of the Chapter 3, which was taken in an extensively burrowed lagoon. Two of these anomalous points lie close to the interval between 10-15 m which is also notable for its elevated Mo, Re, and U concentrations (Fig. 4.5b). However, average $\delta^{238/235}U$ values inside and outside this interval are not significantly different, -0.17±0.23‰ and -0.18±0.06‰, respectively.

Short, high resolution $\delta^{238/235}U$ profiles taken around the Brunhes/ Matayama reversal at Sites 1003 and 1004 also record short term $\delta^{238/235}U$ variations of up to 0.2‰ with some evidence of vertical structure at this resolution (Fig. 4.6 b,c). While the average $\delta^{238/235}U$ value measured at Site 1004 is similar to that of Site 1006 (-0.18±0.23‰), the average at Site 1003 was considerably higher (0.05±0.13‰). The difference is especially striking considering that samples at Site 1003 and 1004 were deposited contemporaneously.

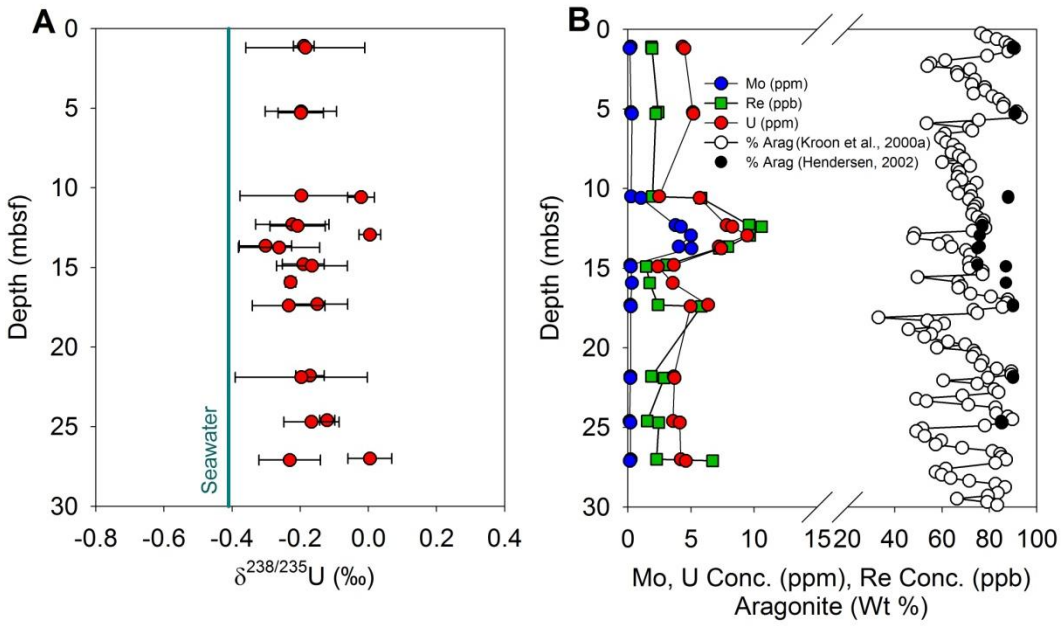

Figure 4.5. Down core geochemical profiles at ODP Leg 166, Site 1006. (A) Down core $\delta^{238/235}$U profile. (B) Redox sensitive metals (Mo, Re, U, *this study*) and previously published measurements of wt% aragonite in samples used in this study (filled circles; Henderson, 2002) and a high resolution profile showing climate-driven cyclicity in the same core (open circles; Kroon et al., 2000a).

Although relatively few samples were measured from Sites 1005, 1008, and 1009, they show a pattern similar to that from the other sites, with four samples giving a $\delta^{238/235}$U average of -0.23±0.14‰, and two additional points with values of -0.02‰ and 0.01‰ (Table 4.1).

4.5.2 Variations in Redox Sensitive Trace Metal Concentrations

Redox sensitive trace metal concentrations range from moderate to high in all of the samples studied and were strongly correlated with one another. At Site

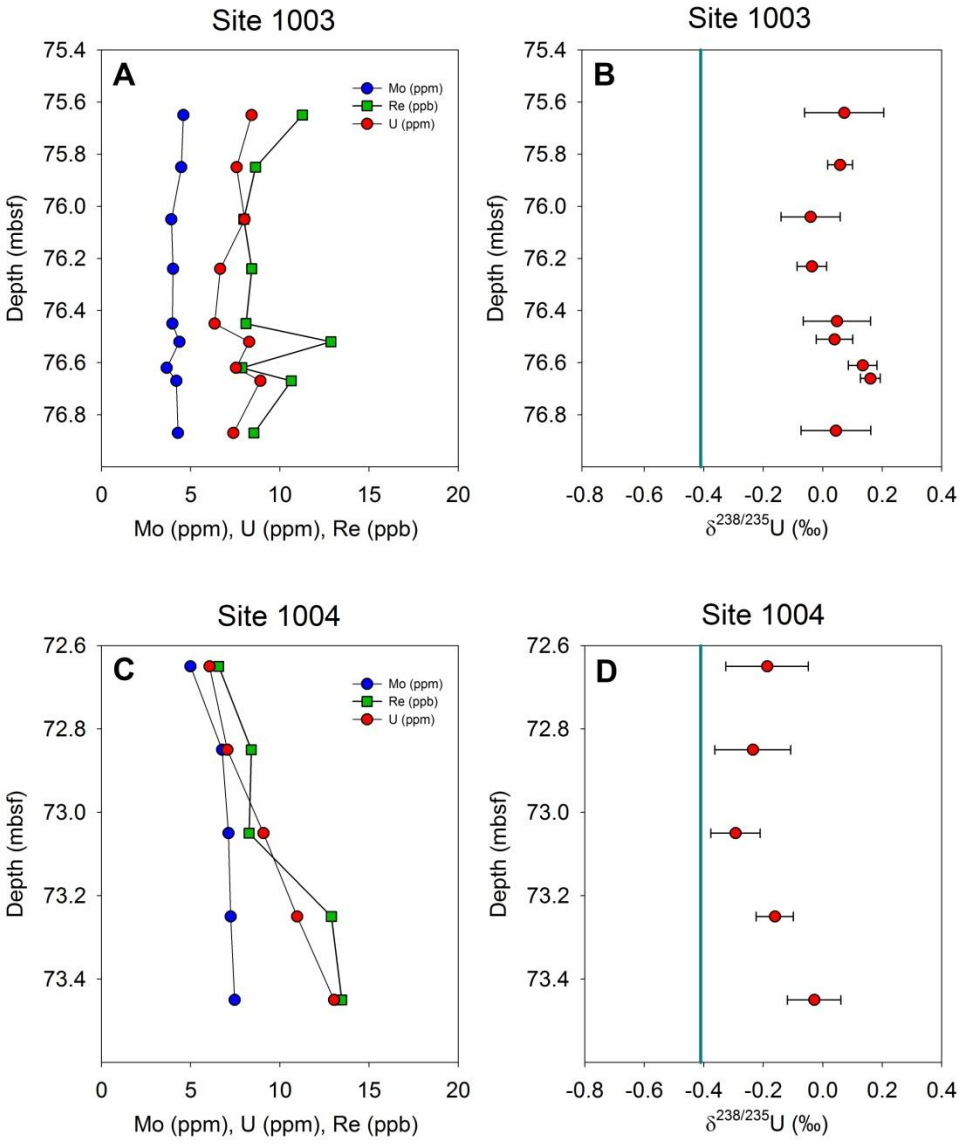

Figure 4.6. Down core geochemical profiles at ODP Leg 166, Sites 1003 and 1004. (A, C) Variations in redox sensitive metals (Mo, Re, U). (B, D) Down core $\delta^{238/235}U$ profiles. Note that the depth scale is greatly expanded compared to Site 1006 in Fig. 4.5.

1006, the intervals between 0-10 m and 15-27 m had lower average concentrations of Mo, U, and Re (4.4 ppm, 0.2 ppm, and 2.6 ppb, respectively). These concentrations are similar to those observed in Bahamian primary carbonate precipitates (Chapter 3, Chapter 5). The remaining samples from Site 1006 and all other sites have higher average Mo, U and Re concentrations (6.6 ppm, 3.2 ppm, 7.1 ppb, respectively). These results are consistent with previous evidence for U reduction in carbonate pore water during burial diagenesis and strongly suggest that the enrichment of redox-sensitive trace metals is related to the presence of pore water sulfide at all sites except Site 1006 (Henderson et al., 1999). The presence or absence of sulfide is especially significant for Mo, resulting a >10X increase in Mo concentrations in sediments with sulfidic pore water. A similar effect has also been observed in shallow push-cores collected from top of the Bahamas Bank, where Mo was strongly enriched in cores with sulfidic pore water, but remained at background concentrations in a core with very low sulfide (Chapter 5).

4.6 Discussion

4.6.1 Correlation Between $\delta^{238/235}U$ and $\delta^{234/238}U(T)$

One of the primary goals of this study was to examine the correlation, if any, between diagenetic alteration of the $^{238}U/^{234}U/^{230}Th$ system and potential shifts in the $^{238}U/^{235}U$ values of bulk carbonate over the last ~780 ky. Many of the samples in this study show clear evidence of alteration of the $^{238}U/^{234}U/^{230}Th$ system (Henderson, 2002). There are two type of evidence for this. First,

Table 4.1 Summary of results from ODP cores.

Sample Identifier (Hole-Section-Depth)	Depth (mbsf)	Age (ka)	U (ppm)	Mo (ppm)	Re (ppb)	$\delta^{238/235}$U (‰)	2σ err (‰)
1003B 9H-5 15-16	75.65	780	8.42	4.6	11.3	0.08	0.13
1003B 9H-5 35-36	75.85	780	7.58	4.5	8.6	0.07	0.02
1003B 9H-5 55-56	76.05	780	8.03	3.9	8.0	-0.01	0.10
1003B 9H-5 74-75	76.24	780	6.65	4.0	8.4	-0.02	0.05
1003B 9H-5 95-96	76.45	780	6.34	4.0	8.1	0.06	0.11
1003A 9H-3 10-11	76.52	780	8.27	4.4	12.9	0.05	0.06
1003A 9H-3 20-21	76.62	780	7.55	3.7	7.9	0.15	0.06
1003A 9H-3 25-26	76.67	780	8.91	4.2	10.6	0.18	0.03
1003A 9H-3 45-46	76.87	780	7.39	4.3	8.6	0.05	0.12
1004A 9H-4 135-136	72.65	780	6.06	5.0	6.6	-0.17	0.14
1004A 9H-5 5-6	72.85	780	7.06	6.8	8.4	-0.22	0.12
1004A 9H-5 25-26	73.05	780	9.08	7.1	8.3	-0.27	0.08
1004A 9H-5 45-46	73.25	780	10.97	7.2	12.9	-0.15	0.06
1004A 9H-5 65-66	73.45	780	13.04	7.5	13.5	-0.01	0.09
1005A 4H-1W 4-6	16.04	228	9.90	3.7	9.8	0.02	0.06
1006A 1H-1 109-110	1.1	11	4.33	0.2	1.9	-0.17	0.03
1006A 1H-1 120-121	1.2	11	4.47	0.2	1.9	-0.17	0.17
1006A 1H-4 70-71	5.2	132	5.15	0.2	2.4	-0.19	0.10
1006A 1H-4 80-81	5.3	132	5.19	0.3	2.2	-0.18	0.07
1006B 2H-4 49-50	10.5	207	2.47	0.2	1.9	-0.17	0.18
1006B 2H-4 60-61	10.6	207	5.70	1.0	5.8	-0.01	0.04
1006A 2H-4 70-71	12.3	339	7.84	3.8	9.6	-0.21	0.11
1006A 2H-4 80-81	12.4	339	8.27	4.3	10.6	-0.19	0.08
1006A 2H-4 134-135	12.94	341	9.47	4.9	9.7	0.02	0.05
1006B 2H-6 65-66	13.65	413	7.21	4.1	7.9	-0.29	0.08
1006B 2H-6 74-75	13.75	413	7.39	5.2	7.3	-0.25	0.12
1006A 2H-6 20-21	14.8	413	3.64	0.2	3.1	-0.17	0.06
1006A 2H-6 30-31	14.9	413	2.38	0.1	1.5	-0.23	0.10
1006A 2H-6 133-134	15.93	387	3.57	0.2	1.7	-0.21	0.02
1006A 3H-1 70-71	17.3	492	6.35	0.2	2.4	-0.13	0.09
1006A 3H-1 80-81	17.4	492	4.98	0.2	5.8	-0.21	0.11
1006A 3H-4 69-70	21.8	580	3.64	0.2	1.9	-0.16	0.04
1006A 3H-4 80-81	21.9	580	3.70	0.2	2.9	-0.18	0.19
1006A 3H-6 50-51	24.6	692	3.58	0.1	1.5	-0.10	0.02
1006A 3H-6 59-60	24.7	692	4.12	0.1	2.4	-0.15	0.08
1006A 4H-1 90-91	27	783	4.21	0.1	2.3	0.02	0.06
1006A 4H-1 100-101	27.1	783	4.59	0.1	6.7	-0.21	0.09
1008A 3H-1 12-13	16.22	204	7.61	4.2	6.9	-0.30	0.16
1008A 4H-5 62-63	32.22	356	8.32	1.3	8.3	-0.25	0.06
1009A 8H-2 140-141	54.7	192	5.50	2.9	4.2	-0.19	0.10
1009A 9H-5 109-110	68.39	247	7.59	1.9	4.3	-0.12	0.10
1009A 11H-2 15-16	75.45	336	7.72	2.9	6.2	-0.01	0.16

Henderson (2002) showed that the $^{230}Th/^{238}U$ activity ratios of some samples used in this study deviate significantly from expected values based on independently known samples ages (Fig. 4.7a, open symbols). Second, Henderson (2002) also used the independent age constraints available to calculate $\delta^{234/238}U(T)$ and show that while these values scattered around the modern seawater value indicating a lack of secular variation in the $\delta^{234/238}U$ of seawater, the values often deviated substantially from the expected seawater value indicating diagenesis (Fig. 4.7b).

In comparison, measurements of $\delta^{238/235}U$ in these same samples show rather consistent values that average -0.2‰ with a constant ~0.2‰ offset from seawater. The exceptions to this are samples from Site 1003 that are significantly heavier and offset from seawater by 0.4-0.6‰. Because contemporaneous samples from Site 1004 and other samples of similar age do not show elevated values, it is highly unlikely that the $\delta^{238/235}U$ shift observed at Site 1003 is a result of secular variations in seawater $\delta^{238/235}U$. As a result, the $\delta^{238/235}U$ shift observed at Site 1003 must have been driven by a unique sedimentation or diagenetic process, such as the emplacement of a turbidite, but the available data set is insufficient to discern among potential hypotheses. Overall, $\delta^{238/235}U$ measurements show no correlation with calculated values of $\delta^{234/238}U(T)$ as shown in Figure 4.8. Samples from Site 1003 appear to form a cluster with unusually heavy $\delta^{238/235}U$ and light $\delta^{234/238}U(T)$, but without more information it is difficult to determine whether this is a causal relationship or a chance correlation.

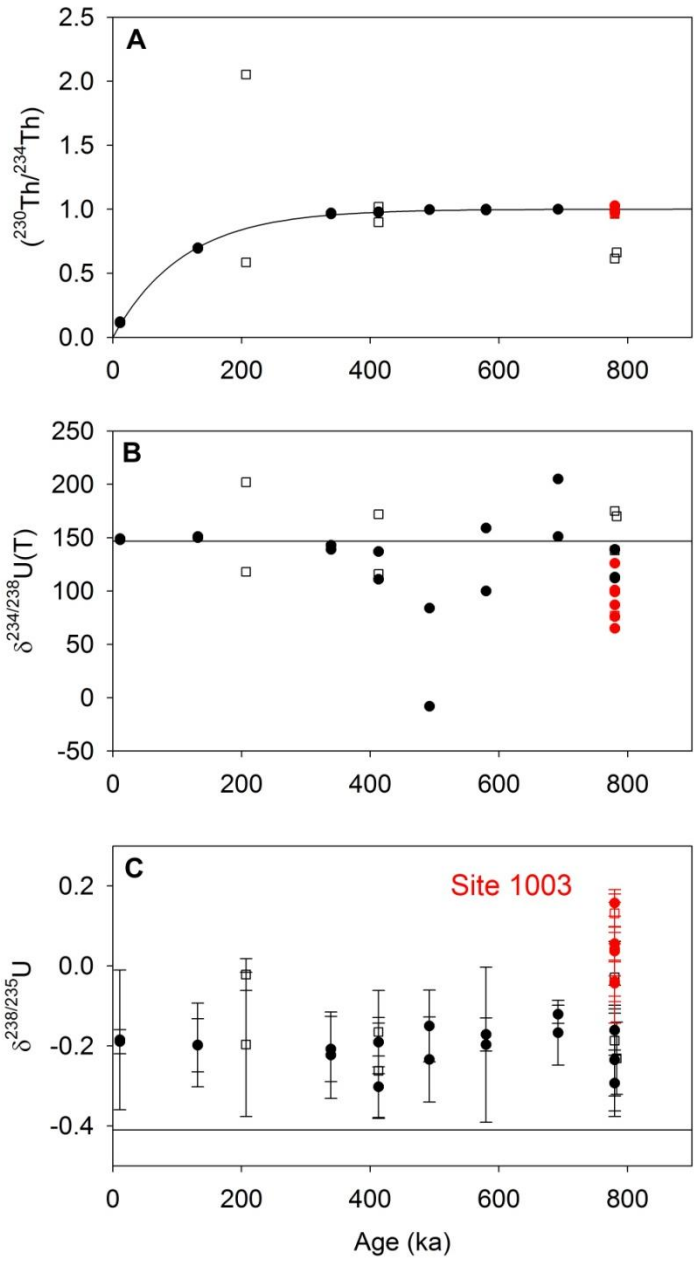

Figure 4.7. (^{230}Th/^{238}Th), $\delta^{234/238}$U(T), and $\delta^{238/235}$U as function of sample age from ODP Leg 166 samples. (A) Comparison of measurement vs. expected (^{230}Th/^{234}Th) activity ratios. Samples which deviate by more than 3% from the expected ratio (solid curve) are shown in open symbols (B) Calculated $\delta^{234/238}$U(T) based on measured $\delta^{234/238}$U values and independent age constraints.

$\delta^{234/238}U$ of modern seawater (146.8‰) is indicated by the horizontal line. (C) Measured values of $\delta^{238/235}U$ (*this study*), with samples from Site 1003 shown in red. The $\delta^{238/235}U$ value of modern seawater (-0.41‰) is indicated by the horizontal line. Data and graphics shown in panels A and B have been redrawn from Henderson (2002).

4.6.2 U concentrations and correlations with redox sensitive metals

As previously recognized by Henderson (2002), U concentrations in drill core samples are significantly elevated relative to typical marine primary precipitates such as calcareous algae, corals, and ooids, that typically contain < 4 ppm U. At Site 1006, the average U concentration is 5.1 ppm, with a range of values up to 9.4 ppm. Samples from nearby sites (1003, 1004, 1005, 1008, and 1009) can range even higher, with concentrations up to 13 ppm (Fig. 4.5, Fig. 4.6, Table 4.1).

Two lines of evidence suggest that pore water redox chemistry plays an important role in determining the extent of U enrichment in Bahamas sediments. First, there is a strong correlation between U and Re concentrations (Fig. 4.9a). These metals both undergo reductive authigenic accumulation under anoxic conditions, and correlations between U and Re concentrations are commonly observed under reducing conditions (Colodner et al., 1995; Crusius and Thomson, 2000; Kendall et al., 2009; Morford and Emerson, 1999; Morford et al., 2005). Second, there is a knee-shaped relationship between Mo and U concentrations where U appears to undergo low levels of authigenic enrichment without

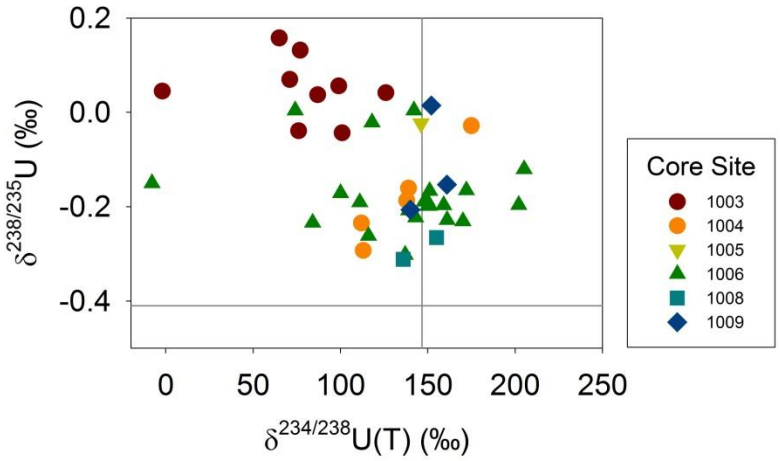

Figure 4.8. Crossplot of $\delta^{238/235}U$ and $\delta^{234/238}U(T)$ data from all samples in this study. Dashed lines represent the average U isotope composition of seawater.

corresponding Mo enrichment, but then both metals are accumulated at higher levels of enrichment (Fig. 4.9b). This pattern of enrichment is consistent with accumulation of U under reducing, but non-sulfidic conditions, followed by strong enrichment of both Mo and U under sulfidic settings, as has been previously observed by many authors (Helz et al., 1996; Morford and Emerson, 1999; Morford et al., 2005; Morford et al., 2007). This interpretation is further supported by the extremely low Mo concentration in many samples from Site 1006, which is known to have anoxic, but non-sulfidic pore waters (Shipboard Scientific Party, 1997). Based on this interpretation, 0.5 ppm Mo and 5.5 ppm U are tentatively and operationally identified as defining a threshold between deposition under anoxic versus sulfidic pore water conditions (Fig. 4.9b).

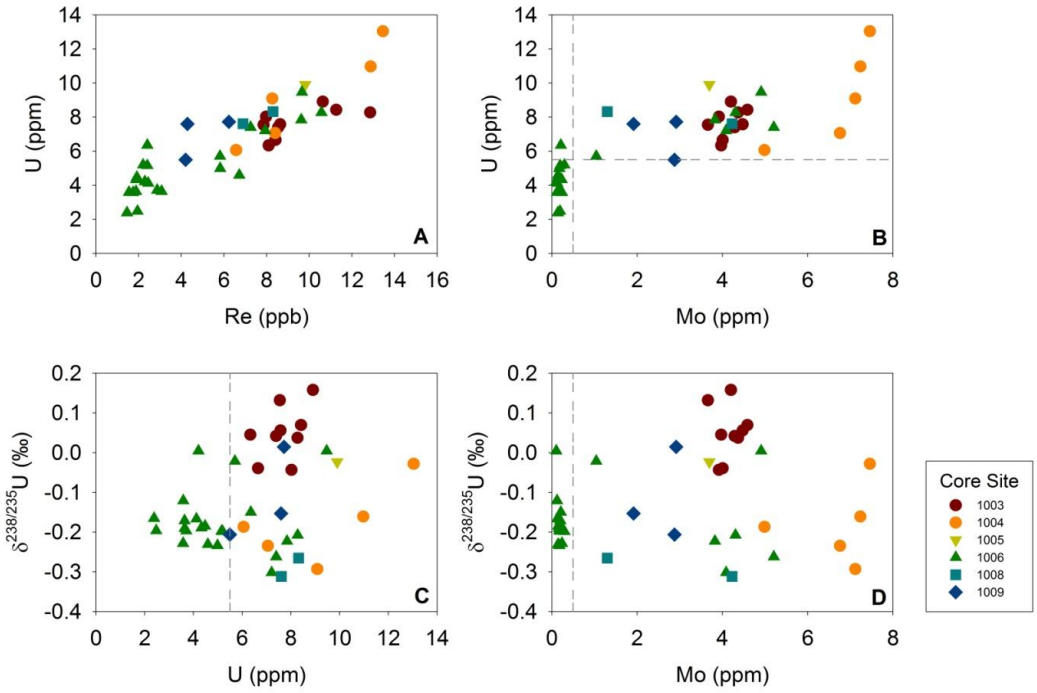

Figure 4.9. Relationships between U, Mo, and Re concentrations and $\delta^{238/235}$U. (A) Correlation between U and Re concentrations (B) Correlation between Mo and U concentrations. (C) Relationship between U concentration and $\delta^{238/235}$U. (D) Relationship between Mo concentration and $\delta^{238/235}$U. The dashed lines in panels B, C, and D indicate tentative Mo and U concentration thresholds that are suggested to define the boundary between sediments with anoxic vs. sulfidic pore waters. Note that in both panels C and D, $\delta^{238/235}$U variability appears to be reduced below the proposed threshold values.

These thresholds, which likely indicate the onset of sulfidic pore water conditions, also appear to define an important boundary for $\delta^{238/235}$U variability (Fig. 4.9c,d). Below these thresholds, $\delta^{238/235}$U values cluster around -0.18 ±

0.11‰ (2sd). Above this threshold, $\delta^{238/235}U$ values cluster around -0.09 ± 0.29‰ (2sd). The additional variability suggests that there may be an additional process that affects the magnitude and/or variability of $\delta^{238/235}U$ fractionation during reductive authigenic accumulation in carbonates. However, a larger data set and mechanistic study of this process are required before this hypothesis can be verified.

4.6.3 Possible Down Slope Trends

Although this study was not specifically designed to map down-slope trends, Figure 4.10 provides a preliminary analysis of trends from the samples available for this study. The strongest trend is a shift toward lower U, Mo, and Re concentrations with increasing distance from the platform margin. $\delta^{238/235}U$ may also display a similar trend, but the unusually high $\delta^{238/235}U$ values at Site 1003 and scarcity of the remaining data at Sites 1004 and 1005 strongly bias this result. These results are consistent with a model of enhanced authigenic accumulation of Mo, U, and Re at sites close to the platform due to higher organic carbon loading and dilution of allochthonus iron delivery by higher carbonate sedimentation rates, leading to sulfidic pore water conditions. Future studies of trace metal concentrations and isotopes along the Bahamas Transect could exploit precise correlations available between cores to separately identify spatial and temporal processes controlling trace metal variations along section and down core.

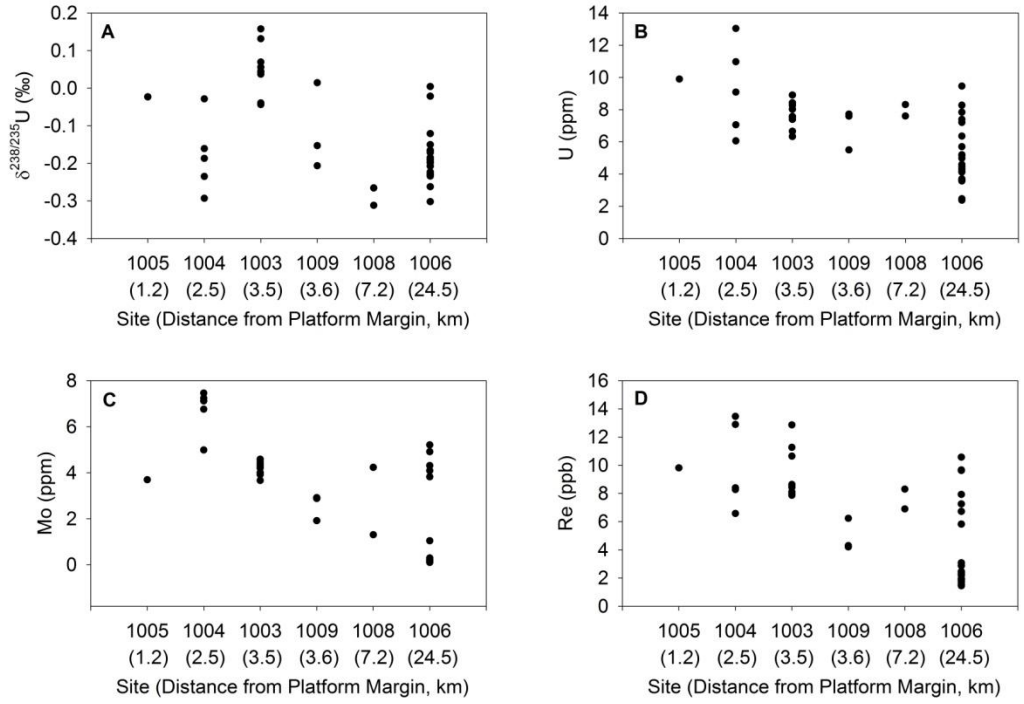

Figure 4.10. Down slope variations in geochemical parameters with increasing distances from the platform margin. (A) Variation in $\delta^{238/235}$U. (B-D) Variation in U, Mo, and Re concentrations. The horizontal axis provides the site number and distance from the platform margin.

4.7 Conclusions

Analysis of $\delta^{238/235}$U in bulk carbonate samples collected during ODP Leg 166 on the western margin of the Bahamas Bank revealed a range of -0.31 to 0.16‰. Notably, all of the 42 samples measured had $\delta^{238/235}$U values significantly heavier than that of modern seawater (-0.41‰, Weyer et al., 2008). The average $\delta^{238/235}$U of Site 1006 sediments is -0.16±0.15‰ (2sd). This value is significantly

heavier than seawater (-0.41‰) but is consistent with measurements of shallow bulk carbonate sediments collected via push cores (Chapter 3). This suggests that the primary fractionation of $\delta^{238/235}U$ in bulk carbonate sediments occurs syndepositionally and is characterized by a +0.2-0.4‰ offset from seawater that occurs due to the incorporation of isotopically heavy U(IV) via reductive authigenic accumulation of U from pore waters.

Down core profiles show little evidence for systematic post-depositional diagenetic alteration of $\delta^{238/235}U$ in sediments dating back to 780 ka, even in samples that show significant alteration of the Th/U system. However, at Site 1003 and in several other scattered samples, very heavy $\delta^{238/235}U$ values (~0-0.16‰) were observed. These samples demonstrate much heavier $\delta^{238/235}U$ values are sometime achievable under particular depositional or diagenetic conditions that are not currently well understood.

U, Mo, and Re concentrations appear to be controlled by reductive authigenesis from sediment pore waters, with preferential accumulation of U and Re under anoxic pore water conditions and accumulation of all three metals under sulfidic pore water conditions. Based on this interpretation, tentative Mo and U threshold concentrations at 0.5 ppm Mo and 5.5 ppm U are defined as the probable boundary between anoxic and sulfidic deposition in these sediments. Below these threshold values, measured $\delta^{238/235}U$ values appear more uniform with a 2sd variation of 0.11‰, while $\delta^{238/235}U$ values in samples associated with sulfidic pore waters show more variability with a 2sd of 0.29‰.

Finally, U, Mo, and Re concentrations, and possibly $\delta^{238/235}U$ values, show decreasing trends with distance from the platform margin. This suggests more proximal sites may have higher organic carbon loading and more reducing pore waters, leading to enhanced reductive accumulation of redox sensitive metals and possibly heavier $\delta^{238/235}U$ values. However, more work and a dedicated sampling strategy is required to eliminate the possibility that temporal variations might contribute to these apparent spatial trends.

Chapter 5

MOLYBDENUM ISOTOPE FRACTIONATION IN SHALLOW BAHAMIAN CARBONATE SEDIMENTS

5.1 Introduction

The marine geochemistry of molybdenum (Mo) is highly sensitive to the redox state of seawater, making it an attractive proxy for the reconstruction of paleoredox variations in the Earth's ocean (Algeo and Lyons, 2006; Emerson and Huested, 1991; Scott et al., 2008). One of most powerful ways of reconstructing the global marine paleoredox variations is through the use Mo isotopes (Anbar, 2004; Arnold et al., 2004; Dahl et al., 2011; Duan et al., 2010; Kendall et al., 2009; Kendall et al., 2011; Siebert et al., 2005; Wille et al., 2007). Because the residence time of Mo in seawater (~700 ka, Anbar, 2004) greatly exceeds ocean mixing timescales (~1500 yr), the isotopic composition of Mo is uniform throughout the open ocean (Nakagawa et al., 2012). In theory, this allows global average paleoredox conditions to be constructed from data at a single location, which is extremely useful when studying Precambrian time periods where it is difficult to convincingly establish the contemporaneous deposition of multiple locations.

To date, most Mo isotope paleoredox reconstructions are based on black shale lithologie that are thought to quantitatively capture seawater Mo and directly record the Mo isotope composition of seawater (Erickson and Helz, 2000; Gordon et al., 2009; Neubert et al., 2008). However, black shales are not ubiquitous in the geologic record and so our conception of ocean redox evolution

may be biased by the conditions of restricted marginal basins in which such shales are sometimes deposited (Arthur and Sageman, 1994). Furthermore, quantitative scavenging of Mo from the water column into sediments only occurs when the water column concentration of H_2S_{aq} exceeds 11 μM, under which conditions the soluble molybdate ion (MoO_4^{-2}) is converted to the particle-reactive tetrathiomolybdate (MoS^{-2}) on the time scale of several months (Erickson and Helz, 2000). Under anoxic, weakly sulfidic, or seasonally varying conditions, Mo isotopes can be fractionated during incorporation into sediments (Brucker et al., 2009; Gordon et al., 2009; Neubert et al., 2008; Siebert et al., 2006). To avoid this complication, shales are routinely screened using iron (Fe) speciation to identify persistently euxinic conditions of deposition prior to Mo isotope analysis (Gordon et al., 2009). However, while this screening process can identify euxinic deposition conditions, it is difficult to prove that any particular threshold guarantees sufficient H_2S_{aq} to quantitatively scavenge Mo.

Recent work has suggested that the incorporation of Mo into marine carbonate sediments may directly record the Mo isotope composition of seawater, thus avoiding the need to demonstrate highly euxinic depositional conditions in shales (Voegelin et al., 2009). Furthermore, carbonates are abundant in the geologic record and are commonly deposited along open ocean margins. Because of this, a well-established Mo isotope proxy based on variations in carbonate rocks would be highly complementary to existing black-shale based records. Indeed, several authors have already attempted to apply this concept to Archean carbonates (Czaja et al., 2012; Voegelin et al., 2010).

However, in order to convincingly interpret Mo isotope variations in the carbonate rock record, it is important to first address the diagenetic processes that might alter Mo isotopes during sedimentation and subsequent deep burial. These processes may occur on a variety of timescales ranging from weeks to millions of years, and may vary from location to location. The goal of this study is to provide an initial reconnaissance of the early diagenetic controls on Mo incorporation into bulk carbonate sediments and to determine which processes, if any, fractionate Mo isotopes during deposition and early burial.

5.2 Materials and Methods

Samples for this study were collected in the southern Exuma Islands, Bahamas, between Lee Stocking and Little Darby Islands in January and July of 2011. A complete description of site locations, samples, and analytical techniques is provided in Chapter 3. A brief overview is provided below.

5.2.1 Sampling Sites and Materials

The sample set for this study consisted of a wide variety of primary carbonate precipitates collected throughout the study region, along with solid phase and pore water samples from 4 shallow push cores (~30-50 cm in length). Core 1 was collected in a shallow turtle grass flat (*Thalassia testudium*), and consisted of 0.1 mm-1 mm carbonate sand with abundant *Halimeda* fragments, and visible amounts of organic matter including *T. testudium* rhizomes and leaves. The area included a large number of shrimp (*Callianassa sp.*) mounds and

burrows, although the core was collected to avoid these features. Core 2 was collected approximately 100 meters southeast of Core 1 on a tidal flat devoid of bottom cover. Sediment consisted of <1mm carbonate sand that was homogenous throughout the core. Core 3 was collected in a *T. testudium* flat similar to Core 1, but in deeper water (~4 m) and in the absence of *Callianassa* burrows. Sediment at this site was similar to that of Core 1 but lacked *Halimeda* fragments. Core 4 was collected in a tidal pond on Norman's Pond Cay, which is connected to the ocean through a 1 m deep manmade channel that was used to facilitate salt production from the 17^{th}-19^{th} centuries (Hein and Winsborough, 2001; Wicklund et al., 1991). Sediment in Core 4 consisted of fine dark-colored carbonate mud, interspersed with larger carbonate sand skeletal fragments, and several intervals of buried microbial laminates. This site was chosen as an organic-rich end-member.

Pore water samples were collected using trace-metal-clean Rhizon pore water samplers, both *in situ* by inserting the samplers directly into the sediment in the field, and *ex situ* via small holes drilled in the core liners upon return to the field laboratory. As discussed in Chapter 3, anaerobic sampling facilities were unavailable at the time of sampling. As a result, despite extreme caution, it is likely that samples were inevitably exposed to a small amount of atmospheric contamination during sampling. The primary effect of this appears to be artificially high pore water trace metal concentrations in some samples due to rapid reoxidation of reduced trace metal rich phases. A complete discussion of pore water sampling, analysis, and results is provided in Chapter 3.

5.2.2 Analytical Methods

Molybdenum isotope measurements were made in the W. M. Keck Laboratory for Environmental Biogeochemistry at Arizona State University. Prior to analysis, sediments were dried at 100°C and homogenized using a ball mill equipped with silicon carbide mortars. Sample aliquots (1.0 g) were ashed at 750°C for 24 hours to remove organics and then dissolved in 10 mL of 3 M nitric acid. Following dissolution, major and trace element concentrations were determined on sample aliquots at 1:2000 dilution using an Thermo X-series 2 quadrapole ICP-MS. Preliminary Mo concentrations were used to prepare aliquots of core samples containing >75 ng Mo, spiked with a ^{97}Mo-^{100}Mo double spike at a spike:sample molar ratio of ~2. Spiked samples were dried down, reconstituted in 2 mL of 0.5 M HCl and loaded onto cation exchange columns containing 2 mL of previously-cleaned cation exchange resin (BioRad AG 50WX8, 200‑400 mesh). The initial eluate was collected, and residual Mo was eluted using additional 4 ml of 0.5 M HCl, leaving behind Fe on the column. Following cation columns, the HCl molarity of the samples was brought up to 4 M with the addition of 2.6 mL of 12.1 M HCl. The resulting solution was loaded onto anion exchange columns containing 1 ml of previously cleaned anion exchange resin (BioRad AG 1X8, 200‑400 mesh). Matrix elements were eluted in an additional 5 ml 4 M HCl. Residual Fe and Zr were eluted using 2 mL of 2 M HNO_3, and finally the Mo was eluted and collected in an additional 6 mL of 2 M HNO_3. Following column chemistry, samples were repeatedly treated with a mixture of 0.5 mL concentrated HNO_3 and 0.2 mL 32% H_2O_2 repeatedly (3X) to oxidize any

organic materials leached from the ion exchange resins. Mo isotopes ($^{98}Mo/^{95}Mo$) and final Mo concentrations (via isotope dilution) were determined on a Thermo Neptune MC-ICP-MS equipped with an ESI Apex Q desolvating nebulizer. The double spike equations were solved using a non-linear optimization approach coded in MATLAB. Isotope data are reported as:

$$\delta^{98/95}Mo\ (‰) = 1000 \times [(^{98}Mo/^{95}Mo_{sample}) / (^{98}Mo/^{95}Mo_{standard}) - 1] \quad \text{Eq. 5.1}$$

relative to the "RochMo2" in-house laboratory standard (Johnson Matthey Specpur, Lot #802309E). Seawater has a $\delta^{98/95}Mo$ of 2.3‰ on this scale (Arnold et al., 2004; Barling and Anbar, 2004; Neubert et al., 2008; Siebert et al., 2003). Analytical precision was determined as $\pm 2\sigma$ of three repeat measurements, and averaged 0.05‰ with a range of 0.01-0.24‰.

5.3 Results

5.3.1 Mo Concentrations in Primary Precipitates

Compared to the average composition of the upper crust, which contains ~ 1.5 ppm Mo, Mo concentrations in primary precipitates were generally low, ranging between 0.1-0.2 ppm (Fig. 5.1, Table 5.1; Taylor and McLennan, 1995). Concentrations were lower in clean carbonate samples containing little associated organic matter (corals, mollusk shells, ooids) and were elevated in algae samples containing visible associated organic matter.

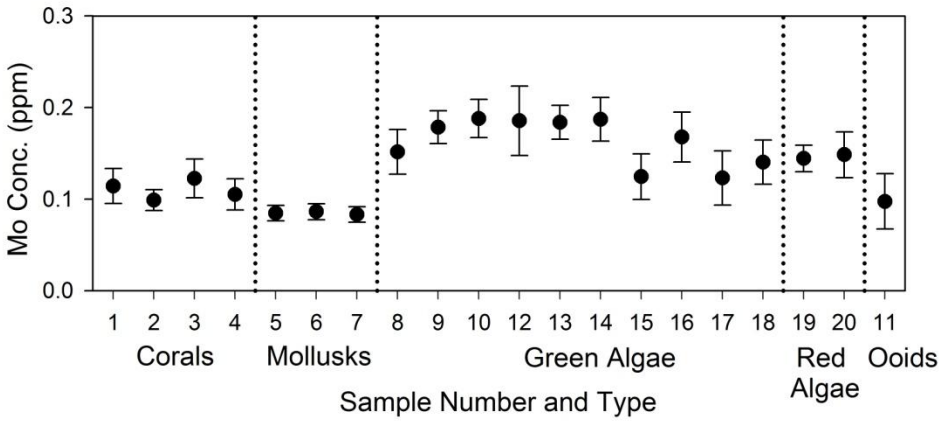

Fig. 5.1. Mo concentrations in a variety of biological and abiological primary carbonate precipitates from the Bahamas. See Table 5.1 for specific sample information.

Although still low compared to average continental crust, the Mo concentrations measured in this study are significantly higher than concentrations determined by Voegelin et al. (2009), who found Mo concentrations ranging from 0.010-0.120 ppm in a variety of primary carbonate precipitates and carbonate sands from around the world. This discrepancy cannot be explained by detrital contamination, as the maximum detrital contribution to these samples calculated from the measured Al concentrations and a crustal Mo:Al ratio of 1.1 ppm/15.4 wt% is ~3% (crustal Mo:Al ratio from Voegelin et al., 2009). One possible explanation for the discrepancy is the difference in analytical techniques. Whereas, Voegelin et al. (2009) used isotope dilution to measure Mo concentrations in samples purified of Ca, primary precipitate Mo concentrations in this study were determined using Q-ICP-MS on 1:2000 dilutions of digested

Table 5.1. Mo concentrations in primary carbonate precipitates.

Sample #	Sample Description	Primary Mineralogy	Mo Conc. (ppm)	2sd error
Corals				
1	*Diploria strigosa*	Arag.	0.11	0.02
2	*Siderastrea radians*	Arag.	0.10	0.01
3	*Porites divaricata*	Arag.	0.12	0.02
4	*Porites asteroids*	Arag.	0.11	0.02
Mollusks				
5	*Tellina listeri*	Arag.	0.08	0.01
6	*Codakia orbicularis*	Arag.	0.09	0.01
7	*Cittarium pica*	Arag.	0.08	0.01
Green Algae				
8	*Acetabularia crenulata* (whole)	Arag.	0.15	0.02
9	*Acetabularia crenulata* (stalk)	Arag.	0.18	0.02
10	*Acetabularia sp.* (head)	Arag.	0.19	0.02
12	*Rhipocephalus phoenix* (stalk)	Arag.	0.19	0.04
13	*Rhipocephalus phoenix* (leaves)	Arag.	0.18	0.02
14	*Halimeda incrassate*	Arag.	0.19	0.02
15	*Penicillus capitatus* (stalk, collected dead)	Arag.	0.12	0.02
17	*Penicillus capitatus* (stalk, collected live)	Arag.	0.17	0.03
18	*Penicillus capitatus* (head, collected live)	Arag.	0.12	0.03
Red Algae				
19	*Neogoniolithon strictum* (Collected Dead)	HMC	0.15	0.02
20	*Neogoniolithon strictum* (Collected Live)	HMC	0.18	0.02
Ooids				
11	Ooids, Lee Stocking Island	Arag.	0.10	0.03

samples. Given the low Mo concentration and high Ca:Mo ratios in the primary precipitate samples, it is difficult to rule out the presence of an unidentified interference. Comparison of measurements of the Mo concentration in a single *Porites* coral sample by isotope dilution and Q-ICP-MS returned 0.069 ppm and

0.093 ppm respectively. Although indicative a significant offset, this comparison seems unable to fully explain the observed discrepancy. Regardless of possible analytical limitations, both data sets agree that Mo concentrations in primary carbonate precipitates are very low (< 0.2 ppm).

5.3.2 Pore Water Chemistry

Pore water samples were analyzed from four short push cores taken throughout the study region to determine chemical conditions during early diagenesis. A complete discussion of the pore water chemistry from these cores can be found in Chapter 3, while results pertinent to this study are summarized here.

Pore water sulfide profiles indicated significant (27-1000 μM) total sulfide concentrations ($\sum H_2S = [H_2S_{aq}] + [HS^-]$) in all cores at the even the shallowest sampling depth (2-3 cm, Fig. 5.2). Total sulfide concentrations generally increased down core, with some evidence for a local sulfide maximum between 10-15 cm. Extensive respiration was also indicated by a decrease in pore water pH from bottom water values of ~8.0 to 7.0-7.1 at >10cm depth.

Because the equilibrium between hydrogen sulfide (H_2S_{aq}) and the bisulfide ion (HS^-) is sensitive to changes in this pH range with important consequences for Mo speciation, the contribution of H_2S_{aq} to total sulfide was calculated using the apparent equilibrium constant for seawater (Millero et al., 1988). Measured pH values on the NBS scale were converted to the seawater

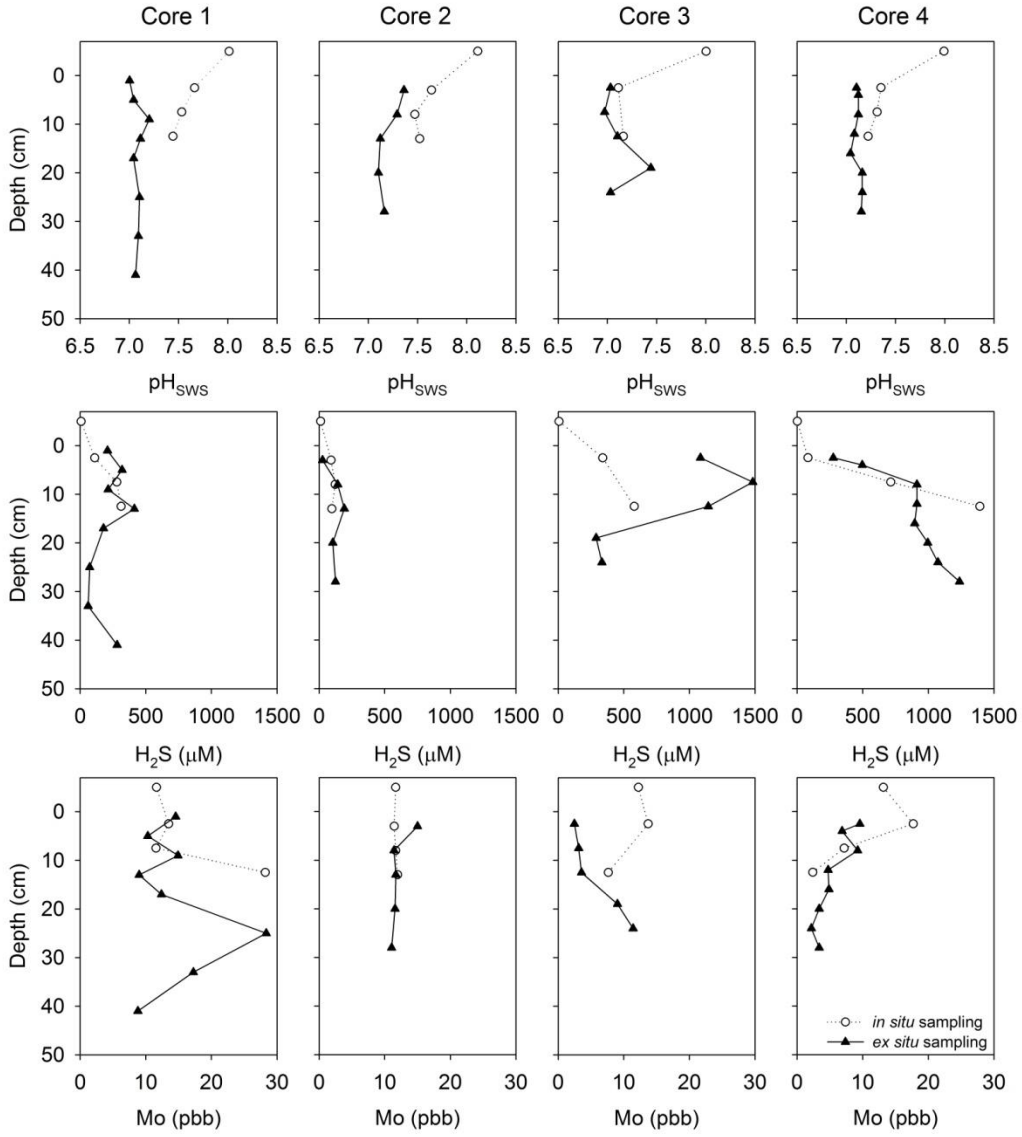

Figure 5.2. Pore water pH, $\sum H_2S$ and dissolved Mo concentrations.

scale for use in this relation assuming a proton activity (f_H) of 0.729 (Perez and Fraga, 1987).

As a result of the high $\sum H_2S$ concentrations and relatively low pH, calculated H_2S_{aq} concentrations were generally high, ranging between ~20-300 μM in Cores 1, 3 and 4 (Table 5.2). H_2S_{aq} concentrations in excess of 11 μM are

Table 5.2. Summary of pore water geochemistry.

Sample	Depth (cm)	Sal. (ppt)	pH_{SWS}	$\sum H_2S$ (μM)	H_2S_{aq} (μM)	Mo (ppb)	Fe (ppb)
Estimated Err. (1sd)	2	0.5	0.05	10	3	10%	10%
Core 1 Bottom Water	-5	37.0	8.01	8	0	11.6	4.7
Core 1 *in situ* 1	2.5	37.5	7.66	111	5	13.5	3.3
Core 1 *in situ* 2	7.5	38.0	7.53	280	16	11.6	11.5
Core 1 *in situ* 3	12.5	38.0	7.44	313	21	28.2	5.5
Core 1 *ex situ* 1	**1**	38.0	7.00	209	35	14.6	101.2
Core 1 *ex situ* 2	**5**	38.0	7.04	320	49	10.3	3.3
Core 1 *ex situ* 3	**9**	37.5	7.20	213	24	14.9	2.5
Core 1 *ex situ* 4	**13**	37.0	7.11	413	55	9.0	3.4
Core 1 *ex situ* 5	**17**	37.5	7.04	178	27	12.4	4.3
Core 1 *ex situ* 6	**25**	38.0	7.10	73	10	28.4	3.0
Core 1 *ex situ* 7	**33**	37.5	7.09	61	9	17.2	1.9
Core 1 *ex situ* 8	**41**	38.0	7.06	282	42	8.8	18.0
Core 2 Bottom Water	-5	37.5	8.11	12	0	11.7	2.4
Core 2 *in situ* 1	3	37.5	7.64	92	4	11.4	12.3
Core 2 *in situ* 2	8	37.0	7.47	123	8	11.7	5.5
Core 2 *in situ* 3	13	37.0	7.52	98	6	12.0	17.3
Core 2 *ex situ* 1	**3**	37.0	7.36	27	2	15.0	2.2
Core 2 *ex situ* 2	**8**	37.5	7.29	142	13	11.4	3.9
Core 2 *ex situ* 3	**13**	37.5	7.12	192	25	11.7	2.0
Core 2 *ex situ* 4	**20**	37.5	7.10	104	14	11.6	2.6
Core 2 *ex situ 5*	**28**	37.5	7.16	125	15	11.0	2.2
Core 3 Bottom Water	-5	37.5	8.00	8	0	12.2	1.3
Core 3 *in situ* 1	2.5	38.0	7.11	340	46	13.7	8.0
Core 3 *in situ* 3	12.5	38.0	7.16	580	70	7.6	5.1
Core 3 *ex situ* 1	**2.5**	38.0	7.03	1084	170	2.5	5.6
Core 3 *ex situ* 2	**7.5**	37.5	6.97	1483	261	3.1	5.2
Core 3 *ex situ* 3	**12.5**	37.5	7.10	1144	157	3.6	63.1
Core 3 *ex situ* 4	**19**	37.5	7.44	290	20	9.12	8.3
Core 3 *ex situ* 5	**24**	37.5	7.03	334	52	11.4	12.2
Core 4 Bottom Water	-5	39.0	7.99	2	0	13.1	11.7
Core 4 *in situ* 1	2.5	39.0	7.35	83	7	17.7	10.4
Core 4 *in situ* 2	7.5	39.0	7.31	714	64	7.2	17.8
Core 4 *in situ* 3	12.5	39.0	7.22	1393	150	2.4	11.0
Core 4 *ex situ* 1	**2.5**	38.0	7.10	276	38	9.6	4.4
Core 4 *ex situ* 2	**4**	38.5	7.12	497	65	6.9	12.6
Core 4 *ex situ* 3	**8**	38.0	7.12	913	120	9.2	4.9
Core 4 *ex situ* 4	**12**	38.0	7.08	913	130	4.7	5.9
Core 4 *ex situ* 5	**16**	38.0	7.04	896	138	4.9	147.9
Core 4 *ex situ* 6	**20**	39.0	7.16	996	121	3.4	3.1
Core 4 *ex situ* 7	**24**	40.0	7.16	1073	130	2.2	4.5
Core 4 *ex situ* 8	**28**	40.5	7.15	1238	153	3.4	4.8

important for the conversion of soluble MoO_4^{-2} to particle reactive MoS_4^{-2}, suggesting that Mo scavenging should be an important process in Cores 1,2, and 4 (Erickson and Helz, 2000). Core 2, taken in a tidal flat, has lower H_2S_{aq} ranging between 3-30 μM, and Mo scavenging is expected to be less pronounced in this core.

Pore water Mo profiles were erratic, most likely due to remobilization of trace metals into pore water by inadvertent O_2 contamination of the pore water (discussed in Chapter 3). Nevertheless, significant depletion of Mo concentrations below seawater values (~10.2 ppb) in cores 3 and 4 provides evidence for a local Mo sink within the sediment. Elevated Mo concentrations in Core 1 are probably an artifact of atmospheric contamination during sampling, but potentially indicate the presence of an authigenic sedimentary Mo pool that is sensitive to reoxidation. Mo pore water concentrations in Core 2, which contained the lowest H_2S_{aq} concentrations, display little variation and are similar to that of seawater.

5.3.3 Mo Concentrations and $\delta^{98/95}$Mo in Core Samples

Mo concentrations in core samples were quite variable between cores (Fig. 5.3, Table 5.3). Core 2 samples were similar to primary carbonate precipitates (0.099-0.170 ppm), while samples from cores 1, 3, and 4 have Mo concentrations 10-100 times higher (1.8-27.6 ppm).

$\delta^{98/95}$Mo varied between 1.07 and 2.5‰, with strong variations between sites and more modest variations within cores. In general, cores with strongly elevated Mo concentrations also display $\delta^{98/95}$Mo values close to seawater (2.3‰),

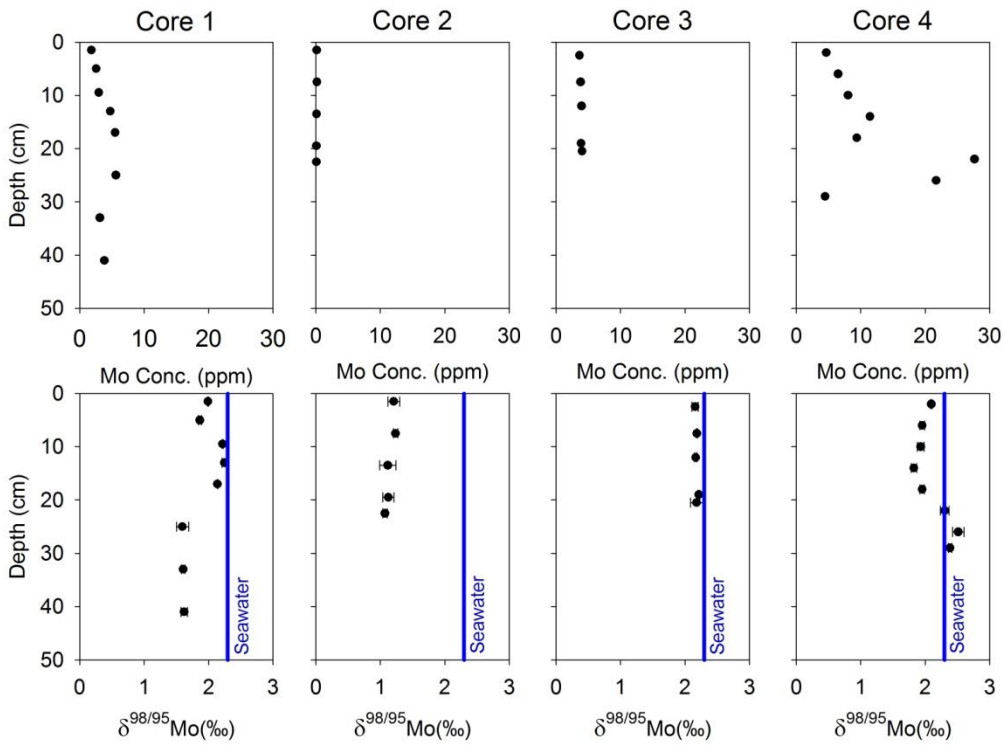

Figure 5.3. Solid phase Mo concentrations and $\delta^{98/95}$Mo variations in shallow sediment cores. Except were visible, error bars are smaller than the symbol size.

while Core 2 with low Mo concentrations is significantly lighter (1.07-1.24‰). This pattern is most clearly seen by comparing the results from Cores 2 and 3 where down core variation in $\delta^{98/95}$Mo is negligible. Cores 1 and 4 generally have heavy Mo isotope compositions approaching or even exceeding that of seawater (1.6-2.5‰) but there is significant down core variation that may reflect time-dependent variations in depositional conditions or post-depositional alteration of $\delta^{98/95}$Mo by processes such as bioturbation.

Table 5.3. Solid-phase Mo concentration and isotope data from sediment cores.

	Depth (cm)	Mo Conc. (ppm)	$\delta^{98/95}$Mo (‰)	2σ err
Core 1				
	0-3	1.844	1.99	0.01
	4-6	2.579	1.87	0.02
	8-11	2.989	2.22	0.01
	12-14	4.760	2.25	0.04
	16-18	5.523	2.14	0.01
	24-26	5.636	1.60	0.09
	32-34	3.148	1.61	0.03
	40-42	3.854	1.62	0.05
Core 2				
	0-3	0.147	1.21	0.09
	6-9	0.170	1.24	0.03
	12-15	0.123	1.12	0.13
	18-21	0.099	1.13	0.09
	21-24	0.114	1.07	0.03
Core 3				
	1-4	3.644	2.16	0.05
	6-9	3.829	2.19	0.01
	10-14	3.974	2.17	0.02
	17-21	3.899	2.22	0.01
	19-22	4.064	2.18	0.10
Core 4				
	0-4	4.678	2.10	0.01
	4-8	6.500	1.96	0.04
	8-12	8.050	1.93	0.05
	12-16	11.448	1.83	0.04
	16-20	9.425	1.95	0.03
	20-24	27.680	2.30	0.07
	24-28	21.703	2.51	0.09
	28-30	4.486	2.39	0.03

5.4 Discussion

Molybdenum isotope variation in carbonates could be a useful tool for reconstructing paleoredox variations in ancient oceans. However, before such variations can be interpreted with confidence, it is important to assess and understand the diagenetic processes that might alter the $\delta^{98/95}$Mo of carbonate sediments both during initial deposition and longer term burial. The goal of this study is to examine the processes effecting the $\delta^{98/95}$Mo of bulk sediment occurring during initial sediment deposition and shallow burial (<50 cm) in shallow water carbonate settings (<5 m depth).

5.4.1 Molybdenum Concentrations

To establish baseline Mo concentrations in primary carbonate precipitates, the Mo concentrations of a wide variety of corals, mollusks, red and green algae, and ooids were measured and found to be consistently less than ~0.2 ppm.

Similar Mo concentrations were found only in 1 of the 4 cores collected. Core 2, collected in a shallow tidal flat setting, contained between 0.099-0.170 ppm Mo. In sharp contrast, the remaining 3 cores contained much higher Mo concentrations ranging from 1.84-27.6 ppm Mo, representing a 10-100 fold enrichment above concentrations found in primary carbonate precipitates. The contribution from detrital Mo to core samples was estimated from measured Al concentrations following Voegelin et al (2009) and found to represent < 1% of the total concentration.

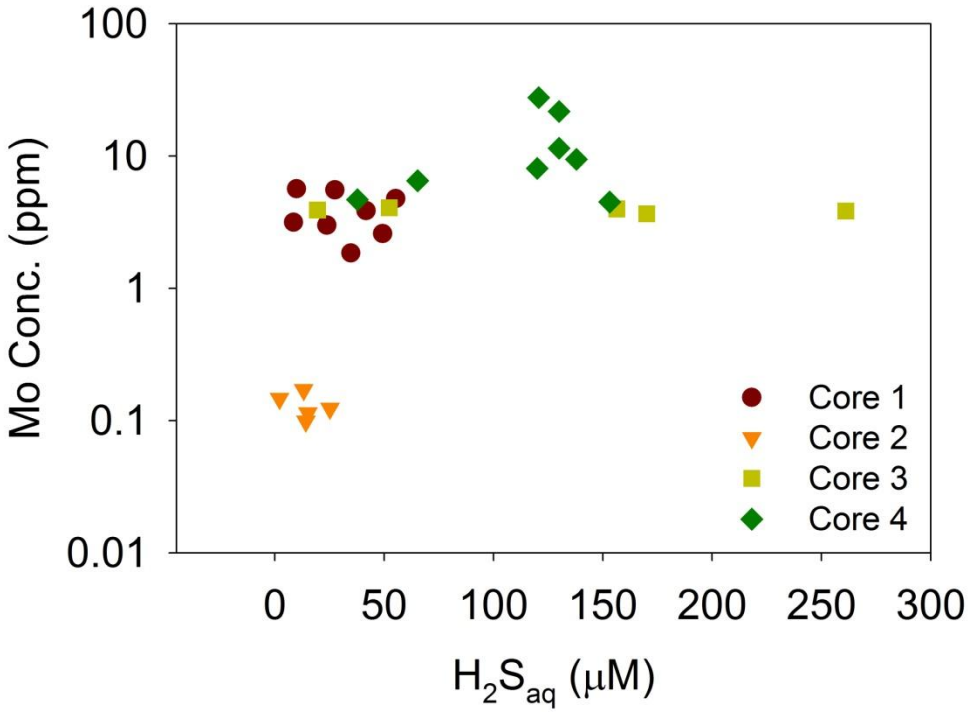

Figure 5.4. Crossplot of the Mo concentrations in core samples with calculated H_2S_{aq} concentrations. Note that the Mo concentration axis is a log scale.

A cross plot of Mo concentrations versus pore water H_2S_{aq} demonstrates a clear separation of Core 2 from other sites (Fig. 5.4). This pattern of variation is consistent with the hypothesis that authigenic accumulation of Mo is controlled by H_2S_{aq} concentrations and the formation of thiomolybdate species (Erickson and Helz, 2000; Helz et al., 1996). Thiomolybdates are thought to be scavenged from solution by absorption to sediment particles, especially organic matter (Algeo and Lyons, 2006). Core 2 also contained the lowest amount of macroscopic organic detritus, which may further contribute to the observed trends in Figure 5.4.

These results demonstrate that a large amount of authigenic Mo can be accumulated in shallow water carbonate sediments, with concentrations

approaching or exceeding those typically associated with siliclastic sediments (McManus et al., 2006; Morford et al., 2005; Neubert et al., 2008). Because of this, the implicit assumption made by previous authors that Mo in carbonates reflects Mo incorporated during primary carbonate precipitation may be incorrect, at least in shallow water settings (Czaja et al., 2012; Voegelin et al., 2010; Voegelin et al., 2009).

5.4.2 Molybdenum Isotopes

In order to reconstruct seawater $\delta^{98/95}$Mo from measured variations in carbonate sediments, it is essential to understand what processes, if any, fractionate $\delta^{98/95}$Mo during early diagenesis. For example, carbonate sediment pore waters commonly contain sulfide at micromolar to millimolar concentrations that are sufficient to strongly affect Mo geochemistry. The formation of thiomolybdate species is thought to fractionate Mo isotopes in sulfidic environments when capture of the resulting tetrathiomolybdate (MoS_4^{-2}) is not quantitative (Dahl et al., 2010; Erickson and Helz, 2000; Nagler et al., 2011; Neubert et al., 2008; Tossell, 2005).

The results of this study suggest some carbonate sediments directly track seawater $\delta^{98/95}$Mo, while others demonstrate a variable offset that ranges up to 1.3‰ lighter than seawater. The magnitude of the offset appears to be controlled by the local depositional environment, and can vary on a spatial scale of 100 m, as illustrated by the strong difference between Cores 1 and 2 that collected within the same embayment, but with very different bottom cover. Core 1 was collected

in a turtle grass (*Thalassia testudium*) flat that was rich in organic matter and contained high levels of pore water sulfide, while Core 2 was collected along a tidal flat mostly barren of vegetation and containing much lower levels of pore water sulfide. Core 3, collected in turtle grass flat at a depth of 4 meters, contained the highest pore water sulfide concentrations measured, and offers the most consistent, direct record of seawater $\delta^{98/95}$Mo.

The factors affecting downcore variations in $\delta^{98/95}$Mo in Cores 1 and Core 4 are difficult to constrain based on the available data. Numerous shrimp mounds and burrows (*Callianassa sp.*) were present close to Core 1. While care was taken to avoid these burrows, it is likely that intensive bioturbation and exposure of sediment to oxygen through burrow ventilation may explain the difference between cores 1 and 3, which were otherwise similar. The very high Mo concentrations in Core 4, collected in an anthropogenically-influenced tidal pond, are most easily explained by tidal pumping of seawater through these permeable, highly-reducing sediments. In this framework, $\delta^{98/95}$Mo variations might be driven by variation in the hydrological controls on tidal pumping, either through anthropogenic manipulation of the pond level or natural accumulation and thickening of the soft sediment package. Distinct horizons in this core, including buried microbial laminations and layers rich in shell debris, suggest that depositional conditions may have varied substantially from present conditions. Changes in depositional conditions could result in $\delta^{98/95}$Mo variations through impacts on the pore water H_2S_{aq} concentrations or by altering the extent to which Mo was quantitatively scavenged into these sediments.

5.4.3 The Role of Pore Water H_2S in the Mo Geochemistry of Carbonate Sediments

Previous studies of Mo isotope variation in carbonates have emphasized the role of Mo incorporation in primary carbonate precipitates. Voegelin et al. (2009) surveyed $\delta^{98/95}$Mo across a wide range of modern ooids, carbonate sands, and biological precipitates and found that $\delta^{98/95}$Mo ranged from 1-2.3‰ with consistently low Mo concentrations (<0.2 ppm). This is similar to results from Core 2 in this study, where Mo is <0.2 ppm and $\delta^{98/95}$Mo is between 1.07-1.24‰.

However, 3 of 4 cores in this study contain much higher bulk Mo concentrations accompanied by heavier $\delta^{98/95}$Mo values, approaching or exceeding that of seawater. In these cores, Mo incorporation during primary carbonate precipitation appears to be much less important than authigenic Mo accumulation during the initial deposition of sediments. The primary difference between the low-Mo core, Core 2, and the 3 high-Mo cores appears to be the concentration of pore water sulfide (Fig. 5.2), and particularly the concentration of H_2S_{aq} (Table 5.2).

Mo geochemistry is strongly affected by the conversion of molybdate (MoO_4^{-2}) to tetrathiomolybdate (MoS_4^{-2}) in the presence of sufficient amounts of H_2S (Erickson and Helz, 2000; Helz et al., 1996). This process occurs through a series of substitutions in which oxygen atoms in molybdate are serially replaced by sulfur, leading to a series of mono-, di-, tri-, and tetrathiomolybdate. However, because the three intermediate species have negligible stability fields, the formation of MoS_4^{-2} occurs as a geochemical switch point when H_2S_{aq} exceeds 11

μM (Erickson and Helz, 2000). Tetrathiomolybdate is thought to be rapidly and quantitatively scavenge to organic matter in sediments, resulting in high sediment Mo concentrations with little or no isotopic fractionation from seawater (Algeo and Lyons, 2006; Dahl et al., 2010; Helz et al., 1996; Nagler et al., 2011; Neubert et al., 2008).

For a known H_2S_{aq} concentration, the speciation of thiomolybdates in seawater can be readily calculated. The speciation equations are as follows:

$$\frac{[MoO_4^{2-}]}{\sum Mo^{VI}} = \left(1 + K_{01}[H_2S_{aq}] + K_{01}K_{12}[H_2S_{aq}]^2 + K_{01}K_{12}K_{23}[H_2S_{aq}]^3 + K_{01}K_{12}K_{23}K_{34}[H_2S_{aq}]^4\right)^{-1} \quad \text{Eq. 5.1}$$

$$\frac{[MoO_3S_1^{2-}]}{\sum Mo^{VI}} = \left(\frac{1}{K_{01}[H_2S_{aq}]} + 1 + K_{12}[H_2S_{aq}]^1 + K_{12}K_{23}[H_2S_{aq}]^2 + K_{12}K_{23}K_{34}[H_2S_{aq}]^3\right)^{-1} \quad \text{Eq. 5.2}$$

$$\frac{[MoO_2S_2^{2-}]}{\sum Mo^{VI}} = \left(\frac{1}{K_{01}K_{12}[H_2S_{aq}]^2} + \frac{1}{K_{12}[H_2S_{aq}]} + 1 + K_{23}[H_2S_{aq}] + K_{23}K_{34}[H_2S_{aq}]^2\right)^{-1} \quad \text{Eq. 5.3}$$

$$\frac{[MoO_1S_3^{2-}]}{\sum Mo^{VI}} = \left(\frac{1}{K_{01}K_{12}K_{23}[H_2S_{aq}]^3} + \frac{1}{K_{12}K_{23}[H_2S_{aq}]^2} + \frac{1}{K_{23}[H_2S_{aq}]} + 1 + K_{34}[H_2S_{aq}]\right)^{-1} \quad \text{Eq. 5.4}$$

$$\frac{[MoS_4^{2-}]}{\sum Mo^{VI}} = \left(\frac{1}{K_{01}K_{12}K_{23}K_{34}[H_2S_{aq}]^4} + \frac{1}{K_{12}K_{23}K_{34}[H_2S_{aq}]^3} + \frac{1}{K_{23}K_{34}[H_2S_{aq}]^2} + \frac{1}{K_{34}[H_2S_{aq}]} + 1\right)^{-1} \quad \text{Eq. 5.5}$$

where K_{01}, K_{12}, K_{23} and $K_{34} = 10^{5.19}$, $10^{4.80}$, $10^{5.00}$, and $10^{4.88}$, respectively (25°C, I = 0.8-2.22, Erickson and Helz, 2000).

By combining the predicted thiomolybdate speciation with the isotopic fractionation for each transition, it is possible to calculate the expected equilibrium $\delta^{98/95}$Mo of each molybdate species. Based on quantum mechanical modeling, Tossel (2005) predicted that the equilibrium $\delta^{98/95}$Mo of dithiomolybdate and tetrathiomolybdate should be -3.3‰ and -6.7‰ lighter than molybdate. Dahl et al. (2010) later extrapolated these results to mono- and

trithiomolydate, assuming that each successive sulfur replacement results in a -1.7‰ shift in $\delta^{98/95}$Mo. Based on these assumptions, the $\delta^{98/95}$Mo of molybdate can be calculated:

$$\delta^{98/95}MoO_4^{2-} = \delta^{98/95}Mo_{SW} + \Delta_S \frac{[MoO_3S_1^{2-}]}{\sum Mo^{VI}} + 2\Delta_S \frac{[MoO_2S_2^{2-}]}{\sum Mo^{VI}} + 3\Delta_S \frac{[MoO_1S_3^{2-}]}{\sum Mo^{VI}} + 4\Delta_S \frac{[MoS_4^{2-}]}{\sum Mo^{VI}} \quad \text{Eq. 5.6}$$

where $\delta^{98/95}Mo_{SW}$ is the total isotopic composition of all Mo species in seawater (~2.3‰) and Δ_S is isotopic fractionation associated with each sulfidation step (-1.7‰). The equilibrium isotopic compositions of the remaining thiomolybdate species are related by:

$$\begin{aligned} \delta^{98/95}MoO_4^{2-} &= \delta^{98/95}MoO_3S_1^{2-} + \Delta_S \\ &= \delta^{98/95}MoO_2S_2^{2-} + 2\Delta_S \\ &= \delta^{98/95}MoO_1S_3^{2-} + 3\Delta_S \\ &= \delta^{98/95}MoS_4^{2-} + 4\Delta_S \end{aligned} \quad \text{Eq. 5.7}$$

The results of these calculations are plotted in Figure 5.5 and demonstrate two important points. Although there is clearly a "switch point" between MoO_4^{2-} and MoS_4^{2-} at 11 μM H_2S_{aq}, tetrathiomolybdate does not become the dominate species until 23.5 μM H_2S_{aq}, more than twice the canonical value, and only becomes the predominant species (>90% of total Mo) at H_2S_{aq} concentrations of 130 μM (Fig. 5.5a). This result has important implications for Mo isotopes as well (Fig. 5.5b). As a result of the extended transition at the switch point, tri- and tetrathiomolybdate remain significantly light compared to the Mo average pool until H_2S_{aq} exceed 20 μM.

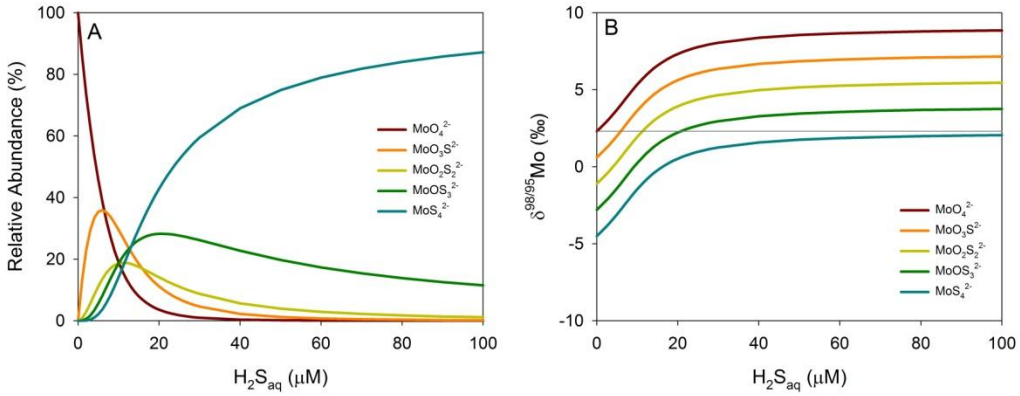

Figure 5.5. Thiomolybdate speciation diagram and equilibrium isotopic composition in seawater. (A) Relative abundance of each Mo species as a function of H_2S_{aq} concentration at equilibrium based on equilibrium constants in Erickson and Helz (2000). (B) Equilibrium isotopic composition of each Mo species as a function of H_2S_{aq} given a total Mo isotopic composition of 2.3‰ (gray horizontal line) and assuming a 1.7‰ offset between each species (Dahl et al., 2010; Nagler et al., 2011; Tossell, 2005).

The results of these calculations are strikingly similar to the relationship between $\delta^{98/95}$Mo and H_2S_{aq} in our core samples (Fig. 5.6). At low H_2S_{aq} concentrations (below ~20 μM), $\delta^{98/95}$Mo values are lighter than seawater and consistent with values measured in primary carbonate precipitates (Voegelin et al., 2009). At higher H_2S_{aq} concentrations, $\delta^{98/95}$Mo values approach those of seawater values as authigenic Mo enrichment via uptake to sediments becomes the dominant process. The calculated equilibrium $\delta^{98/95}$Mo values for tri- and tetrathiomolybdate closely bound the observed data and suggests that equilibrium

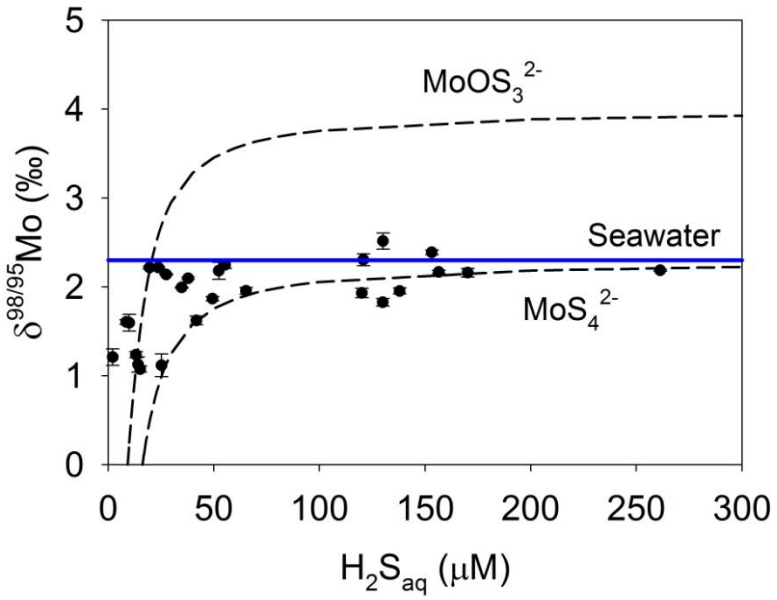

Figure 5.6. Relationship between $\delta^{98/95}$Mo of bulk carbonates sediments and pore water H_2S_{aq}. The blue line indicates the Mo isotopic composition of open ocean seawater. Dashed black lines indicated the calculated isotope composition of tri- and tetrathiomolybdate, assuming that the isotopic composition of the total Mo pool is 2.3‰ (see text for details). Error bars indicated the 2σ uncertainty of replicate measurements.

partitioning among thiomolybdates controls the isotopic composition of Mo sequestered in these cores.

Recently, Helz et al. (2011) proposed that the dominant process responsible for scavenging Mo from solution was the formation of a novel Fe-Mo-S mineral with a composition similar to $FeMo_{0.6}S_{2.8}$. A precipitate with similar composition has been previously observed in laboratory experiments

(Helz et al., 1996). Helz et al. (2011) used *in situ* observations to constrain the stoichiometry and solubility product of this precipitate. The suggested stoichiometry for this reaction is:

$$FeMo_{0.6}S_{2.8} + 0.8H^{+} \rightleftharpoons Fe^{2+} + 0.6MoS_4^{2-} + 0.4H_2S_{aq} \qquad \text{Eq. 5.8}$$

for which the solubility product is defined:

$$Q_{FeMoS} = \frac{\left[aFe^{2+}\right]\left[aMoS_4^{2-}\right]^{0.6}\left[H_2S_{aq}\right]^{0.4}}{10^{-0.8pH}} \qquad \text{Eq. 5.9}$$

where [aX] denotes the activity of species X. The equilibrium solubility product for this species was estimated to be $K_{sp} = 10^{-8.3\pm0.7}$ (Helz et al., 2011).

In order to evaluate the potential significance of this reaction at the sites in this study, the speciation calculations detailed in Helz et al. (2011) were repeated for the pore water chemistry in this study using the data in Table 5.2. Following Helz et al. (2011), the Davies equation was to calculate activity coefficients in seawater. The activity coefficients for monovalent and divalent ions, γ_1 and γ_2 are given by:

$$\gamma_1 = 10^{-0.5\cdot1^2\left(\frac{I^{0.5}}{1+I^{0.5}}-0.3I\right)} = 0.756 \quad (I = 0.72) \qquad \text{Eq. 5.10}$$

$$\gamma_2 = 10^{-0.5\cdot2^2\left(\frac{I^{0.5}}{1+I^{0.5}}-0.3I\right)} = 0.326 \quad (I = 0.72) \qquad \text{Eq. 5.11}$$

Based on reducing porewater conditions, pore water iron was assumed to be present as Fe^{2+}. Equation 5.5 was used to determine the total concentration of MoS_4^{2-}. Ion pairing effects were accounted for assuming the speciation of Fe^{2+} and MoS_4^{2-} could be modeled:

$$\sum Fe = [Fe^{2+}] + [FeCl^{+}] + [FeSO_{4,aq}] + [FeCO_{3,aq}] + [Fe(HS)_{2,aq}] \quad \text{Eq. 5.12}$$

$$\sum MoS_4^{2-} = [MoS_4^{2-}] + [CaMoS_{4,aq}] + [MgMoS_{4,aq}] \quad \text{Eq.5.13}$$

The activities of Fe^{2+} and MoS_4^{2-} can then be calculated:

$$[aFe^{2+}] = \gamma_2 \sum Fe \cdot \left(1 + 10^{-0.12}[Cl^-] + 10^{0.96}[SO_4^{2-}] + 10^{4.33}[CO_3^{2-}] + 10^{6.45}\gamma_2\left(\gamma_1[HS^-]\right)^2\right)^{-1} \quad \text{Eq. 5.14}$$

$$[aMoS_4^{2-}] = \gamma_2 \cdot [MoS_4^{2-}]\left(1 + \frac{372\gamma_2^{\,2}}{10^{0.12I}}[Ca^{2+}] + \frac{1070\gamma_2^{\,2}}{10^{0.12I}}[Mg^{2+}]\right)^{-1} \quad \text{Eq 5.15}$$

The terms in Eq. 5.15 are taken directly from Helz et al. (2011). The coefficients in Eq. 5.14 are derived from two sources. The first three equilibrium constants in Eq 5.14 were measured in seawater and account for the significant inorganic Fe^{2+} species in seawater in the absence of sulfide (Santana-Casiano et al., 2006). The final term accounts for the formation of $Fe(HS)_{2,aq}$ at I=0, and has been corrected for ion strength effects in the above equation (Davison et al., 1999). The saturation state of $FeMo_{0.6}S_{2.8}$ can then be calculated:

$$\Omega_{QFeS} = \frac{Q_{FeMoS}}{K_{FeMoS}} \quad \text{Eq. 5.16}$$

The resulting profiles are within an order of magnitude of saturation with respect to the putative mineral phase (Fig. 5.7). Given the uncertainties in pore water trace metal concentrations and the limitations of Fe-speciation due to effects such as organic ligands, this agreement seems encouraging. The role of a FeMoS phase seems possible, if not certain, in these sediments.

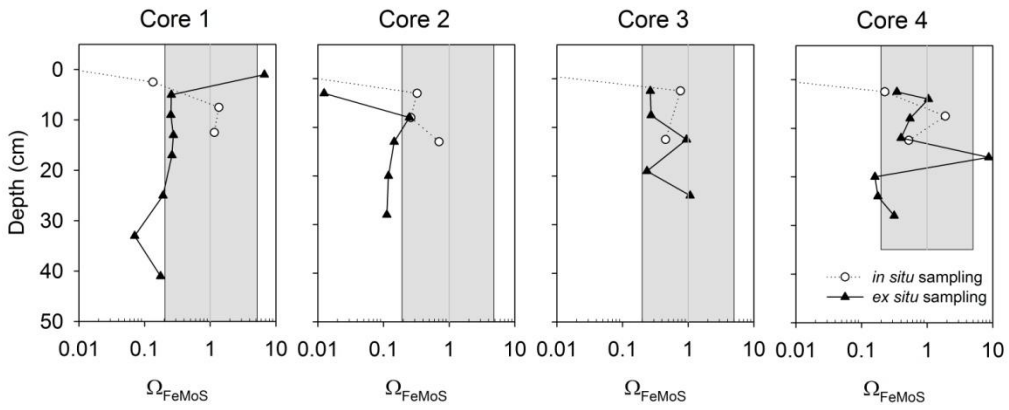

Figure 5.7. Saturation index of the putative FeMoS phase reported by Helz et al. (2011) calculated for the pore water samples in this study. Bottom water samples (not shown) are strongly undersaturated and plot offscale to the upper left. The gray box represents saturation states that are within error of the proposed saturation constant.

5.5 Conclusions

The purpose of this study was to examine the potential for early diagenetic fractionation during the preservation of $\delta^{98/95}$Mo records in shallow marine carbonate sediments. A comprehensive understanding of these processes is essential to properly interpret $\delta^{98/95}$Mo variation in ancient carbonate sediments (e.g. Czaja et al., 2012; Voegelin et al., 2010).

The results demonstrate that direct incorporation of Mo during primary carbonate precipitation is likely the dominant process controlling down core Mo concentrations and isotopes at low levels of pore water sulfide (< 20μ M H_2S_{aq}). Under these conditions, measured Mo concentrations were <0.2 ppm and $\delta^{98/95}$Mo

was ~1.6‰, in agreement with previous published measurements of primary carbonate precipitates (Voegelin et al., 2009).

In contrast however, in three of the four cores we examined, higher levels of pore water sulfide (20 – 300 μM H_2S_{aq}) were accompanied by 10-100 fold increase in sediment Mo concentrations and a $\delta^{98/95}$Mo shift toward the value of seawater. These measurements are consistent with the authigenic accumulation of Mo via the formation of thiomolybdate species and subsequent scavenging to sediments.

Authigenic accumulation of Mo from sulfidic pore waters in marine carbonate sediments is likely to be an important process in shallow-water carbonate sections. With relatively high Mo concentrations (1-10's of ppm), such sections should be easy to identify in the Phanerozoic geologic record and are useful because Mo accumulated under these conditions closely approximates the $\delta^{98/95}$Mo of seawater. In Precambrian sections, lower seawater Mo concentrations may limit the magnitude of enrichment, making it more difficult to distinguish authigenic enrichment in carbonates. In these sections, proxies for pore water sulfide concentrations such as organic content or iron speciation might be useful tools for determining the likely degree of enrichment.

Future work on $\delta^{98/95}$Mo variations in modern carbonate sediments should focus on expanding the spatial and temporal limits of this study, particularly with a focus on deeper platform margin sediments and longer cores. With lower organic content, some deeper water cores may not contain sufficient pore water sulfide to result in authigenic Mo accumulation. Furthermore, this study covers

only the earliest phase of diagenesis to burial depths < 50 cm. The extent to which $\delta^{98/95}$Mo patterns are altered during later burial and diagenesis must be explored before reliable conclusions can be drawn from the geological record. Ultimately, by studying patterns of Mo isotope diagenesis in carbonates over a range of depths and time scales, it should be possible to accurately reconstruct the $\delta^{98/95}$Mo paleoseawater record, and from this information discern variations in global marine paleoredox conditions.

Chapter 6

CONCLUSIONS, APPLICATIONS, AND FUTURE RESEARCH DIRECTIONS

6.1. Summary of Findings

This dissertation advances our understanding of the Mo and U paleoredox proxies in two important ways. First, Chapter 2 provides a direct estimate of the $^{238}U/^{235}U$ apparent fractionation factor during the reduction of U in euxinic marine settings. This fractionation factor is thought to be the dominant driver of fractionation in the marine $^{238}U/^{235}U$ system. The new value, $\varepsilon = 0.61 \pm 0.12‰$ (2sd) is larger than previous estimates of fractionation in euxinic settings (~0.4‰, Weyer et al., 2008) and terrestrial settings (~0.4‰, Brennecka et al. 2010, 0.46±0.13‰ (2sd), Bopp et al. 2010). More importantly however, Chapter 2 demonstrates how local drawdown of U can lead to Raleigh fractionation of $^{238}U/^{235}U$ in restricted marine basins. When this occurs, the isotopic offset between open ocean seawater and U in the basin sediments becomes a function of the extent of U drawdown from the water column. In the extreme case of nearly quantitative draw down, the expected fractionation between open ocean seawater and basin sediments would be completely suppressed, similar to the behavior of Mo in euxinic basins. Because the actual extent of U drawn down would be difficult or impossible to reconstruct from the rock record, caution is warranted when attempting to use $\delta^{238/235}U$ measurements from restricted basins to reconstruct open ocean sea water values.

The second contribution of this dissertation is the examination of the factors controlling $\delta^{238/235}U$ and $\delta^{98/95}Mo$ preservation in bulk marine carbonates. Because carbonate sediments are abundant in the geologic record and are often deposited on open ocean margins, they avoid many of limitations of black shales, albeit at the expense of increased concerns about diagenesis. The purpose of Chapters 3-5 was to begin exploring the processes controlling deposition and the diagenetic potential of Mo and U isotope records in bulk carbonate sediments. The overarching conclusion of these chapters is that the deposition of Mo and U in carbonate sediments is not primarily controlled by co-precipitation with the primary carbonate minerals as was expected, but instead is controlled by authigenic accumulation of Mo and U from reducing, sulfidic pore waters. As a result, Mo and U concentrations in carbonate sediments can be elevated above concentrations in primary precipitates, and the isotopic composition Mo and U in carbonate sediments is similar values expected for anoxic or euxinic settings.

Chapter 4 builds on Chapter 3 by providing the first direct attempt to detect post-depositional diagenesis of $\delta^{238/235}U$ using drill core samples collected from the western margin of the Grand Bahamas Bank (ODP Leg 166). The results of this study demonstrate that, while the fractionation of $\delta^{238/235}U$ between seawater and bulk carbonate sediments is somewhat variable, most of the variance is restricted to a small number of samples. The remaining data set is characterized by a reliable and fairly consistent offset between sediments and sea water.

6.2 Synergistic Use of $\delta^{238/235}$ and $\delta^{98/95}$Mo in Carbonates

One of the major inherent challenges facing non-traditional stable isotope paleoredox proxies is the problem of multiple sinks. When faced with three or more isotopically distinct sinks, the solution to the isotope mass balance problem becomes non-unique. One potential solution to this problem is through the combination two or more complimentary redox-sensitive stable isotope systems, which in theory allow one additional sink to be resolved for each additional isotope system. However, this requires that seawater isotope variations can be reconstructed for two or more elements from the same samples in the same lithologies. Based on the work described above, it appears that this could be achievable using measurements of $\delta^{238/235}$U and $\delta^{98/95}$Mo in bulk carbonate sediments, provided sufficient care is taken to identify depositional conditions and assess the potential for post-depositional diagenesis.

Table 6.1. Relationships between Mo and U burial fractions.

	Mo	**U**
Oxic	$1 - X_{anox}^{Mo} - X_{eux}^{Mo}$	$\frac{R_{oxic}^{U/Mo}\left(1 - X_{anox}^{Mo} - X_{eux}^{Mo}\right)}{R_{oxic}^{U/Mo}\left(1 - X_{anox}^{Mo} - X_{eux}^{Mo}\right) + R_{anox}^{U/Mo}X_{anox}^{Mo} + R_{eux}^{U/Mo}X_{eux}^{Mo}}$
Suboxic /Anoxic	X_{anox}^{Mo}	$\frac{R_{anox}^{U/Mo}X_{anox}^{Mo}}{R_{oxic}^{U/Mo}\left(1 - X_{anox}^{Mo} - X_{eux}^{Mo}\right) + R_{anox}^{U/Mo}X_{anox}^{Mo} + R_{eux}^{U/Mo}X_{eux}^{Mo}}$
Euxinic	X_{eux}^{Mo}	$\frac{R_{eux}^{U/Mo}X_{eux}^{Mo}}{R_{oxic}^{U/Mo}\left(1 - X_{anox}^{Mo} - X_{eux}^{Mo}\right) + R_{anox}^{U/Mo}X_{anox}^{Mo} + R_{eux}^{U/Mo}X_{eux}^{Mo}}$

Below, a technique for combining Mo and U isotope proxies is demonstrated for a case with three sinks (oxic, suboxic/anoxic, and euxinic). The first step is to express the relative size of each U sink as a function of the size of the Mo sink (Table 6.1). To relate the removal of U to Mo in each sink, each Mo sink is multiplied by the ratio of U:Mo accumulation rate in modern sinks (Fig. 6.1), and normalized to 100% by dividing by the total predicted U sink. One can then use the expressions in Table 6.1 to write an isotope mass balance equation for both Mo and U:

$$\delta_{SW}^{Mo} = \delta_{input}^{Mo} - X_{eux}^{Mo}\Delta_{eux}^{Mo} + X_{anox}^{Mo}\Delta_{anox}^{Mo} + \left(1 - X_{anox}^{Mo} - X_{eux}^{Mo}\right)\Delta_{oxic}^{Mo} \qquad \text{Eq. 6.1}$$

$$\delta_{SW}^{U} = \delta_{input}^{U} - \left(1 - f_{hyd}\right)\frac{R_{eux}^{U/Mo}X_{eux}^{Mo}\Delta_{eux}^{U} + R_{anox}^{U/Mo}X_{anox}^{Mo}\Delta_{anox}^{U} + R_{oxic}^{U/Mo}\left(1 - X_{anox}^{Mo} - X_{eux}^{Mo}\right)\Delta_{oxic}^{U}}{R_{eux}^{U/Mo}X_{eux}^{Mo} + R_{anox}^{U/Mo}X_{anox}^{Mo} + R_{oxic}^{U/Mo}\left(1 - X_{anox}^{Mo} - X_{eux}^{Mo}\right)}$$

Eq. 6.2

These equations depend only on two unknowns, X_{eux}^{Mo} and X_{anox}^{Mo}, denoting the burial fraction of Mo in anoxic and euxinic sinks. The remaining terms express the isotopic fractionation factors (e.g., Δ_{eux}^{Mo}), Mo/U burial ratios (e.g., $R_{eux}^{U/Mo}$) and the isotopic composition of inputs and seawater (e.g., δ_{input}^{Mo} and δ_{SW}^{Mo}). The term f_{hyd} allows for a constant fractionation of U to be removed in hydrothermal systems with no isotopic fractionation.

With 2 equations and 2 unknowns, it is possible to uniquely constrain the extent of anoxia versus euxinia in the global ocean. Figure 6.2 shows the results of a calculation where the contoured isolines depict the predicted values of

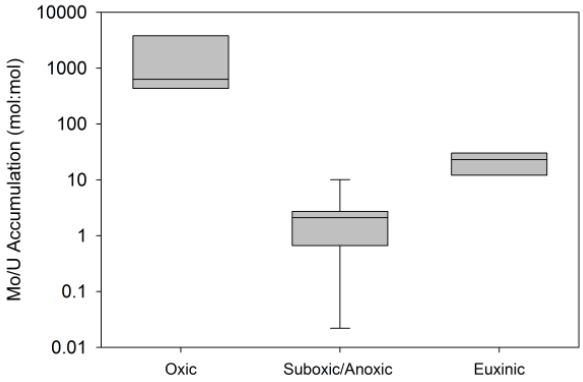

Figure 6.1. Relative accumulation rates of authigenic Mo and U under various redox conditions from modern marine settings. Data are from manganese crusts (Koschinsky and Hein, 2003), continental margin sediments (McManus et al., 2006), and restricted euxinic basins (Zheng et al., 2002; Zheng et al., 2000).

Table 6.2 Model parameter values.

Parameter	Symbol	Value
Ratio of U:Mo Mass Accumulation Rates		
Euxinic Sediments	$R_{eux}^{U/Mo}$	1/20
Suboxic/Anoxic Sediments	$R_{anox}^{U/Mo}$	1/10
Oxic Sediments	$R_{oxic}^{U/Mo}$	1/700
$^{238}U/^{235}U$ Isotope Fractionation (‰)		
River Input	δ_{input}^{U}	-0.3
Euxinic Sinks	Δ_{eux}^{U}	0.4
Suboxic/Anoxic Sinks	Δ_{anox}^{U}	0.1
Oxic Sinks	Δ_{oxic}^{U}	-0.2
Proportion of Hydrothermal Sinks	f_{hyd}	10
$^{98}Mo/^{95}Mo$ Isotope Fractionation (‰)		
River Input	δ_{input}^{Mo}	0.6
Euxinic Sinks	Δ_{eux}^{Mo}	0.0
Suboxic/Anoxic Sinks	Δ_{anox}^{Mo}	-0.7
Euxinic Sinks	Δ_{oxic}^{Mo}	-3.0

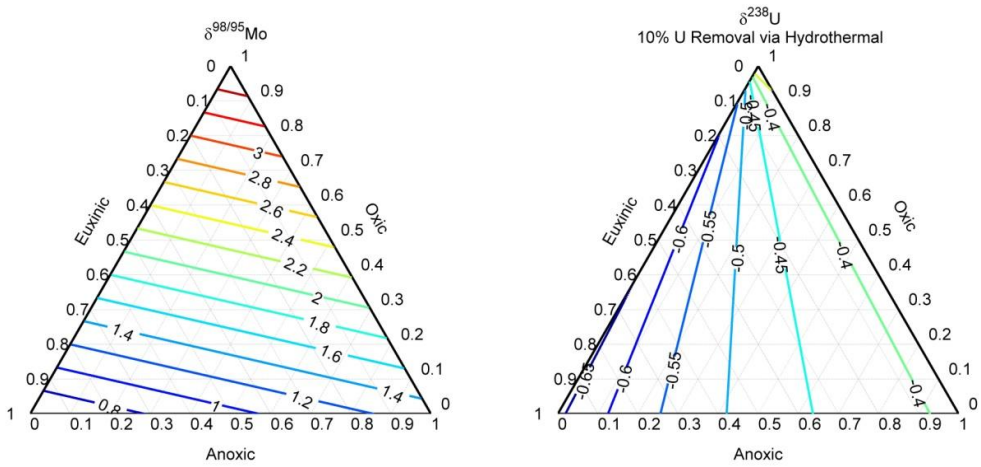

Figure 6.2. Ternary diagrams depicting predicted seawater $\delta^{98/95}$Mo and $\delta^{238/235}$U values (colored contours) as a function of the proportion of oxic, suboxic/anoxic, and euxinic Mo sinks.

seawater $\delta^{238/235}$U and $\delta^{98/95}$Mo on ternary diagrams for the three component mixing between the portions of oxic, anoxic, and euxinic sinks given the parameter values in Table 6.2. Because the contoured isolines on the two plots are nearly perpendicular, knowledge of any pair of seawater $\delta^{238/235}$U and $\delta^{98/95}$U values uniquely specifies the relative magnitude of oxic, suboxic/anoxic, and euxinic sinks.

In the near future, approaches like that depicted in Figure 6.2 will be combined with the availability of multiple isotope paleoredox proxies to better deconvolute paleoredox signals. If successfully applied, this approach could provide answers to persistent questions about the paleoredox evolution of Earth's atmosphere and oceans. For example, this approach could provide a much better understanding of the timing and extent of oxygenated and sulfidic water masses

between the first evolution of oxygenic photosynthesis and the Great Oxidation Event at ~2.4 Ga (Anbar et al., 2007; Kendall et al., 2010; Reinhard et al., 2009; Wille et al., 2007). Similar, this multiple proxy system would be much better suited to answering questions about the timing and extent of Proterozoic euxinia (Canfield, 1998; Poulton et al., 2004, 2010; Scott et al., 2008).

REFERENCES

Abe, M., Suzuki, T., Fujii, Y., Hada, M., and Hirao, K., 2008, An *ab initio* molecular orbital study of the nuclear volume effects in uranium isotope fractionations: Journal of Chemical Physics, v. 129, 164309.

Algeo, T.J., and Lyons, T.W., 2006, Mo-total organic carbon covariation in modern anoxic marine environments: Implications for analysis of paleoredox and paleohydrographic conditions: Paleoceanography, v. 21, p. PA1016.

Almgren, T., Dyrssen, D., and Fonselius, S., 1983, Determination of alkalinity and total carbonate., *in* Grasshoff, M.E.K., and Kremling, K., eds., Methods of Seawater Analysis, Verlag- Chemie, p. 99-123.

Anbar, A.D., 2004, Molybdenum stable isotopes: Observations, interpretations and directions, *in* Johnson, C.M., Beard, B.L., and Albarede, F., eds., Geochemistry of Non-Traditional Stable Isotopes, Volume 55: Reviews in Mineralogy & Geochemistry, p. 429-454.

Anbar, A.D., Duan, Y., Lyons, T.W., Arnold, G.L., Kendall, B., Creaser, R.A., Kaufman, A.J., Gordon, G.W., Scott, C., Garvin, J., and Buick, R., 2007, A whiff of oxygen before the Great Oxidation Event?: Science, v. 317, p. 1903-1906.

Andersen, M.B., Stirling, C.H., Potter, E.K., and Halliday, A.N., 2004, Toward epsilon levels of measurement precision on U-234/U-238 by using MC-ICPMS: International Journal of Mass Spectrometry, v. 237, p. 107-118.

Andersen, M.B., Stirling, C.H., Zimmermann, B., and Halliday, A.N., 2010, Precise determination of the open ocean $^{234}U/^{238}U$ composition: Geochemistry Geophysics Geosystems, v. 11, Q12003.

Anderson, R.F., Fleisher, M.Q., and Lehuray, A.P., 1989a, Concentration, oxidation state, and particulate flux of uranium in the Black Sea: Geochimica et Cosmochimica Acta, v. 53, p. 2215-2224.

Anderson, R.F., Lehuray, A.P., Fleisher, M.Q., and Murray, J.W., 1989b, Uranium deposition in Saanich Inlet sediments, Vancouver Island: Geochimica et Cosmochimica Acta, v. 53, p. 2205-2213.

Archer, C., and Vance, D., 2008, The isotopic signature of the global riverine molybdenum flux and anoxia in the ancient oceans: Nature Geoscience, v. 1, p. 597-600.

Arnold, G.L., Anbar, A.D., Barling, J., and Lyons, T.W., 2004, Molybdenum isotope evidence for widespread anoxia in mid-proterozoic oceans: Science, v. 304, p. 87-90.

Arthur, M.A., and Sageman, B.B., 1994, Marine Black Shales: Depositional Mechanisms and Environments of Ancient Deposits: Annual Review of Earth and Planetary Sciences, v. 22, p. 499-551.

Ayotte, J.D., Gronberg, J.M., and Apodaca, L.E., 2011, Trace Elements and Radon in Groundwater Across the United States: U.S. Geological Survey Scientific Investigations Report 2011-5059. 115 pp.

Banner, J.L., and Hanson, G.N., 1990, Calculation of simultaneous isotopic and trace element variations during water-rock interaction with applications to carbonate diagenesis: Geochimica et Cosmochimica Acta, v. 54, p. 3123-3137.

Barling, J., and Anbar, A.D., 2004, Molybdenum isotope fractionation during adsorption by manganese oxides: Earth and Planetary Science Letters, v. 217, p. 315-329.

Barling, J., Arnold, G.L., and Anbar, A.D., 2001, Natural mass-dependent variations in the isotopic composition of molybdenum: Earth and Planetary Science Letters, v. 193, p. 447-457.

Barnes, C.E., and Cochran, J.K., 1990, Uranium removal in oceanic sediments and the oceanic U balance: Earth and Planetary Science Letters, v. 97, p. 94-101.

—, 1991, Geochemistry of uranium in Black Sea sediments: Deep-Sea Research Part A-Oceanographic Research Papers, v. 38, p. S1237-S1254.

Bopp, C.J., Lundstrom, C.C., Johnson, T.M., and Glessner, J.J.G., 2009, Variations in U-238/U-235 in uranium ore deposits: Isotopic signatures of the U reduction process?: Geology, v. 37, p. 611-614.

Bopp, C.J., Lundstrom, C.C., Johnson, T.M., Sanford, R.A., Long, P.E., and Williams, K.H., 2010, Uranium U-238/U-235 Isotope Ratios as Indicators of Reduction: Results from an in situ Biostimulation Experiment at Rifle, Colorado, USA: Environmental Science & Technology, v. 44, p. 5927-5933.

Brennecka, G.A., Borg, L.E., Hutcheon, I.D., Sharp, M.A., and Anbar, A.D., 2010a, Natural variations in uranium isotope ratios of uranium ore concentrates: Understanding the U-238/U-235 fractionation mechanism: Earth and Planetary Science Letters, v. 291, p. 228-233.

Brennecka, G.A., Herrmann, A.D., Algeo, T.J., and Anbar, A.D., 2011a, Rapid expansion of oceanic anoxia immediately before the end-Permian mass extinction: Proceedings of the National Academy of Sciences, v. 108, p. 17631-17634.

Brennecka, G.A., Wasylenki, L.E., Bargar, J.R., Weyer, S., and Anbar, A.D., 2011b, Uranium isotope fractionation during adsorption to Mn-oxyhydroxides: Environmental Science & Technology, v. 45, p. 1370-1375.

Brennecka, G.A., Wasylenki, L.E., Weyer, S., and Anbar, A.D., 2008, Experiments demonstrate that Uranium isotopes fractionate during adsorption to Mn-oxides: Geochimica et Cosmochimica Acta, v. 72, p. A114-A114.

Brennecka, G.A., Weyer, S., Wadhwa, M., Janney, P.E., Zipfel, J., and Anbar, A.D., 2010b, $^{238}U/^{235}U$ Variations in Meteorites: Extant ^{247}Cm and Implications for Pb-Pb Dating: Science, v. 327, p. 449-451.

Brucker, R.L.P., McManus, J., Severmann, S., and Berelson, W.M., 2009, Molybdenum behavior during early diagenesis: Insights from Mo isotopes: Geochemistry Geophysics Geosystems, v. 10, Q06010.

Bubb, J.N., and Atwood, D.K., 1968, Recent dolomitization of Pleistocene limestones by hypersaline brines, Great Inaqua Island, Bahamas: AAPG Bulletin, v. 52, p. 522.

Burdige, D.J., Hu, X.P., and Zimmerman, R.C., 2010, The widespread occurrence of coupled carbonate dissolution/reprecipitation in surface sediments on the Bahamas Bank: American Journal of Science, v. 310, p. 492-521.

Burdige, D.J., and Zimmerman, R.C., 2002, Impact of sea grass density on carbonate dissolution in Bahamian sediments: Limnology and Oceanography, v. 47, p. 1751-1763.

Burdige, D.J., Zimmerman, R.C., and Hu, X., 2008, Rates of carbonate dissolution in permeable sediments estimated from pore-water profiles: The role of sea grasses: Limnology and Oceanography, v. 53, p. 549-565.

Canfield, D.E., 1998, A new model for Proterozoic ocean chemistry: Nature, v. 396, p. 450-453.

Chen, J.H., Edwards, R.L., and Wasserburg, G.J., 1986, U-238,U-234 and TH-232 in seawater: Earth and Planetary Science Letters, v. 80, p. 241-251.

Chung, G.S., and Swart, P.K., 1990, The concentration of uranium in freshwater vadose and phreatic cements in a Holocene ooid cay; a method of

identifying ancient water tables: Journal of Sedimentary Research, v. 60, p. 735-746.

Clark, S., and Johnson, T., 2008, Effective isotopic fractionation factors for solute removal by reactive sediments: a laboratory microcosm and slurry study: Environmental Science & Technology, v. 42, p. 7850-7855.

Cline, J.D., 1969, Spectrophotometric determination of hydrogen sulfide in natural waters: Limnology and Oceanography, v. 14, p. 454–458.

Cochran, J.K., Carey, A.E., Sholkovitz, E.R., and Surprenant, L.D., 1986, The geochemistry of uranium and thorium in coastal marine sediments and sediment pore waters: Geochimica et Cosmochimica Acta, v. 50, p. 663-680.

Colodner, D., Edmond, J., and Boyle, E., 1995, Rhenium in the Black Sea - comparison with molybdenum and uranium: Earth and Planetary Science Letters, v. 131, p. 1-15.

Condon, D.J., McLean, N., Noble, S.R., and Bowring, S.A., 2010, Isotopic composition (U-238/U-235) of some commonly used uranium reference materials: Geochimica et Cosmochimica Acta, v. 74, p. 7127-7143.

Crusius, J., and Thomson, J., 2000, Comparative behavior of authigenic Re, U, and Mo during reoxidation and subsequent long-term burial in marine sediments: Geochimica et Cosmochimica Acta, v. 64, p. 2233-2242.

Czaja, A.D., Johnson, C.M., Roden, E.E., Beard, B.L., Voegelin, A.R., Nagler, T.F., Beukes, N.J., and Wille, M., 2012, Evidence for free oxygen in the Neoarchean ocean based on coupled iron-molybdenum isotope fractionation: Geochimica et Cosmochimica Acta, v. 86, p. 118-137.

Dahl, T.W., Anbar, A.D., Gordon, G.W., Rosing, M.T., Frei, R., and Canfield, D.E., 2010, The behavior of molybdenum and its isotopes across the chemocline and in the sediments of sulfidic Lake Cadagno, Switzerland: Geochimica et Cosmochimica Acta, v. 74, p. 144-163.

Dahl, T.W., Canfield, D.E., Rosing, M.T., Frei, R.E., Gordon, G.W., Knoll, A.H., and Anbar, A.D., 2011, Molybdenum evidence for expansive sulfidic water masses in similar to 750 Ma oceans: Earth and Planetary Science Letters, v. 311, p. 264-274.

Davison, W., Phillips, N., and Tabner, B.J., 1999, Soluble iron sulfide species in natural waters: Reappraisal of their stoichiometry and stability constants: Aquatic Sciences - Research Across Boundaries, v. 61, p. 23-43.

Derry, L.A., 2010, A burial diagenesis origin for the Ediacaran Shuram-Wonoka carbon isotope anomaly: Earth and Planetary Science Letters, v. 294, p. 152-162.

Dix, G.R., 2001, Origin of Sr-rich magnesian calcite mud in a Holocene pond basin (Lee Stocking Island, Bahamas): Journal of Sedimentary Research, v. 71, p. 167-175.

Dix, G.R., and Mullins, H.T., 1988, A regional perspective of shallow-burial diagenesis of deep-water periplatform carbonates from the northern Bahamas, *in* Austin, J.A.J., and Schlager, W., eds., Proc. ODP, Sci. Results, 101: College Station, TX, Ocean Drilling Program, p. 279–302.

Dong, W., and Brooks, S., 2006, Determination of the formation constants of ternary complexes of uranyl and carbonate with alkaline earth metals (Mg^{2+}, Ca^{2+}, Sr^{2+}, and Ba^{2+}) using anion exchange method: Environmental Science & Technology, v. 40, p. 4689-4695.

Droxler, A.W., Bruce, C.H., Sager, W.W., and Watkins, D.H., 1988, Pliocene–Pleistocene variations in aragonite content and planktonic oxygen-isotope record in Bahamian periplatform ooze, Hole 633A, *in* Austin, J.A.J., and Schlager, W., eds., Proc. ODP, Sci. Results, 101: College Station, TX, Ocean Drilling Program, p. 221–224.

Duan, Y., Anbar, A.D., Arnold, G.L., Lyons, T.W., Gordon, G.W., and Kendall, B., 2010, Molybdenum isotope evidence for mild environmental oxygenation before the Great Oxidation Event: Geochimica et Cosmochimica Acta, v. 74, p. 6655-6668.

Dunk, R.M., Mills, R.A., and Jenkins, W.J., 2002, A reevaluation of the oceanic uranium budget for the Holocene: Chemical Geology, v. 190, p. 45-67.

Eberli, G.P., 2000, The record of Neogene sea-level changes in the prograding carbonates along the Bahamas Transect—Leg 166 synthesis, *in* Swart, P.K., Eberli, G.P., Malone, M.J., and Sarg, J.F., eds., Proc. ODP, Sci. Results, 166: College Station, TX, Ocean Drilling Program, p. 167–177.

Eberli, G.P., Swart, P.K., and Malone, M.J., 1997, Proceedings of the Ocean Drilling Program, Initial Reports, Volume 166: College Station, Texas, Ocean Drilling Program, p. 850.

Edwards, R.L., Gallup, C.D., and Cheng, H., 2003a, Uranium-series dating of marine and lacustrine carbonates: Reviews in Mineralogy and Geochemistry, v. 52, p. 363-405.

—, 2003b, Uranium-series dating of marine and lacustrine carbonates: Uranium-Series Geochemistry, v. 52, p. 363-405.

Emerson, S.R., and Huested, S.S., 1991, Ocean anoxia and the concentrations of molybdenum and vanadium in seawater: Marine Chemistry, v. 34, p. 177-196.

Erickson, B.E., and Helz, G.R., 2000, Molybdenum(VI) speciation in sulfidic waters: Stability and lability of thiomolybdates: Geochimica et Cosmochimica Acta, v. 64, p. 1149-1158.

Feldmann, M., and McKenzie, J.A., 1998, Stromatolite-thrombolite associations in a modern environment, Lee Stocking Island, Bahamas: Palaios, v. 13, p. 201-212.

Filippelli, G.M., 2002, The global phosphorus cycle, *in* Kohn, M.J., Rakovan, J., and Hughes, J.M., eds., Phosphates: Geochemical, Geobiological, and Materials Importance, Volume 48: Reviews in Mineralogy & Geochemistry, p. 391-425.

Frei, R., Gaucher, C., Poulton, S.W., and Canfield, D.E., 2009, Fluctuations in Precambrian atmospheric oxygenation recorded by chromium isotopes: Nature, v. 461, p. 250-253.

Furman, F.C., Woody, R.E., Rasberry, M.A., Keller, D.J., and Gregg, J.M., 1993, Carbonate and evaporite mineralogy of Holocene (<1900 RCYBP) sediments at Salt Pond, San Salvador Island, Bahamas: Preliminary study, *in* White, B., ed., Proceedings of the Sixth Symposium on the Geology of the Bahamas: San Salvador, Bahamas, Bahamian Field Station.

Garrels, R.M., and Mackenzie, F.T., 1971, Evolution of Sedimentary Rocks: New York, W.W. Norton and Co., 397 p.

Goldberg, T., Archer, C., Vance, D., and Poulton, S.W., 2009, Mo isotope fractionation during adsorption to Fe (oxyhydr)oxides: Geochimica et Cosmochimica Acta, v. 73, p. 6502-6516.

Goldberg, T., Archer, C., Vance, D., Thamdrup, B., McAnena, A., and Poulton, S.W., 2012, Controls on Mo isotope fractionations in a Mn-rich anoxic marine sediment, Gullmar Fjord, Sweden: Chemical Geology, v. 296, p. 73-82.

Gordon, G.W., Lyons, T.W., Arnold, G.L., Roe, J., Sageman, B.B., and Anbar, A.D., 2009, When do black shales tell molybdenum isotope tales?: Geology, v. 37, p. 535-538.

Grotzinger, J.P., 1989, Facies and evolution of Precambrian carbonate depositional systems: emergence of the modern platform archetype, *in* Crevello, P.D., Wilson, J.L., Sarg, J.F., and Read, J.F., eds., Controls on

Carbonate Platforms and Basin Development . Vol. 44.: Tulsa, OK, Society of Economic Paleontologists and Mineralogists, p. 79-106.

Hein, M.K., and Winsborough, B.M., 2001, Oestrupia grandis sp nov., a new benthic marine diatom from the Bahamas: Diatom Research, v. 16, p. 325-341.

Helz, G.R., Bura-Nakic, E., Mikac, N., and Ciglenecki, I., 2011, New model for molybdenum behavior in euxinic waters: Chemical Geology, v. 284, p. 323-332.

Helz, G.R., Miller, C.V., Charnock, J.M., Mosselmans, J.F.W., Pattrick, R.A.D., Garner, C.D., and Vaughan, D.J., 1996, Mechanism of molybdenum removal from the sea and its concentration in black shales: EXAFS evidence: Geochimica et Cosmochimica Acta, v. 60, p. 3631-3642.

Henderson, G.M., 2002, Seawater (234U/238U) during the last 800 thousand years: Earth and Planetary Science Letters, v. 199, p. 97-110.

Henderson, G.M., and Anderson, R.F., 2003, The U-series toolbox for paleoceanography: Uranium-Series Geochemistry, v. 52, p. 493-531.

Henderson, G.M., and Onions, R.K., 1995, U-234/U-238 ratios in quaternary planktonic foraminifera: Geochimica et Cosmochimica Acta, v. 59, p. 4685-4694.

Henderson, G.M., Rendle, R.H., Slowey, N.C., and Reijmer, J.J.G., 2000, U-Th dating and diagenesis of Pleistocene highstand sediments from the Bahamas Slope, *in* Swart, P.K., Eberli, G.P., Malone, M.J., and Sarg, J.F., eds., Proc. ODP, Sci. Results, 166: College Station, TX, Ocean Drilling Program, p. 23–31.

Henderson, G.M., Slowey, N.C., and Haddad, G.A., 1999, Fluid flow through carbonate platforms: constraints from U-234/U-238 and Cl- in Bahamas pore-waters: Earth and Planetary Science Letters, v. 169, p. 99-111.

Hua, B., Xu, H.F., Terry, J., and Deng, B.L., 2006, Kinetics of uranium(VI) reduction by hydrogen sulfide in anoxic aqueous systems: Environmental Science & Technology, v. 40, p. 4666-4671.

Jacobsen, S.B., and Kaufman, A.J., 1999, The Sr, C and O isotopic evolution of Neoproterozoic seawater: Chemical Geology, v. 161, p. 37-57.

Kendall, B., Creaser, R.A., Gordon, G.W., and Anbar, A.D., 2009, Re-Os and Mo isotope systematics of black shales from the Middle Proterozoic Velkerri and Wollogorang Formations, McArthur Basin, northern Australia: Geochimica et Cosmochimica Acta, v. 73, p. 2534-2558.

Kendall, B., Gordon, G.W., Poulton, S.W., and Anbar, A.D., 2011, Molybdenum isotope constraints on the extent of late Paleoproterozoic ocean euxinia: Earth and Planetary Science Letters, v. 307, p. 450-460.

Kendall, B., Reinhard, C.T., Lyons, T., Kaufman, A.J., Poulton, S., and Anbar, A.D., 2010, Pervasive oxygenation along late Archaean ocean margins: Nature Geoscience, v. 3, p. 647-652.

Kigoshi, K., 1971, Alpha-recoil thorium-234: Dissolution into water and the uranium-234/uranium-238 disequilibrium in nature: Science, v. 173, p. 47-48.

Klinkhammer, G.P., and Palmer, M.R., 1991, Uranium in the oceans - Where it goes and why: Geochimica et Cosmochimica Acta, v. 55, p. 1799-1806.

Knauth, L.P., and Kennedy, M.J., 2009, The late Precambrian greening of the Earth: Nature, v. 460, p. 728-732.

Kontakiotis, G., Mortyn, P.G., Antonarakou, A., Martinez-Boti, M.A., and Triantaphyllou, M.V., 2011, Field-based validation of a diagenetic effect on G. ruber Mg/Ca paleothermometry: Core top results from the Aegean Sea (eastern Mediterranean): Geochemistry Geophysics Geosystems, v. 12, Q09004.

Koschinsky, A., and Hein, J.R., 2003, Uptake of elements from seawater by ferromanganese crusts: solid-phase associations and seawater speciation: Marine Geology, v. 198, p. 331-351.

Kramer, P.A., Swart, P.K., De Carlo, E.H., and Schovsbo, N.H., 2000, Overview of interstitial fluid and sediment geochemistry, Sites 1003–1007 (Bahamas Transect), *in* Swart, P.K., Eberli, G.P., Malone, M.J., and Sarg, J.F., eds., Proc. ODP, Sci. Results, 166: College Station, TX, Ocean Drilling Program, p. 179–195.

Kroon, D., Reijmer, J.J.G., and Rendle, R., 2000a, Mid- to late-Quaternary variations in the oxygen isotope signature of *Globigerinoides ruber* at Site 1006 in the western subtropical Atlantic., *in* Swart, P.K., Eberli, G.P., Malone, M.J., and Sarg, J.F., eds., Proc. ODP, Sci. Results, 166: College Station, TX, Ocean Drilling Program, p. 13–22.

Kroon, D., Williams, T., Pirmez, C., Spezzaferri, S., Sato, T., and Wright, J.D., 2000b, Coupled early Pliocene–middle Miocene bio-cyclostratigraphy of Site 1006 reveals orbitally induced cyclicity patterns of Great Bahama Bank carbonate production., *in* Swart, P.K., Eberli, G.P., Malone, M.J., and Sarg, J.F., eds., Proc. ODP, Sci. Results, 166: College Station, TX, Ocean Drilling Program, p. 155–166.

Ku, T.L., 1965, An evaluation of U234/U238 method as a tool for dating pelagic sediments: Journal of Geophysical Research, v. 70, p. 3457-3474.

Ku, T.L., Knauss, K.G., and Mathieu, G.G., 1977, Uranium in open ocean - Concentration and isotopic composition: Deep-Sea Research, v. 24, p. 1005-1017.

Lasemi, Z., Boardman, M.R., and Sandberg, P.A., 1989, Cement origin of supratidal dolomite, Andros Island, Bahamas: Journal of Sedimentary Petrology, v. 59, p. 249-257.

Lovley, D.R., Roden, E.E., Phillips, E.J.P., and Woodward, J.C., 1993, Enzymatic iron and uranium reduction by sulfate-reducing bacteria: Marine Geology, v. 113, p. 41-53.

Malone, M.J., Slowey, N.C., and Henderson, G.M., 2001, Early diagenesis of shallow-water periplatform carbonate sediments, leeward margin, Great Bahama Bank (Ocean Drilling Program Leg 166): Geological Society of America Bulletin, v. 113, p. 881-894.

McManus, J., Berelson, W.M., Severmann, S., Poulson, R.L., Hammond, D.E., Klinkhammer, G.P., and Holm, C., 2006, Molybdenum and uranium geochemistry in continental margin sediments: Paleoproxy potential: Geochimica et Cosmochimica Acta, v. 70, p. 4643-4662.

McManus, J., Nagler, T.F., Siebert, C., Wheat, C.G., and Hammond, D.E., 2002, Oceanic molybdenum isotope fractionation: Diagenesis and hydrothermal ridge-flank alteration: Geochemistry Geophysics Geosystems, v. 3, 1078.

McNeil, D.F., and Kislak, J.I., 2000, Paleomagnetism of carbonate sediments from Hole 1006A, Bahamas Transect, Leg 166: Proc. ODP Sci. Results, v. 166, p. 123-128.

Melim, L.A., Westphal, H., Swart, P.K., Eberli, G.P., and Munnecke, A., 2002, Questioning carbonate diagenetic paradigms: evidence from the Neogene of the Bahamas: Marine Geology, v. 185, p. 27-53.

Miller, C.A., Peucker-Ehrenbrink, B., Walker, B.D., and Marcantonio, F., 2011, Re-assessing the surface cycling of molybdenum and rhenium: Geochimica et Cosmochimica Acta, v. 75, p. 7146-7179.

Miller, D.N., 1961, Early diagenetic dolomite associated with salt extraction process, Inaqua, Bahamas: Journal of Sedimentary Research, v. 31, p. 473-476.

Millero, F.J., 1995, Thermodynamics of the carbon dioxide system in the oceans: Geochimica et Cosmochimica Acta, v. 59, p. 661-677.

Millero, F.J., Plese, T., and Fernandez, M., 1988, The dissociation of hydrogen sulfide in seawater: Limnology and Oceanography, v. 33, p. 269-274.

Montoya-Pino, C., Weyer, S., Anbar, A.D., Pross, J., Oschmann, W., van de Schootbrugge, B., and Arz, H.W., 2010, Global enhancement of ocean anoxia during Oceanic Anoxic Event 2: A quantitative approach using U isotopes: Geology, v. 38, p. 315-318.

Morford, J.L., and Emerson, S., 1999, The geochemistry of redox sensitive trace metals in sediments: Geochimica et Cosmochimica Acta, v. 63, p. 1735-1750.

Morford, J.L., Emerson, S.R., Breckel, E.J., and Kim, S.H., 2005, Diagenesis of oxyanions (V, U, Re, and Mo) in pore waters and sediments from a continental margin: Geochimica et Cosmochimica Acta, v. 69, p. 5021-5032.

Morford, J.L., Martin, W.R., and Carney, C.M., 2009, Uranium diagenesis in sediments underlying bottom waters with high oxygen content: Geochimica et Cosmochimica Acta, v. 73, p. 2920-2937.

Morford, J.L., Martin, W.R., Kalnejais, L.H., François, R., Bothner, M., and Karle, I.-M., 2007, Insights on geochemical cycling of U, Re and Mo from seasonal sampling in Boston Harbor, Massachusetts, USA: Geochimica et Cosmochimica Acta, v. 71, p. 895-917.

Murray, J.W., 2006, Introduction - Recent US research cruises to the Black Sea: Deep-Sea Research Part II-Topical Studies in Oceanography, v. 53, p. 1737-1739.

Nagler, T.F., Neubert, N., Bottcher, M.E., Dellwig, O., and Schnetger, B., 2011, Molybdenum isotope fractionation in pelagic euxinia: Evidence from the modern Black and Baltic Seas: Chemical Geology, v. 289, p. 1-11.

Nakagawa, Y., Takano, S., Firdaus, M.L., Norisuye, K., Hirata, T., Vance, D., and Sohrin, Y., 2012, The molybdenum isotopic composition of the modern ocean: Geochemical Journal, v. 46, p. 131-141.

Neubert, N., Heri, A.R., Voegelin, A.R., Nagler, T.F., Schlunegger, F., and Villa, I.M., 2011, The molybdenum isotopic composition in river water: Constraints from small catchments: Earth and Planetary Science Letters, v. 304, p. 180-190.

Neubert, N., Nagler, T.F., and Bottcher, M.E., 2008, Sulfidity controls molybdenum isotope fractionation into euxinic sediments: Evidence from the modern Black Sea: Geology, v. 36, p. 775-778.

Nikolayev, D., Lazarev, K., and Drozhzhin, V., 1977, Trends in the distribution of U, Io, Ra and Th in the Black and Azov Seas: Geochimica International, v. 14, p. 141-146.

Noordmann, J., Weyer, S., Sharma, M., and Georg, R.B., 2009, Variations of the U-238/U-235 isotope composition in rivers: Geochimica et Cosmochimica Acta, v. 73, p. A951-A951.

Pearce, C.R., Burton, K.W., Pogge von Strandmann, P.A.E., James, R.H., and Gislason, S.R., 2010, Molybdenum isotope behaviour accompanying weathering and riverine transport in a basaltic terrain: Earth and Planetary Science Letters, v. 295, p. 104-114.

Perez, F.F., and Fraga, F., 1987, The pH measurements in seawater on the NBS scale: Marine Chemistry, v. 21, p. 315-327.

Poulson, R.L., Siebert, C., McManus, J., and Berelson, W.M., 2006, Authigenic molybdenum isotope signatures in marine sediments: Geology, v. 34, p. 617-620.

Poulton, S.W., Fralick, P.W., and Canfield, D.E., 2004, The transition to a sulphidic ocean similar to 1.84 billion years ago: Nature, v. 431, p. 173-177.

—, 2010, Spatial variability in oceanic redox structure 1.8 billion years ago: Nature Geoscience, v. 3, p. 486-490.

Rademacher, L.K., Lundstrom, C.C., Johnson, T.M., Sanford, R.A., Zhao, J.Z., and Zhang, Z.F., 2006, Experimentally determined uranium isotope Fractionation during reduction of hexavalent U by bacteria and zero valent iron: Environmental Science & Technology, v. 40, p. 6943-6948.

Raiswell, R., and Canfield, D.E., 1998, Sources of iron for pyrite formation in marine sediments: American Journal of Science, v. 298, p. 219-245.

Reeder, R.J., Nugent, M., Lamble, G.M., Tait, C.D., and Morris, D.E., 2000, Uranyl incorporation into calcite and aragonite: XAFS and luminescence studies: Environmental Science & Technology, v. 34, p. 638-644.

Reeder, R.J., Nugent, M., Tait, C.D., Morris, D.E., Heald, S.M., Beck, K.M., Hess, W.P., and Lanzirotti, A., 2001, Coprecipitation of uranium(VI) with calcite: XAFS, micro-XAS, and luminescence characterization: Geochimica et Cosmochimica Acta, v. 65, p. 3491-3503.

Regenberg, M., Nurnberg, D., Schonfeld, J., and Reichart, G.J., 2007, Early diagenetic overprint in Caribbean sediment cores and its effect on the

geochemical composition of planktonic foraminifera: Biogeosciences, v. 4, p. 957-973.

Reinhard, C.T., Raiswell, R., Scott, C., Anbar, A.D., and Lyons, T.W., 2009, A Late Archean Sulfidic Sea Stimulated by Early Oxidative Weathering of the Continents: Science, v. 326, p. 713-716.

Rendle, R.H., Reijmer, J.J.G., Kroon, D., and Henderson, G.M., 2000, Mineralogy and sedimentology of the Pleistocene to Holocene on the Leeward margin of Great Bahama Bank., *in* Swart, P.K., Eberli, G.P., Malone, M.J., and Sarg, J.F., eds., Proc. ODP, Sci. Results, 166: College Station, TX, Ocean Drilling Program, p. 61-76.

Renshaw, J.C., Butchins, L.J.C., Livens, F.R., May, I., Charnock, J.M., and Lloyd, J.R., 2005, Bioreduction of uranium: Environmental implications of a pentavalent intermediate: Environmental Science & Technology, v. 39, p. 5657-5660.

Robinson, L.F., Belshaw, N.S., and Henderson, G.M., 2004, U and Th concentrations and isotope ratios in modern carbonates and waters from the Bahamas: Geochimica et Cosmochimica Acta, v. 68, p. 1777-1789.

Robinson, L.F., Henderson, G.M., and Slowey, N.C., 2002, U–Th dating of marine isotope stage 7 in Bahamas slope sediments: Earth and Planetary Science Letters, v. 196, p. 175-187.

Romaniello, S.J., and Derry, L.A., 2010, Validation of an intermediate-complexity model for simulating marine biogeochemistry under anoxic conditions in the modern Black Sea: Geochemistry Geophysics Geosystems, v. 11, Q08002.

Santana-Casiano, J.M., González-Dávila, M., and Millero, F.J., 2006, The role of Fe(II) species on the oxidation of Fe(II) in natural waters in the presence of O2 and H2O2: Marine Chemistry, v. 99, p. 70-82.

Scott, C., Lyons, T.W., Bekker, A., Shen, Y., Poulton, S.W., Chu, X., and Anbar, A.D., 2008, Tracing the stepwise oxygenation of the Proterozoic ocean: Nature, v. 452, p. 456-459.

Sexton, P.F., and Wilson, P.A., 2009, Preservation of benthic foraminifera and reliability of deep-sea temperature records: Importance of sedimentation rates, lithology, and the need to examine test wall structure: Paleoceanography, v. 24, PA2208.

Shinn, E.A., Ginsburg, R.N., and Lloyd, R.M., 1965, Recent supratidal dolomite from Andros Island, Bahamas, *in* Pray, L.C., and Murray, R.C., eds.,

Dolomitization and Limestone Diagenesis: Tulsa, Oklahoma, SEPM, p. 112-123.

Shipboard Scientific Party, 1997, Site 1006, *in* Swart, P.K., Eberli, G.P., and Malone, M.J., eds., Proc. ODP, Init. Repts., 166: College Station, TX, Ocean Drilling Program, p. 233–287.

Siebert, C., Kramers, J.D., Meisel, T., Morel, P., and Nagler, T.F., 2005, PGE, Re-Os, and Mo isotope systematics in Archean and early Proterozoic sedimentary systems as proxies for redox conditions of the early Earth: Geochimica et Cosmochimica Acta, v. 69, p. 1787-1801.

Siebert, C., McManus, J., Bice, A., Poulson, R., and Berelson, W.M., 2006, Molybdenum isotope signatures in continental margin marine sediments: Earth and Planetary Science Letters, v. 241, p. 723-733.

Siebert, C., Nagler, T.F., von Blanckenburg, F., and Kramers, J.D., 2003, Molybdenum isotope records as a potential new proxy for paleoceanography: Earth and Planetary Science Letters, v. 211, p. 159-171.

Slowey, N.C., Wilber, R.J., Haddad, G.A., and Henderson, G.M., 2002, Glacial-to-Holocene sedimentation on the western slope of Great Bahama Bank: Marine Geology, v. 185, p. 165-176.

Smith, D.E., Harrison, S., Firth, C.R., and Jordan, J.T., 2011, The early Holocene sea level rise: Quaternary Science Reviews, v. 30, p. 1846-1860.

Stewart, B.D., Neiss, J., and Fendorf, S., 2007, Quantifying constraints imposed by calcium and iron on bacterial reduction of uranium(VI): Journal of Environmental Quality, v. 36, p. 363-372.

Stirling, C.H., Andersen, M.B., Potter, E.K., and Halliday, A.N., 2007, Low-temperature isotopic fractionation of uranium: Earth and Planetary Science Letters, v. 264, p. 208-225.

Sturchio, N.C., Antonio, M.R., Soderholm, L., Sutton, S.R., and Brannon, J.C., 1998, Tetravalent uranium in calcite: Science, v. 281, p. 971-973.

Swart, P.K., 2000, The oxygen isotopic composition of interstitial waters: evidence for fluid flow and recrystallization in the margin of Great Bahama Bank, *in* Swart, P.K., Eberli, G.P., Malone, M.J., and Sarg, J.F., eds., Proc. ODP, Sci. Results, 166: College Station, TX Ocean Drilling Program, p. 91–98.

Swart, P.K., Eberli, G.P., and Malone, M.J., 1997, Proceedings of the Ocean Drilling Program, Volume 166 Scientific Results: College Station, TX Ocean Drilling Program, 195 p.

Swart, P.K., and Guzikowski, M., 1988, Interstitial-water chemistry and diagenesis of periplatform sediments from the Bahamas, ODP Leg 101., *in* Austin, J.A.J., and Schlager, W., eds., Proc. ODP, Sci. Results, 101: College Station, TX, Ocean Drilling Program, p. 363–380.

Taylor, S., and McLennan, S., 1995, The geochemical evolution of the continental crust: Reviews of Geophysics, v. 33, p. 241-265.

Teal, C.S., Mazzullo, S.J., and Bischoff, W.D., 2000, Dolomitization of Holocene shallow-marine deposits mediated by sulfate reduction and methanogenesis in normal-salinity seawater, northern Belize: Journal of Sedimentary Research, v. 70, p. 649-663.

Teodoru, C.R., Friedl, G., Friedrich, J., Roehl, U., Sturm, M., and Wehrli, B., 2007, Spatial distribution and recent changes in carbon, nitrogen and phosphorus accumulation in sediments of the Black Sea: Marine Chemistry, v. 105, p. 52-69.

Thurber, D.L., 1962, Anomalous U234/U238 in nature: Journal of Geophysical Research, v. 67, p. 4518-4520.

Toole, J., Thomson, J., Wilson, T.R.S., and Baxter, M.S., 1984, A sampling artifact affecting the uranium content of deep-sea porewaters obtained from cores: Nature, v. 308, p. 263-266.

Tossell, J.A., 2005, Calculating the partitioning of the isotopes of Mo between oxidic and sulfidic species in aqueous solution: Geochimica et Cosmochimica Acta, v. 69, p. 2981-2993.

van Heuven, S., Pierrot, D., Rae, J.W.B., Lewis, E., and Wallace, D.W.R., 2011, MATLAB Program Developed for CO2 System Calculations. ORNL/CDIAC-105b: Oak Ridge, Tennessee, Carbon Dioxide Information Analysis Center, Oak Ridge National Laboratory, U.S. Department of Energy.

Veeh, H.H., Calvert, S.E., and Price, N.B., 1974, Accumulation of uranium in sediments and phosphorites on the south west African shelf: Marine Chemistry, v. 2, p. 189-202.

Verbruggen, A., Alonso, A., Eykens, R., Kehoe, F., Kuhn, H., Richter, S., and Aregbe, Y., 2008, Preparation and certification of IRMM-3636, IRMM-3636a, and IRMM-3636b, Institute for Reference Materials and Measurements, 27 p.

Voegelin, A.R., Nagler, T.F., Beukes, N.J., and Lacassie, J.P., 2010, Molybdenum isotopes in late Archean carbonate rocks: Implications for early Earth oxygenation: Precambrian Research, v. 182, p. 70-82.

Voegelin, A.R., Nagler, T.F., Pettke, T., Neubert, N., Steinmann, M., Pourret, O., and Villa, I.M., 2012, The impact of igneous bedrock weathering on the Mo isotopic composition of stream waters: Natural samples and laboratory experiments: Geochimica et Cosmochimica Acta, v. 86, p. 150-165.

Voegelin, A.R., Nagler, T.F., Samankassou, E., and Villa, I.M., 2009, Molybdenum isotopic composition of modern and Carboniferous carbonates: Chemical Geology, v. 265, p. 488-498.

Wasylenki, L.E., Rolfe, B.A., Weeks, C.L., Spiro, T.G., and Anbar, A.D., 2008, Experimental investigation of the effects of temperature and ionic strength on Mo isotope fractionation during adsorption to manganese oxides: Geochimica et Cosmochimica Acta, v. 72, p. 5997-6005.

Wasylenki, L.E., Weeks, C.L., Bargar, J.R., Spiro, T.G., Hein, J.R., and Anbar, A.D., 2011, The molecular mechanism of Mo isotope fractionation during adsorption to birnessite: Geochimica et Cosmochimica Acta, v. 75, p. 5019-5031.

Weyer, S., Anbar, A.D., Gerdes, A., Gordon, G.W., Algeo, T.J., and Boyle, E.A., 2008, Natural fractionation of $^{238}U/^{235}U$: Geochimica et Cosmochimica Acta, v. 72, p. 345-359.

Wheat, C.G., Mottl, M.J., and Rudnicki, M., 2002, Trace element and REE composition of a low-temperature ridge-flank hydrothermal spring: Geochimica et Cosmochimica Acta, v. 66, p. 3693-3705.

Whitaker, F.F., Smart, P.L., Vahrenkamp, V.C., Nicholson, H., and Wogelius, R.A., 2009, Dolomitization by Near-Normal Seawater? Field Evidence from the Bahamas, Dolomites, Blackwell Publishing Ltd., p. 109-132.

Wicklund, R.I., Hepp, L.J., and Wenz, G.A., 1991, Preliminary Studies on the Early Life History of the Queen Conch, *Strombus gigas*, in the Exuma Cays, Bahamas: Proceedings of the Gulf & Caribbean Fisheries Institute, v. 40, p. 283-298.

Wille, M., Kramers, J.D., Nagler, T.F., Beukes, N.J., Schroder, S., Meisel, T., Lacassie, J.P., and Voegelin, A.R., 2007, Evidence for a gradual rise of oxygen between 2.6 and 2.5 Ga from Mo isotopes and Re-PGE signatures in shales: Geochimica et Cosmochimica Acta, v. 71, p. 2417-2435.

Wright, J.D., and Kroon, D., 2000, Planktonic foraminiferal biostratigraphy of Leg 166., *in* Swart, P.K., Eberli, G.P., Malone, M.J., and Sarg, J.F., eds.,

Proc. ODP, Sci. Results, 166: College Station, TX, Ocean Drilling Program, p. 3–12.

Zektser, I.S., and Dzhamalov, R.G., 1981, Groundwater discharge to the pacific ocean: Hydrological Sciences Bulletin-Bulletin Des Sciences Hydrologiques, v. 26, p. 271-279.

Zheng, Y., Anderson, R.F., Van Geen, A., and Fleisher, M.Q., 2002, Preservation of particulate non-lithogenic uranium in marine sediments: Geochimica et Cosmochimica Acta, v. 66, p. 3085-3092.

Zheng, Y., Anderson, R.F., van Geen, A., and Kuwabara, J., 2000, Authigenic molybdenum formation in marine sediments: A link to pore water sulfide in the Santa Barbara Basin: Geochimica et Cosmochimica Acta, v. 64, p. 4165-4178.